universität wien

MASTERARBEIT / MASTER'S THESIS

Titel der Masterarbeit / Title of the Master's Thesis

„Investigation of binding of the two MCHR1 ligands SNAP-7941 and FE@SNAP on brown adipose tissue“

verfasst von / submitted by

Katarína Benčurová, BSc

angestrebter akademischer Grad / in partial fulfilment of the requirements for the degree of

Master of Science (MSc)

Wien, 2018 / Vienna, 2018

Studienkennzahl lt. Studienblatt / degree programme code as it appears on the student record sheet:	A 066 838
Studienrichtung lt. Studienblatt / degree programme as it appears on the student record sheet:	Masterstudium Ernährungswissenschaften
Betreut von / Supervisor:	Univ.-Prof. Mag. Dr. Karl-Heinz Wagner
Mitbetreut von / Co-Supervisor:	Mag. Dr. Cécile Philippe

Acknowledgement

I would like to say a big thank you, to all people supporting and motivating me throughout my study and this thesis, be it with a shared coffee and conversation or just making the lessons even more enjoyable. Thank you!

I would like to express my big gratitude to Univ. Prof. Dr. Karl-Heinz Wagner for taking on my master thesis and kindly supervising it.

I am deeply grateful to Mag. Dr. Cécile Philippe, for offering me the possibility to do this extremely interesting master thesis that was full of variance and never boring. Thank you! I could learn so much. Thanks for the discussions, making time to listen about my new discoveries and the always friendly advice.

A very hearty thanks to Mag. Theresa Balber. Thank you for the constant support, discussions about everything that I found out and about everything that didn't make any sense. Thank you for helping me to make some sense. For the enormous amount of time you spent with me. For being always friendly and helpful, although sometimes, there was maybe one too many question.

I am grateful to the whole team in the department, for making me feel welcome and happy there with you. For offering a helping hand. For giving your point of view.

I would like to express my gratitude to Mag. Dr. Lukas Nics. Without you, my thesis would be about something completely different.

My deep and eternal gratitude to Jozef. For listening, being there and being my rock.

And finally, I would like to thank my parents very much. For support, motivation, listening. For making my study possible and never giving up on me.

Table of contents

List of abbreviations

AC	adenylate cyclase
ADRB1, 2, 3	β_1-, β_2-, β_3-adrenergic receptor
ATGL	adipose triglyceride lipase
BAT	brown adipose tissue
BCA	bicinchoninic acid
BCRP	breast cancer resistance protein
BMP	bone morphogenetic protein
BSA	bovine serum albumin
BW	body weight
cAMP	cyclic adenosine monophosphate
CHO-K1	Chinese hamster ovary (CHO) cell line
CHO-K1-ADRB3	CHO-K1 cell line stably transfected with beta-3 adrenergic receptor
CL 316243	5-[(2*R*)-2-[[(2*R*)-2-(3-Chlorophenyl)-2-hydroxyethyl]amino]propyl]-1,3 benzodioxole-2,2-dicarboxylic acid
cpm	counts per minute
cps	counts per second
[^{11}C]SNAP-7941	carbon-11 labelled analogue of racemic SNAP-7941
CREB	cAMP response element-binding
C/EBPα, -β, -δ	CCAAT (cytosine-cytosine-adenosine-adenosine-thymidine)/enhancer binding-protein α, β, δ
DPBS	Dulbecco's phosphate-buffered saline
FBS	fetal bovine serum
FE@SNAP	(±)-(2-Fluoroethyl)-3-{[(3-{4-[3-(acetylamino)phenyl]-1-piperidinyl}propyl)amin]carbonyl}-4-(3,4-difluorophenyl)-6-(methoxymethyl)-2-oxo-1,2,3,4-tetra-hydro-5-pyrimidenecarboxylate
FFAs	free fatty acids
FGF21	fibroblast growth factor 21
FNDC5	fibronectin type III domain-containing protein 5
[^{18}F]FDG	[^{18}F]fluorodeoxyglucose
[^{18}F]FE@SNAP	[^{18}F]-fluoroethylated analogue of SNAP-7941
GLUT 1,4	glucose transporter type 1,4
GPCR	G protein-coupled receptor
HSL	hormone-sensitive lipase

IC_{50}	half maximum inhibitory constant (concentration of the radioligand causing 50% inhibition of radioligand binding)
IBMX	3-isobutyl-1-methylxanthine
[^{125}I]CYP	[^{125}I]-(-)-Iodocyanopindolol
K_d	equilibrium dissociation constant
K_i	equilibrium inhibitor constant
k_{on}	association rate constant
k_{off}	dissociation rate constant
MCH	melanin-concentrating hormone
MCHR1, 2	melanin-concentrating hormone receptor 1, 2
mRNA	messenger RNA
Myf5	myogenic factor 5
PEI	polyethylenimine
PET	positron emission tomography
PET/CT	positron emission tomography coupled with computed tomography
PGC-1α	PPAR-γ coactivator-1alpha
Pgp	P-glycoprotein
PKA	protein kinase A
PPAR-γ	peroxisome proliferator-activated receptor gamma
PRDM16	PR (positive regulatory) domain containing 16
PTH	parathyroid hormone
RL	radioligand
p38 MAPK	p38 mitogen-activated protein kinase
SNAP-7941	(+)-methyl (4S)-3-{[(3-{4-[3-(acetylamino)phenyl]-1-piperidinyl}propyl)amino]carbonyl}-4-(3,4-difluorophenyl)-6-(methoxymethyl)-2-oxo-1,2,3,4-tetrahydro-5-pyrimidinecarboxylate hydrochloride
SPECT	single photon emission computed tomography
TCA	tricarboxylic acid cycle
T_3	3,3',5-triiodo-L-thyronine
UCP1	uncoupling protein 1
WAT	white adipose tissue
µPET	micro-PET
5'AMP	adenosine monophosphate

List of figures

List of tables

1. Introduction

Melanin concentrating hormone (MCH), a neuropeptide playing a key role in energy homeostasis, as well as brown adipose tissue (BAT), an energy dissipating organ, are studied as potential targets for treatment of obesity and endocrine diseases.

Recently, both systems have been connected when [^{11}C]SNAP-7941 and its [^{18}F]-fluoroethylated analogue [^{18}F]FE@SNAP – two potential positron emission tomography (PET) tracers for the melanin-concentrating hormone receptor 1 (MCHR1) – showed uptake in BAT of rats. However, the expression of the MCHR1 in BAT has not been reported in literature yet. Furthermore, the nonradioactive analogue SNAP-7941 increased the accumulation of [^{18}F]fluorodeoxyglucose ([^{18}F]FDG) in BAT of anaesthetized rats. The later observation shifted interest to β_3-adrenergic receptor (ADRB3), since ADRB3 agonists stimulate glucose uptake in BAT.

Therefore, the affinity of SNAP-7941 and FE@SNAP to ADRB3 was determined and the interaction of the potential PET tracers with brown adipocytes as well as the influence of SNAP-7941 and FE@SNAP on the [^{18}F]FDG uptake of brown adipocytes studied.

This master thesis was conducted from February till September 2017 in the Division of Nuclear Medicine of the Medical University Vienna in the research group of Radiopharmacy and Experimental Nuclear Medicine under supervision of Univ. Prof. Dr. Karl-Heinz Wagner from the Department of Nutritional Sciences of University Vienna and co-supervision of Mag. Dr. Cécile Philippe, head of the research group making the above mentioned *in vivo* observations.

2. Literature survey

2.1 Melanin-concentrating hormone and melanin-concentrating hormone receptor 1

Melanin-concentrating hormone (MCH) is a hypothalamic neuropeptide regulating a variety of functions in the mammalian brain. It plays a key role in energy homeostasis and body weight. Studies have shown that the central administration of MCH stimulates food intake. Expression of the neuropeptide is increased in *ob*/*ob* mice and responds to nutritional signals, such as fasting and leptin deficiency (1, 2, 3, 4). Leptin negatively regulates the expression of melanin-concentrating hormone receptor 1 as well (2). Mice overexpressing MCH were significantly heavier than wild type mice when fed a high-fat diet. They were fatter and developed hyperinsulinemia, hyperleptinemia as well as impaired glucose response (4). Furthermore, MCHR1 antagonism was shown to have antiobesity effects in diet-induced obese mice (5).

The peptide MCH binds to two G protein-coupled receptors (GPCRs), termed melanin-concentrating hormone receptor 1 and 2 (MCHR1 and MCHR2) (6, 7). In rodents however, only MCHR1 is functional. Since appropriate animal models are lacking, the physiological role of MCHR2 remains largely unknown (8).

MCH as well as MCHR1 are predominantly expressed in the brain. Neurons that contain MCH are located in areas involved in regulation of ingestive behaviour, such as zona incerta and lateral hypothalamus (1). In rodents, messenger ribonucleic acid (mRNA) for MCHR1 is expressed in tongue, eye, skeletal muscle, testis, pituitary gland, kidney, and white adipose tissue (WAT) as well (2, 6). In humans, MCHR1 is also expressed in peripheral tissues, eg in human colonic cells and has been implicated in inflammatory processes in the intestine (9). Furthermore, MCH as well as MCHR1 are expressed in the pancreatic islets and exogenous MCH was shown to stimulate insulin release (10).

The MCH/MCHR1 system is involved in a variety of pathologies, especially in endocrine disorders like obesity and diabetes, but also in gut inflammation, depression, anxiety or colitis (3, 8, 9) (Figure 1). Hence, the system is a new target for the treatment of human disorders (11, 12).

Positron emission tomography (PET) is a suitable tool to monitor the mentioned pathologies *in vivo* (13). Nowadays, the radionuclide-based PET belongs to the most sensitive molecular imaging techniques, whereas, central to this imaging is the development of appropriate PET imaging probes (14). A PET tracer provides the basis for image quality and clinical interpretation. It consists of two parts: First, a positron emitting radionuclide, amongst most commonly used – fluorine-18, galium-68 or carbon-11, as a working basis for signal detection with a dedicated PET device such as positron emission tomography coupled with computed tomography (PET/CT) scanner. Secondly, a vehicle

molecule defining the biological characteristics and responsible for the interactions within the living organism. This molecular structure has to provide high selectivity and specificity towards the target (15).

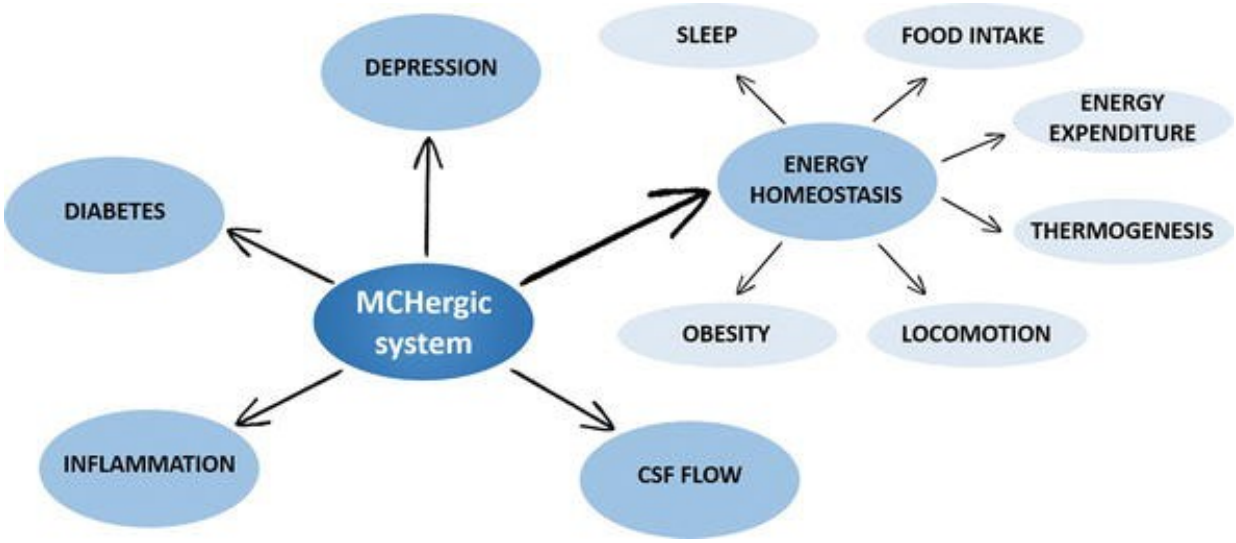

Figure 1: Involvement of the MCH/MCHR1 system
The MCH/MCHR1 system plays an important role in regulation of energy homeostasis and is involved in pathogenesis of endocrine diseases. Furthermore, it has been related to depression and inflammatory processes in gut and is of importance to the flow of cerebrospinal fluid (CSF) (8)

A PET tracer for the MCHR1 could help to gain a deeper understanding of the role and distribution of the dedicated receptor as well as guide pharmacological intervention via the MCHR1. Moreover, a PET tracer could also simplify a dose selection of MCHR1 antagonists, of which the development for the treatment of obesity is pursued. Furthermore, possible quantification of the MCHR1 as a risk factor as well as an early diagnostic tool for diseases like adiposity, diabetes and insulin resistance makes specific MCHR1 imaging of high clinical interest (8, 16).

2.2 [^{11}C]SNAP-7941 and [^{18}F]FE@SNAP – the first potential PET tracers for MCHR1

The research group of Radiopharmacy and Experimental Nuclear Medicine of the Medical University Vienna (Vienna, Austria) developed the first potential PET tracer for MCHR1 in 2012. [^{11}C]SNAP-7941 (Figure 2B) is a carbon-11 labelled analogue (11) of the already published MCHR1 ligand (+)-methyl (4S)-3-{[(3-{4-[3-(acetylamino)phenyl]-1-piperidinyl}propyl)amino]carbonyl}-4-(3,4-difluorophenyl)-6-(methoxymethyl)-2-oxo-1,2,3,4-tetrahydro-5-pyrimidinecarboxylate hydrochloride (SNAP-7941) (3) (Figure 2A). SNAP-7941 was shown to have antidepressant, anxiolytic as well as anorectic effects, which was not caused by malaise nor toxicity (3). One of the main reasons why this compound was

chosen as target for radioactive labelling (11) was its excellent binding affinity (equilibrium dissociation constant K_d = 0.18 nM) (3). Like most of the PET tracers for receptor systems, SNAP-7941 is an antagonist, which prevents potential reaction cascades (17). A fluoroethylated analogue, [^{18}F]FE@SNAP (Figure 2C), was successfully synthesized by the research group afterwards, comprising the advantage of the longer half-life of fluorine-18 (109.8 min) compared to carbon-11 (20.3 min) (13, 18). Currently, these first two PET tracers for MCHR1 are evaluated in preclinical settings (12, 16, 17, 18, 19).

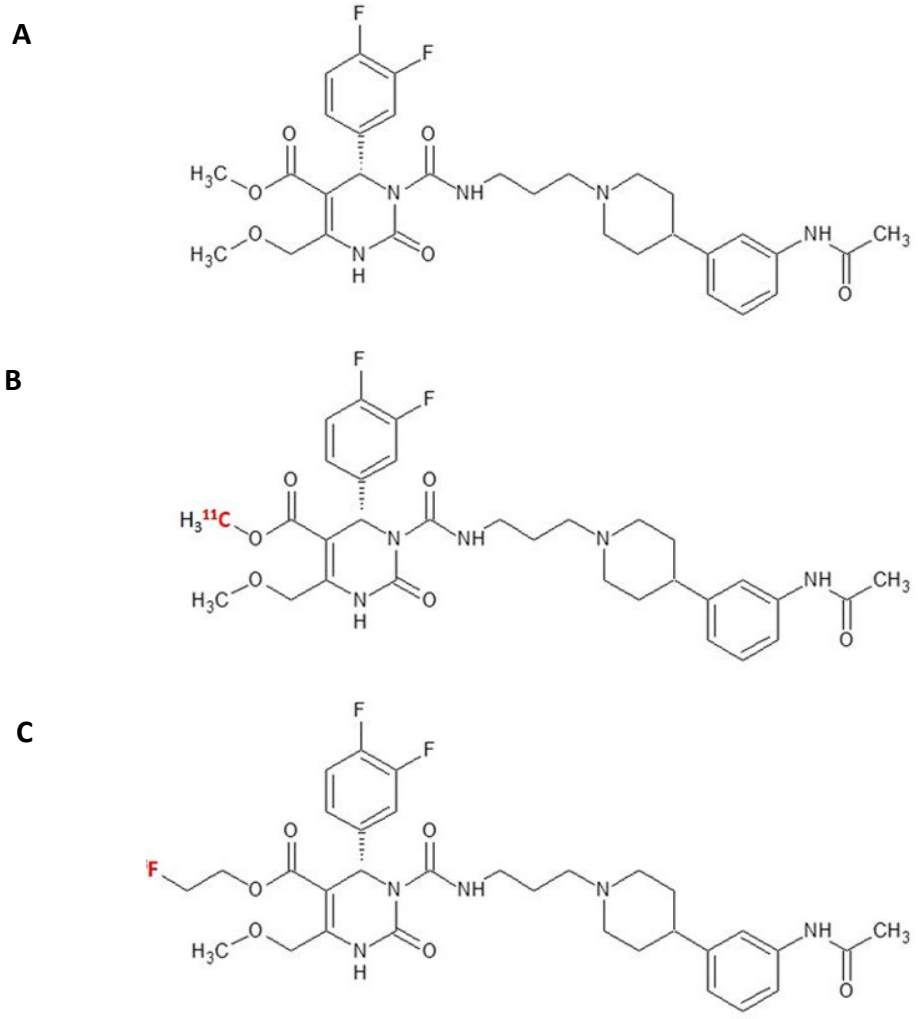

Figure 2: Chemical structures of MCHR1 ligands: SNAP-7941 (**A**), [^{11}C]SNAP-7941 (**B**) and [^{18}F]FE@SNAP (**C**). The red coloured atom marks the position of the radioisotope introduced by labelling (adapted from (16)).

In *in vitro* binding assays conducted on CHO-K1 (Chinese hamster ovary) cell membranes expressing the human MCHR1 or MCHR2 respectively, SNAP-7941 and FE@SNAP evinced high binding affinity to the MCHR1 (12, 16, 18) mandatory for potential MCHR1 PET tracer (18). K_i-values (equilibrium inhibitor constants) for human MCHR1 were 3.91 ± 0.74 nM for (±)-SNAP-7941, the respective

racemate, which was used as the unlabelled compound in these experiments, and 9.98 ± 1.12 nM for FE@SNAP (16). High selectivity of the compounds was observed (K_i >1000 nM for MCHR2). The metabolic stability in human plasma, as well as the stability against carboxylesterase and microsomes was high and the plasma free fraction should be sufficient for potential brain imaging for both substances (12, 18).

[^{11}C]SNAP-7941 is assumed to be a P-glycoprotein (Pgp) and breast cancer resistance protein (BCRP) substrate, due to its significantly increased uptake in the brain of healthy rats after blocking with the Pgp/BCRP inhibitor tariquidar (12). Passive penetration of [^{18}F]FE@SNAP through blood-brain barrier should be possible according to immobilized artificial membrane chromatography (18).

The uptake of [^{11}C]SNAP-7941 as well as of [^{18}F]FE@SNAP was indeed observed in organs expressing MCHR1 (eg eyes, skeletal muscle) (6) in healthy rats (12, 19). The *ex vivo* autoradiography of the brains of healthy rats after intravenous application of [^{18}F]FE@SNAP into conscious animals (exclusion of anaesthetic influence on imaging results) evinced specific uptake in the lateral hypothalamus as well as ventricular system (19). High uptake of [^{11}C]SNAP-7941 and of [^{18}F]FE@SNAP in ventricular system of healthy rats as well as significant reduction of this uptake after displacement with SNAP-7941 could also be observed in small animal imaging (16).

The high binding affinity of the non-labelled derivatives as well as the specific uptake of both radiotracers suggest that [^{18}F]FE@SNAP as well as [^{11}C]SNAP-7941 could serve as useful imaging and therapy monitoring tools for MCHR1 related pathologies (16, 17, 19).

2.3 Brown adipose tissue

Adipose tissue has a major role for the regulation of metabolic function (20), being an energy storing organ. On the other hand it is a thermogenic tissue with contribution to energy expenditure (21). This is due to the existence of different classes of the fat – white, brown and beige. They differ in aspects like developmental origin, gene expression profile, secretome and play divergent roles in energy homeostasis, but they are also all functionally coordinated by sympathetic nervous system and endocrine control (20, 22). The comparison of the different types is shown in Table 1.

White adipose tissue (WAT) is a key determinant of healthy metabolism and metabolic dysfunction (22). WAT is an energy storing tissue, located subcutaneously or visceral and is activated in response to high-fat diet (23). It outstrips brown adipose tissue (BAT) in terms of percentage body mass by far, but activated BAT is an important contributor to nutritional homeostasis as well as energy balance,

through its heat dissipating properties (22). Due to this unique metabolic function, BAT has been in focus of recent metabolic research.

Table 1: Comparison of white, beige and brown adipocytes (adapted from (23))

	White adipocytes	Beige adipocytes	Brown adipocytes
Localisation - Humans	Subcutaneous, intra-abdominal	Cervical, parasternal, supraclavicular, para- and prevertebral	Cervical, parasternal, supraclavicular, para- and prevertebral
- Rodents	Subcutaneous, intra-abdominal	Predominantly subcutaneous	Interscapular, perivascular
Developmental origin	Myf5-negative	Myf5-negative	Myf5-positive
Lipid droplets	Unilocular	Uni/Multilocular	Multilocular
Mitochondrial content	Low	Low to high	High
UCP1 expression	Low	Basal: low Stimulated: high	High
Adaptive thermogenesis	Negative	Basal: low Stimulated: high	High
Energy metabolism	Energy storage	Stimulated: energy dissipation	Energy dissipation
Activators	High fat diet	Cold, catecholamines, β-adrenergic agonists, vitamin A derivatives, BMPs, FGF21, irisin, etc.	

Due to its name giving brown colour, BAT can macroscopically easily be distinguished from WAT, which has a white or yellowish colour (24). There are not only brown adipocytes in BAT, but also the endothelial cells of capillaries, the interstitial cells and preadipocytes (25). Brown adipocytes are usually spheres with a nucleus located in the centre of the cell and numerous mitochondria with well-defined cristae. The lipids are organized in many small vacuoles (multilocular) (26, 27), in contrast to white adipocytes, which are unilocular (one large lipid droplet occupying almost the whole cytoplasm) and relatively scarce in mitochondria. Furthermore, brown fat tissue is densely vascularized (23, 27).

Brown adipocytes share a common precursor with skeletal muscle cells. Both cell types come from a lineage expressing myogenic factor 5 Myf5 (Myf5+cells) (Figure 3). Transcriptional regulator positive regulatory domain containing 16 (PRDM16) controls the cell fate switch between skeletal myoblasts and brown fat cells, when it binds to peroxisome proliferator-activated receptor gamma (PPAR-γ) and

stimulates brown adipogenesis. White adipocytes as well as beige adipocytes do not arise from Myf5 expressing precursors (28), they derive from Myf5 negative cells (Myf5-cells) via distinct precursor cells (20) (Figure 3).

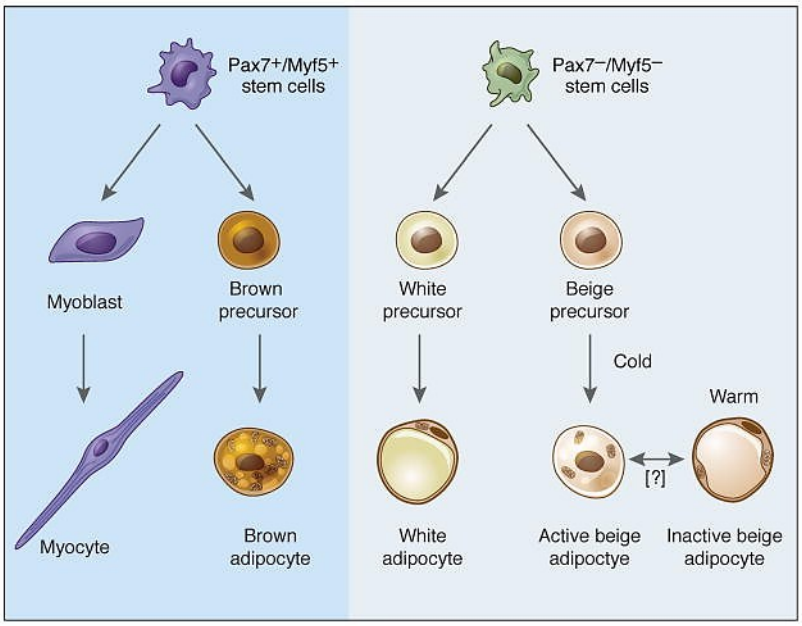

Figure 3: Origins of distinct types of adipocytes (20)

BAT has a unique ability to regulate energy expenditure. Brown adipocytes are capable of dissipating energy, a process called uncoupled respiration, resulting in increased oxidation of fatty acids, glucose uptake and heat production (adaptive or non-shivering thermogenesis). This depends on the expression of a protein called uncoupling protein 1 (UCP1), an inner mitochondrial membrane protein, central regulator of the thermogenic process in BAT. UCP1 short-circuits the mitochondrial proton gradient, so that oxygen consumption is no longer coupled to adenosine triphosphate (ATP) synthesis. As a consequence, heat is generated. The process of thermogenesis can be activated by certain stimuli like cold exposure, adrenergic compounds or genetic alterations (23, 25, 29). The thermogenic activity of BAT has been for long time appreciated particularly in infants as well as small mammals, where it plays a vital role in maintaining core body temperature, but also for hibernators for arousal from hibernation (24, 25).

Recently, the presence of active BAT was also discovered in adult humans (30, 31, 32), as an active and “trainable” tissue responsive to physiological stimuli, such as cold (22, 31, 32) (Figure 4). Induction of BAT activity with cold is associated with enhanced thermogenesis, energy expenditure and beneficial effects on fat mass and glucose metabolism and correlates negatively with obesity. Active

BAT can be detected by [^{18}F]FDG PET/CT (23, 33) (Figure 4). [^{18}F]FDG is a glucose analogue and the most wildly used PET tracer worldwide. In comparison to normal glucose, [^{18}F]FDG stays trapped in the cell. This "metabolic trapping" is due to the fact, that the hydroxyl group on the second position in the glucose molecule is substituted with fluorine-18. The gaining of energy from glucose in a cell is accomplished by glycolysis. After phosphorylation in position 6 an isomerization follows. However, this second step needs a hydroxyl group in position 2 to enable cyclisation, which is in [^{18}F]FDG substituted with positron emitting fluorine-18. [^{18}F]FDG cannot be further metabolized and stays in the cell. The alterations in glucose management as well as tissues with high glucose demand can be detected using [^{18}F]FDG (15).

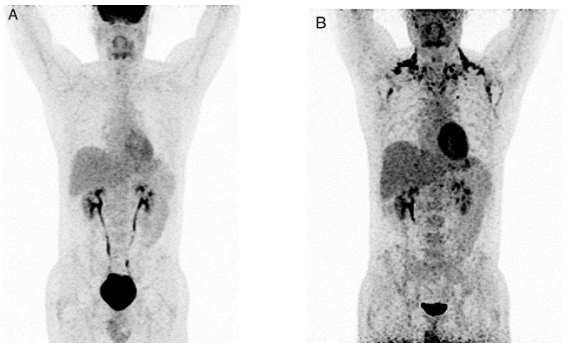

Figure 4: Representative [^{18}F]FDG PET/CT scans before (A) and after (B) short-term exposure to cold. [^{18}F]FDG-positive depots of BAT are visible at typical cervical, clavicular and paravertebral regions (adapted from (33)).

Beige adipocytes can emerge in white fat depots under certain stimuli, such as genetic factors, cold, adrenergic stimulation or exercise. They possess characteristics of both, white and brown fat cells, depending upon the stimuli. The induction of a BAT-like cellular and molecular program in WAT is called "browning" or "beiging". This is associated with increased energy expenditure and protection against obesity and type 2 diabetes mellitus. BAT activity is furthermore decreased in metabolical states of obesity and hyperglycaemia. The brown and/or beige adipocytes with their energy dissipating properties therefore hold promise as a therapeutic concept against obesity and related problems – pharmacological stimulation of energy expenditure (21, 22, 23, 33).

In human BAT, there is an evidence for both brown and beige fat cells. This can be in part explained by the large heterogeneity of the studied human fat samples (21). [^{18}F]FDG-positive BAT depots are located cervical (deep neck region), clavicular, para- (Figure 4) and prevertebral (23, 33). *"The close proximity to the vasculature of the neck has led to evolutionary speculation that the heat generating qualities of BAT may have been relevant for temperature regulation of the blood flowing to the brain"* (21). In rodents, BAT is localized in interscapular and perivascular regions (23).

Adipogenesis occurs in two phases at the cellular level. During determination, the possible alternate fates of a precursor cell become restricted and the cell becomes committed to adipose lineage, becoming a preadipocyte. Later, during the terminal differentiation, preadipocyte acquires the characteristics of a mature adipocyte (20).

Factors that promote this terminal differentiation have been recently depicted in an extensive review by Rosen and Spiegelman (20). The above mentioned PPAR-γ is a "master regulator" of fat cell formation and a very potent adipogenic factor; many other transcriptional factors that have been identified as promoting or inhibiting adipogenesis do this at least partially by induction or repression of PPAR-γ. Cytosine-cytosine-adenosine-adenosine-thymidine (CCAAT)/enhancer-binding proteins (C/EBPs) α, β, and δ along with noncoding RNA are important inducers of adipogenesis. For brown fat adipogenesis PPAR-γ coactivator-1alpha (PGC1α), a dominant regulator of mitochondrial biogenesis, oxidative metabolism and thermogenesis in BAT, is of further importance (20). Endocrine regulators of the adipose thermogenic program include fibronectin type III domain-containing protein 5 (FNDC5) and irisin, natriuretic peptides, retinoids and retinaldehyde dehydrogenase, bone morphogenetic proteins (BMPs) as well as parathyroid hormone (PTH), PTH-related peptide and others (21, 23, 34) (Figure 5).

BAT has a very high relative uptake of glucose and even though the total amount of BAT in body is not large, it can potentially be a significant glucose-clearing organ (35). There are two pathways increasing glucose uptake in BAT with effects on different glucose transporter (GLUT) isoforms. The first is stimulated by insulin, causing a translocation of GLUT4, the insulin-regulated glucose transporter, from the intracellular stores to the plasma membrane. It is also possible, that in the presence of insulin, GLUT4 is recycled from the cell surface (27, 36). The second metabolic pathway is stimulated by norepinephrine during the activation of thermogenesis and can be mimicked by β_3-adrenergic agonists like 5-[(2*R*)-2-[[(2*R*)-2-(3-Chlorophenyl)-2-hydroxyethyl]amino]propyl]-1,3 benzodioxole-2,2-dicarboxylic acid (CL 316243), being thus mediated by β_3-adrenergic receptor (37, 38). It was shown, that the proliferating brown adipocytes have high levels of GLUT1 mRNA and low levels of GLUT4 mRNA. The GLUT4/GLUT1 ratio increases during the differentiation and mature brown fat cells have high levels of GLUT4 mRNA. Interestingly, the treatment with norepinephrine or CL 316243 increased GLUT1 mRNA and decreased GLUT4 mRNA in mature brown adipocytes as reported in a study by Dallner and co-workers (35). Moreover, GLUT1 protein expression on the plasma membrane was highly increased (35). This is in contrast with findings by a Japanese-American group suggesting that norepinephrine stimulates glucose transport in brown adipocytes by increasing the affinity of GLUT1 for its ligand without increasing the amount of GLUT1 in plasma membrane (36). Interestingly, GLUT4 was shifted to an intracellular vesicular compartment due to the norepinephrine treatment which

makes it plausible, that even though GLUT4 is heavily expressed in brown adipocytes, it does not contribute to norepinephrine-induced glucose uptake (35). Cold stimulates the uptake of glucose in BAT through norepinephrine release as well. This effect is used when detecting BAT in humans with [^{18}F]FDG PET/CT scans after cold exposure.

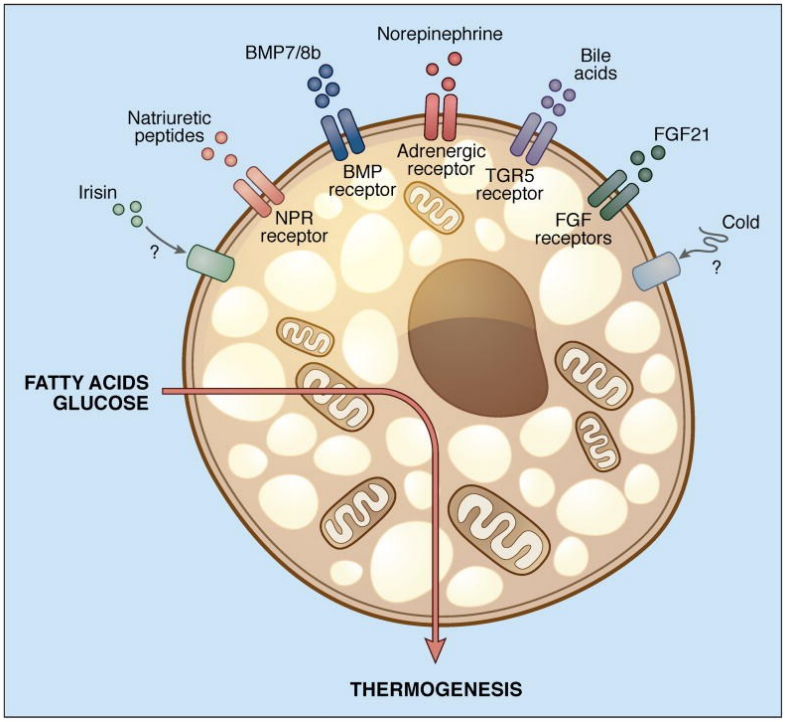

Figure 5: Activators of development and function of brown/beige fat
Some of the inducers of browning and enhanced thermogenesis appear to work in the first place by inducing the formation of new beige (eg irisin) or brown adipocytes (eg BMP7) while others may act on recruitment and enhancement of thermogenic potential (20)

2.4 β_3-adrenergic receptor

Different classes of receptors mediate the central and peripheral, metabolic and neuroendocrine effects of the neurotransmitters norepinephrine (noradrenaline) and epinephrine (adrenaline). These membrane proteins coupled to G proteins (primarily G_s proteins) are called adrenergic receptors or adrenoceptors and have been subclassified according to their pharmacological properties and physiological actions into: α_1-, α_2-, β_1-, β_2- and β_3-adrenergic receptors (39, 40, 41, 42). In brown adipose tissue, ß$_3$-adrenergic receptor (ADRB3) is the predominantly expressed adrenergic receptor subtype (25, 43).

Adrenergic receptors are expressed in almost all peripheral tissues and in the central nervous system and they fulfil a variety of functions. They have been of interest as targets for drug action. Drugs

interacting with adrenergic receptors are in use against different diseases including hypertension, angina pectoris, asthma, depression and others. β_1-adrenergic receptors (ADRB1) are predominantly expressed in the heart and mediate increases in cardiac rate, force of contraction or stimulation of renin secretion. β_2-adrenergic receptors (ADRB2) that mediate smooth muscle relaxation are particularly expressed in respiratory system, but also in blood vessels and uterus (42, 44).

In 1989 a human gene encoding for ADRB3 has been isolated (39). Before, the receptor has been often referred to as the "atypical β-adrenoceptor", because of its insensitivity to the commonly used β-adrenergic antagonists (39, 42). The amino acid sequence of the human β_3-adrenergic receptor (hADRB3) is 51% and 46% identical to that of human ADRB2 and ADRB3 (39). The receptor is about 30-fold more affine for norepinephrine compared to epinephrine (45). As a G protein-coupled receptor, the ADRB3 comprises seven transmembrane domains (39), with three intracellular and three extracellular loops. The N-terminus is extracellular and glycosylated, the C-terminal ending is intracellular, but in contrast to ADRB1 and ADRB2 does not possess a site for phosphorylation with protein kinase A. There is a disulphide bond between two cysteine residues of the second and third extracellular loop essential for the receptor activity and binding of ligands (41). It seems that ADRB3 might exist in at least two different agonist conformational states (40).

Transfection of Chinese hamster ovary cells with ADRB3 (CHO-K1-ADRB3 cells) has allowed better characterization of the receptor. The exposure of these cells to norepinephrine or epinephrine leads to an increase in cyclic adenosine monophosphate (cAMP) accumulation (39), through stimulation of adenylate cyclase (AC) (46). ADRB3 is present in different tissues, primarily in adipose tissue but also in muscle, heart, brain, gastrointestinal tract and urogenitary apparatus and has effects on lipid and glucose metabolism as well as energy utilization (39, 41). Stimulation of ADRB3 by norepinephrine or other adrenergic agonists increases the glucose transport as described more detailed above (41).

In adipose tissue, the ADRB3 is a mediator of lipolysis, in BAT also of thermogenesis (22, 25, 47). The process has been described in more detail in reviews from Peirce *et al.* (22) and from Fenzl and Kiefer (23). Sympathetic nervous system activation via cold releases the catecholamine norepinephrine that binds to β-adrenergic receptors. Binding to ADRB3 coupled to $G_{\alpha s}$ leads to an activation of adenylate cyclase increasing the intracellular concentration of cAMP. This activates protein kinase A (PKA) phosphorylating proteins on lipid droplets, such as hormone-sensitive lipase (HSL), which is hereby activated and perilipin, where the phosphorylation causes deactivation allowing the activation of adipose triglyceride lipase (ATGL). The result is lipolysis: the release of fatty acids from their storage in form of triglycerides. Lipolysis and free fatty acids (FFAs) stimulate thermogenesis. The expression of UCP1 is increased through the p38 mitogen-activated protein kinase (p38 MAPK) cascade (Figure 6). Furthermore, FFAs are oxidized and through the generation of electron carriers cause an

electrochemical gradient and drive ATP synthesis. UCP1 dissipates the electrochemical gradient that drives the synthesis of ATP which results in the release of large amounts of energy as heat (22, 23, 25, 48) (Figure 7).

Several substances, which were already described to bind to ADRB3, have been employed in this thesis. The two radioligands used in competitive binding studies with ADRB3 were [^{125}I]-(-)-Iodocyanopindolol ([^{125}I]CYP), a β_1-/β_2-adrenergic antagonist and partial agonist on ADRB3 (46) that binds to the receptor specifically and saturably (39, 45, 46, 49) and [^{3}H]-CGP-12177 (50), which is also a partial agonist on ADRB3 (40, 45). The β-blocker pindolol behaves as partial agonist for ADRB3 (39, 40, 45) and the β_1-/β_2-adrenergic antagonist propranolol exhibited somewhat differing effects in various studies. It behaved as a very weak and partial agonist on ADRB3 (40, 46) or exhibited even extremely weak inverse agonistic effects (almost antagonist) (45). Carazolol was shown to be a potent and selective ADRB3 agonist (49).

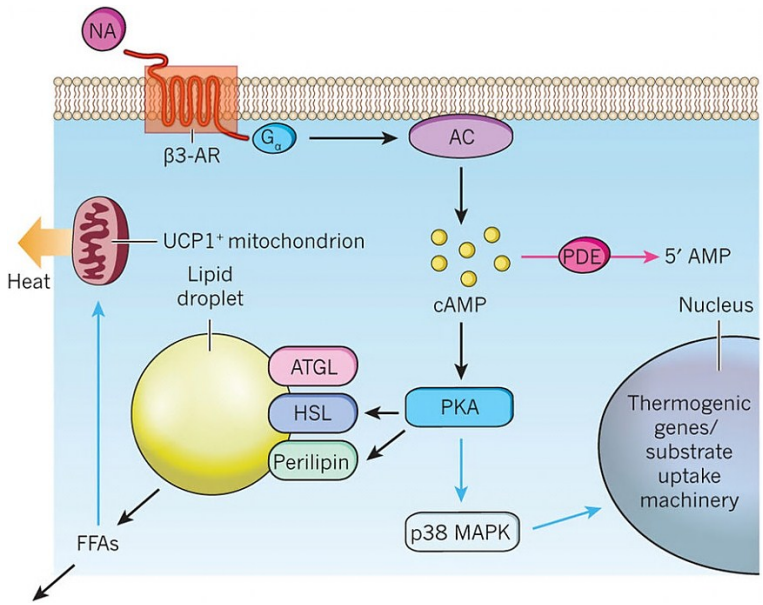

Figure 6: Lipolysis and thermogenesis in adipocytes (22)
NA: noradrenaline, β3-AR: β_3-adrenergic receptor, PDE: phosphodiesterase, 5′ AMP: adenosine monophosphate

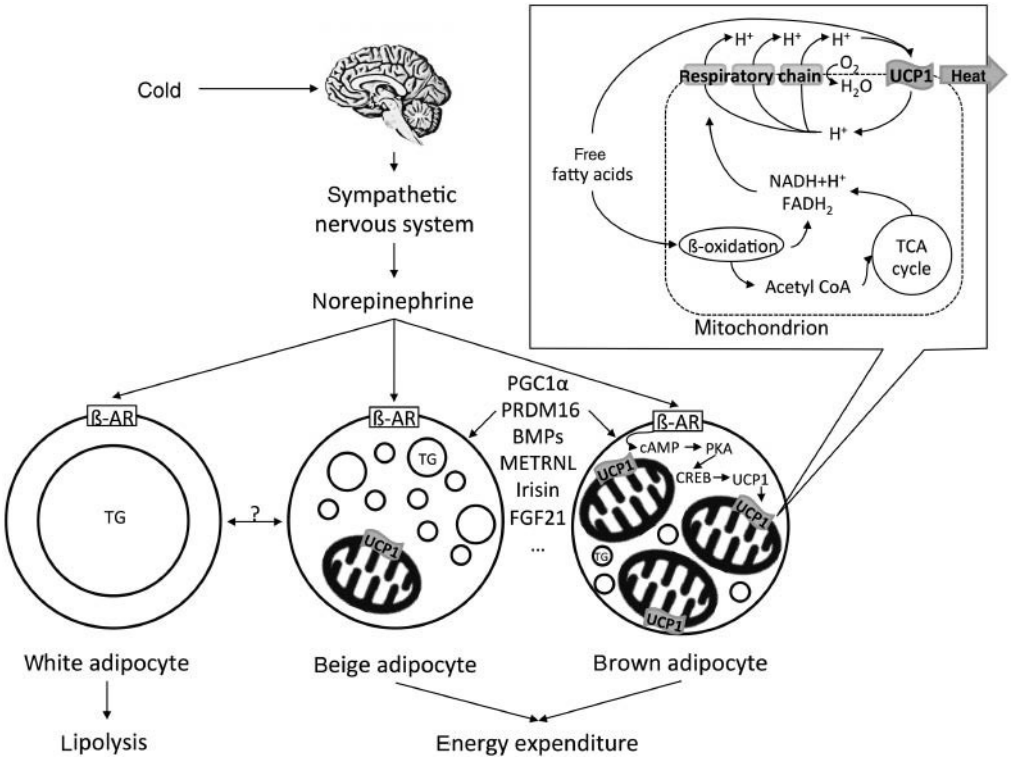

Figure 7: Effect of the activation of the sympathetic nervous system via cold on three adipocyte types (23)
β-AR: β-adrenergic receptor, TG: triglyceride, METRNL: meteorin-like, FGF21: fibroblast growth factor 21, CREB: cAMP response element-binding, Acetyl CoA: acetyl coenzyme A, TCA: tricarboxylic acid cycle

2.5 Theory of radioligand binding assays

One of the main aims of radioligand binding studies in pharmacology is to determine affinities of ligands for a receptor as well as to better understand the mechanism behind the interaction. Three types of radioligand binding experiments can be distinguished: kinetic, saturation and competition assays (51). Within this master thesis, kinetic and competitive experiments have been performed.

Kinetic studies are mostly used to characterize novel radioligands and to establish the optimal assay conditions (52). The binding of one or more concentrations of the radioactive labelled ligand is measured over time to obtain information about the association and dissociation of the ligand from the receptor characeterized by the association (k_{on}) and dissociation (k_{off}) rate constants (51).

Both saturation and competition binding studies are equilibrium studies. The principle behind this kind of experiments is the idea that an association of a radioligand with its receptor and dissociation of the resulting ligand-receptor complex are reversible processes occurring concomitantly until an equilibrium has been reached (52).

Saturation binding studies are performed using a series of concentrations of a radioligand and its binding to the receptor is measured at equilibrium (51). This allows the determination of K_d, the

equilibrium dissociation constant, and of the number of binding sites. K_d is the concentration at which the ligand binds half of its binding sites and therefore a measure for the ligand's affinity to the receptor (binding site). The lower the K_d-value, the higher the affinity of the ligand (52).

"Binding of the ligand to the receptor follows the law of mass action. The ligand and receptor associate and form a ligand-receptor complex, or they may dissociate again" (52) (Figure 8).

$$\text{receptor} + \text{ligand} \leftrightarrow \text{receptor} \cdot \text{ligand}$$

Figure 8: Law of mass action (52)

When in state of equilibrium, the rate of formation of new ligand-receptor complexes equals the rate of dissociation of these complexes (52) (Figure 9).

$$[\text{ligand}] \times [\text{receptor}] \times k_{on} = [\text{receptor} \cdot \text{ligand}] \times k_{off}$$

Figure 9: Equilibrium state (52)

Once equilibrium is reached, the K_d-value, a measure of the tendency of the receptor-ligand complex to dissociate, can be determined (51) (Figure 10).

$$K_d = \frac{k_{off}}{k_{on}} = \frac{[\text{ligand}] \times [\text{receptor}]}{[\text{receptor} \cdot \text{ligand}]}$$

Figure 10: Equilibrium dissociation constant K_d (51)

Competitive binding experiments are performed using a single radioligand concentration and a variety of concentrations of the competing substance (53). They allow the determination of IC_{50}, the concentration of the competitive inhibitor causing 50% inhibition of radioligand binding (52). Data are best fitted with non-linear regression (54) giving the IC_{50} as the point of inflection of the competitive binding curve (52) (Figure 11). Competitive binding curves are obtained by plotting the amount of the bound radioligand, usually expressed as counts per minute (y-axis) against the concentration of the unlabelled competitor on a logarithmic scale (x-axis). The top of the monophasic curve corresponds to total radioligand binding, which is the amount of radioligand bound in the absence of the unlabelled competing drug. The bottom corresponds to non-specific binding (54) (Figure 11), which can be determined when the radioligand is incubated in additional presence of a high concentration of a

competitor (52) (≥ 100 K_d) in order to block specific sites with this unlabelled substance, so that the radioligand can bind only non-specifically (54). The non-specific binding can be caused by binding to receptors other than the target receptor, to cell membrane lipids but also by binding to the wall of the test tube. Specific binding can be calculated as the difference between total and non-specific binding (52).

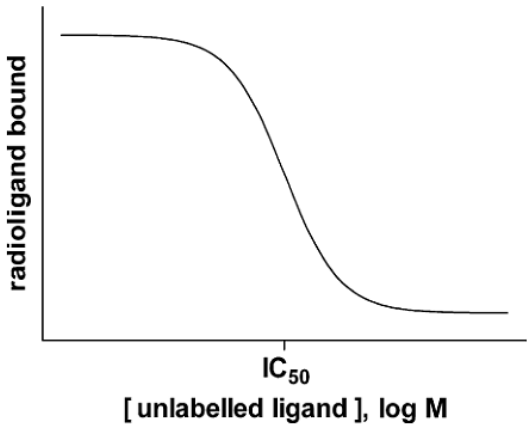

Figure 11: Competitive binding curve (52)

The equilibrium inhibition constant for binding of the unlabelled drug (K_i) can be calculated using the Cheng-Prusoff equation (55) (Figure 12) and is a measure for the affinity of the unlabelled drug.

$$K_i = \frac{IC_{50}}{1 + \frac{[RL]}{K_d}}$$

Figure 12: Cheng-Prusoff equation (55)
[RL] = concentration of the used radioligand (RL)

2.6 Conventional radioligand binding techniques

The conventional radioligand binding methods are commonly used for determination of the affinity of ligands (K_d or K_i) (52) as explained in section 2.5. Radioligand binding can be performed using cell membrane preparations or whole cells (56).

These methods allow a variety of conditions and samples to be processed (56). A typical measurement includes handling of a large sample size applying the same number of cells or the same concentration of membranes (57). The assay consists of three main steps: incubation, separation of bound and unbound ligand and measurement of activity of the bound ligand (56).

First, assay buffers and cell or membrane suspension are prepared, followed by radioligand incubation within tubes (56) or wells. During this step, the radioligand binds to its target until a binding equilibrium has been reached (52). When establishing a new assay, ideal conditions need to be experimentally found. This involves the duration and temperature of incubation, radioligand concentration and buffer. Ion composition and pH value are important parameters of the buffer used (56). Hypotonic buffers with chelating substances such as ethylenediaminetetraacetic acid are often used. Chelating substances prevent endogenous enzymes from degrading membranes or proteins. Higher temperature allows the equilibrium to be achieved faster and hereby shorten the incubation time (52).

"At the end of the incubation period bound and unbound radioligand must be separated" (52). Two methods are mostly used; vacuum filtration and centrifugation (52). Filtration is the more frequently used technique and filtration devices such as elaborate harvesters can be employed. With these, large sample numbers can be processed simultaneously. The incubation medium is sucked through filters. To minimize non-specific binding, rinsing a few times after filtration is necessary. Ice-cold buffers minimize dissociation of the bound ligand. Ideally, the receptor-ligand complex should be completely trapped within the filters (51, 52). The filters can be pretreated with substances like polyethyleneimine or bovine serum albumin to further minimize the non-specific binding (51).

When using whole cells, not only receptor binding but also specific cell uptake via transporters, internalization and diffusion can be investigated. Therefore, cells are cultivated in well plates and incubated with different concentrations of the radioligand for different time points. Cell supernatant, containing the unbound (free) radioligand and cell fraction can be collected separately.

This is the case with [^{18}F]FDG, a glucose analogue, actively transported via glucose transporter into the cell, where cell uptake and not binding is determined. For these experiments, only intact living cells and no membranes can be used and no K_i nor K_d can be determined.

The third step of the conventional binding method is quantification of the radioactive content of the sample (56). For beta emitters such as tritium, scintillation fluid is necessary prior to counting with a dedicated Beta Counter. Gamma emitters (eg iodine-125) can be measured directly using appropriate hardware (52, 56).

2.7 Real-time assays using LigandTracer® Technology

The technology of LigandTracer® was first described by Björke and Andersson in 2006 (57) and is commercially available from Ridgeview Instruments AB (Uppsala, Sweden). The method is semi-

automated and monitors the interactions of ligands with adherent cells in real-time thereby providing an advantage especially when working with novel radioligands. Not only information about affinity of the ligand, but also knowledge about cell uptake or retention can be obtained and be of importance eg when preparing cells for other procedures (57, 58).

To perform the measurement, cells are seeded only onto one part of the cell dish designated as the target area. The opposite part without cells is the reference area. During the measurement the cell dish rotates on an inclined support, consequently the liquid is continuously stirred. The detector is located above the upper part of this support and either target region or reference region is in the field of detector (Figure 13). The liquid accumulates in the lower end of the dish and is therefore not in the field of detection. Both areas, the one with and the other without cells, are repeatedly measured with an output signal being a difference between the maximum radioactivity of the target area and the background signal derived from the reference region per rotation round in counts per second (cps). The obtained signal is an accurate measurement of the amount of the cell-associated radioligand. This is followed over time, providing an accurate measurement of the kinetics of the interaction. The operator obtains a binding curve that displays the amount of ligand bound or taken up over time and contains information about affinity, kinetics and complexity of radioligand binding (57, 58, 59, 60). In Figure 14 an example of a kinetic binding curve is shown. Radioligand association was performed with two concentrations of the radioligand, followed by removal of cell medium, which allows the radioligand to dissociate.

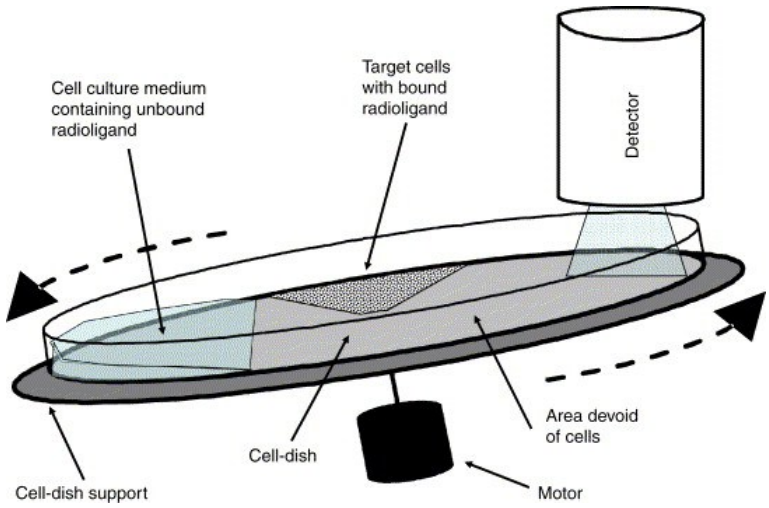

Figure 13: Schematic of the LigandTracer® Instrument prototype (58)

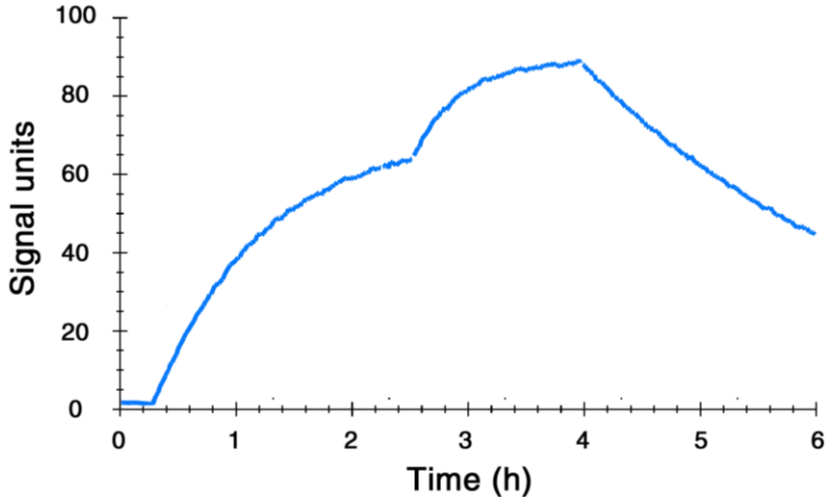

Figure 14: Example of LigandTracer® binding curve (adapted from (61))

The main advantage of kinetic measurements is the large amount of data points obtained and the fact, that the interactions between the ligands and cells can be followed in real-time. The method saves labour time as well as reagents compared to manual methods, improving hereby the productivity and safety. Furthermore, an *in situ* reference area is used for background correction in continuous operation and provides real-time binding traces with superior time-resolution. The main disadvantage is – as that the cells must be present only in a defined area – the more elaborate preparation of the petri dish. Furthermore, cells need to be adherent and cells in suspension cannot be used, unless these are anchored to the cell culture dish prior to use (57, 58, 59).

2.8 Connection between MCHR1 ligands and brown adipose tissue – project background

Recent micro-PET (µPET) experiments have shown an accumulation of [^{18}F]FE@SNAP and [^{11}C]SNAP-7941 (applied in pM-concentration) in brown adipose tissue of naïve rats. Furthermore, a trend towards uptake enhancement after displacement with SNAP-7941 (pharmacological dose: 15 mg/kg body weight (BW)) was observed. However, contradictory observations were made in awake rats: A specific (blockable) uptake was observed when [^{18}F]FE@SNAP was injected to conscious freely moving rats via a catheter implanted into the jugular vein. An influence of anaesthesia on the uptake could therefore be excluded. Significant reduction of [^{18}F]FE@SNAP uptake was observed after blocking with SNAP-7941 (15 mg/kg BW). These experiments suggest the sensitivity of BAT activation towards environmental effects and question the possible expression of MCHR1 within this tissue, that has not been reported yet (62, 63).

Furthermore, administration of SNAP-7941 (15 mg/kg BW) caused an increased [^{18}F]FDG accumulation in BAT of anaesthetized rats (63). This suggests an adrenergic stimulation of glucose uptake in brown adipocytes as is the case with norepinephrine or β_3-adrenergic agonists like CL 316243 via the ADRB3 (37, 63).

The relationship between MCHR1 ligands and β_3-adrenergic receptors in BAT emerged in the focus of the research group as well as my master thesis. Both, antagonism of the MCHR1 as well as activation of BAT, are investigated as potential targets for treatment of obesity. Thus, the clarification of the role of MCHR1 ligands in BAT is of high interest (62, 63).

3. Aim

As pharmacological doses of SNAP-7941 (15 mg/kg BW) increased the uptake of [^{18}F]FDG in BAT of anaesthetized rats and specific (blockable) uptake of [^{18}F]FE@SNAP in BAT of non-anaesthetized rats were observed in previous experiments (62, 63), we hypothesized that the MCHR1 ligands SNAP-7941 and FE@SNAP bind to ADRB3, since MCHR1 expression was not described in BAT so far.

Therefore, we aimed at the determination of the affinity of these two ligands to ADRB3. Competition binding studies (filtration method) using cell membranes expressing hADRB3 were performed and compared with competitive real-time whole cell-binding studies. Moreover, we aimed at a deeper understanding of the *in vivo* observations and thus characterization of the interaction of the PET tracers [^{11}C]SNAP-7941 and [^{18}F]FDG with brown adipocytes. Hence, binding behavior of [^{11}C]SNAP-7941, [^{18}F]FE@SNAP and [^{18}F]FDG was investigated using murine brown preadipocytes, mature brown adipocytes and CHO-K1 cells expressing hADRB3.

4. Materials and Methods

4.1 Materials

4.1.1 Cell lines and membrane preparations

The commercial CHO-K1 cell membranes expressing hADRB3 (human Adrenergic ß$_3$ Receptor) (Product No.: ES-035-M400UA) (64) and the CHO-K1 cells stably expressing hADRB3 (human Adrenergic ß$_3$ Receptor Cell Line) (Product No: ES-035-CV) (65) were both purchased from PerkinElmer® (Waltham, USA). CHO-K1 cells were a generous gift from Professor Karl-Norbert Klotz (University of Würzberg, Germany). Murine brown preadipocytes were kindly donated from the Department of Medicine III, Clinical Division of Endocrinology and Metabolism of Medical University of Vienna (Vienna, Austria).

4.1.2 Chemicals

The test compounds carazolol, pindolol and (S)-(−)-Propranolol hydrochloride (propranolol), melanin concentrating hormone (active sequence – 6-17), solvent dimethyl sulfoxide (DMSO), sodium chloride (NaCl), tris(hydroxymethyl)aminomethane (Tris), ethylenediaminetetraacetic acid (EDTA), 4-(2-hydroxyethyl)piperazine-1-ethanesulfonic acid (HEPES), bovine serum albumin (BSA), polyethylenimine (PEI), Protease Inhibitor Cocktail (Catalog No: P2714), insulin (human recombinant), 3,3',5-triiodo-L-thyronine (T_3), 3-isobutyl-1-methylxanthine (IBMX), indomethacin, dexamethasone and Oil Red O stain were purchased from Sigma-Aldrich (St. Louis, USA).

Ethanol, 2-propanol, hydrochloric acid (HCl) and Mayer's hemalum solution (haematoxylin) and formaldehyde solution min. 37% were obtained from Merck KGaA (Darmstadt, Germany).

CL 316243 was purchased from Tocris Bioscience (Bristol, UK) in form of disodium salt.

Scintillation cocktail (Ultima Gold™ XR LSC Cocktail for aqueous samples) was purchased from PerkinElmer® (Waltham, USA).

Radioligands [^{3}H]-CGP-12177 (Product No.: NET1061) (66) and [^{125}I]CYP (Product No.: NEX189) were purchased from PerkinElmer® (Waltham, USA).

The test compounds SNAP-7941 and FE@SNAP were synthesized in collaboration with the Department of Pharmaceutical Chemistry and the Department of Organic Chemistry of the University of Vienna (Vienna, Austria) (67).

Cell culture media and reagents were purchased from gibco® (Paisley, UK) or gibco® (Grand Island, USA) and are listed in Table 2.

Pierce™ BCA Protein Assay Kit was obtained from Thermo Fisher Scientific (Waltham, USA) (68).

Table 2: Chemicals

Chemical	Source	Chemical	Source
BSA	Sigma-Aldrich	Indomethacin	Sigma-Aldrich
Carazolol	Sigma-Aldrich	Insulin	Sigma-Aldrich
CL 316143	Tocris Bioscience	[^{125}I]CYP	PerkinElmer®
Dexamethasone	Sigma-Aldrich	L-Glutamine 200 mM (100X)	gibco®
DMSO	Sigma-Aldrich	MCH	Sigma-Aldrich
Dulbecco's modified eagle medium (DMEM)	gibco®	NaCl	Sigma-Aldrich
Dulbecco's phosphate-buffered saline (DPBS)	gibco®	Oil Red O stain	Sigma-Aldrich
EDTA	Sigma-Aldrich	PEI	Sigma-Aldrich
Ethanol	Merck KGaA	Pen Strep ((penicillin – 10.000 Units/mL and streptomycin – 10.000 µg/mL)	gibco®
F-12 Nut Mix (Ham) (1X) medium	gibco®	Pierce™ BCA Protein Assay Kit	Thermo Fisher Scientific
FE@SNAP	synthesized (collaboration Medical University Vienna and Unversity of Vienna) (67)	Pindolol	Sigma-Aldrich
Fetal bovine serum (FBS)	gibco®	Propranolol	Sigma-Aldrich
Formaldehyde solution min. 37%	Merck KGAaA	Protease Inhibitor Cocktail	Sigma-Aldrich

Geneticin®	gibco®	SNAP-7941	synthesized (collaboration Medical University Vienna and University of Vienna) (67)
Haematoxylin	Merck KGAaA	Sodium Pyruvate 100 mM (100X) (pyruvate)	gibco®
HCl	Merck KGAaA	T_3	Sigma-Aldrich
HEPES	Sigma-Aldrich	Tris	Sigma-Aldrich
[^{3}H]-CGP-12177	PerkinElmer®	Trypsin (Trypsin-EDTA (0.05%))	gibco®
IBMX	Sigma-Aldrich	2-Propanol	Merck KGAaA

4.1.3 Disposables

Test tubes were purchased from Sarstedt AG & Co (Nümbrecht, Germany) and scintillation vials from PerkinElmer® (Waltham, USA). Whatman GF/B Filter Paper was obtained from Brandel Inc. (Gaithersburg, USA).

SETON centrifuge tubes (SETON open-top centrifuge tubes (polyclear)) were purchased from Seton Scientific (Petaluma, USA), Eppendorf tubes and pipette tips from Eppendorf (Hamburg, Germany) were used.

Cell dishes (Cellstar® cell culture dishes) and T75 cm^2, T175 cm^2 cell culture flasks (Cellstar® cell culture flasks) were obtained from Greiner Bio-One GmbH (Frickenhausen, Germany), CryoTube™ Vials from Thermo Fisher Scientific (Waltham, USA). 6-well plates (Corning® Costar® 6 well cell culture plates) were purchased from Corning Inc (Corning, USA). Millex®-GS Sterile Filter Units (0.22 µm) from Merck KGAaA (Darmstadt, Germany) were used for sterile filtration. In cell culture, VWR® Disposable Serological Pipets (VWR International, Radnor, USA) were used.

4.2 Instrumentation

Competitive binding studies using filtration for separation were performed with Brandel® Harvester (Brandel, Gaithersburg, USA) (Figure 15). Radioactivity was measured with Hidex 300SL Beta Counter

(Hidex, Turku, Finnland). For incubation at 27 °C, GFL Water Bath Type 1003 from GFL Gesellschaft für Labortechnik GmbH (Burgwedel, Germany), was used.

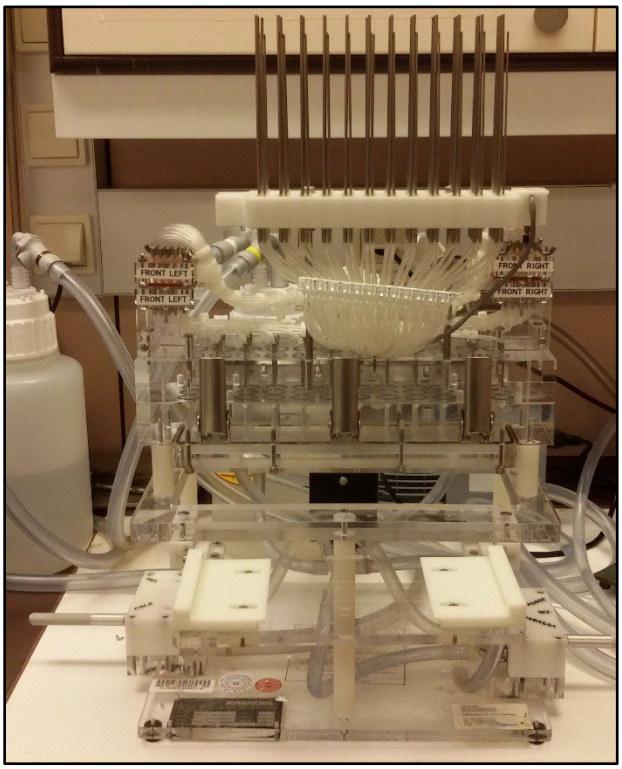

Figure 15: Brandel® Harvester
In the Department of Biomedical Imaging and Image-guided Therapy, Medical University of Vienna, Austria

For centrifugation, Hettich® ROTANTA 460 RC centrifuge (membrane preparation) and Hettich® ROTANTA TRC centrifuge (cell culture) from Hettich (Kirchlengern, Germany) were employed. Ultracentrifuge SORVALL OTD Combi was purchased from Thermo Fisher Scientific (Waltham, USA).

All steps requiring sterile work in cell culture were performed under Laminar-Flow Hood BioWizard Silver SL-130 from Kojair Tech Oy (Vilppula, Finnland). Cells were counted using Cell Scepter™ from Merck KGaA (Darmstadt, Germany) and incubated in CO_2-Incubator C200 (Labotect GmbH, Göttingen, Germany). Pipetboy acu 2 (INTEGRA Biosciences GmbH, Biebertal, Germany) and pipettes from Eppendorf (Hamburg, Germany) were used for pipetting. Microscope Axio Observer (Zeiss, Jena, Germany) in the Department of Pathophysiology and Allergy Research of Medical University of Vienna (Vienna, Austria) and Olympus CK2 Inverted Microscope (Olympus K.K., Tokio, Japan) were used.

LigandTracer® experiments were performed using LigandTracer® Grey, Yellow and White (Figure 16) from Ridgeview Instruments AB (Uppsala, Sweden). Bi-distilled water was acquired from Milli-Q® water purification system from Merck KGAaA (Darmstadt, Germany). The fume hood (Captair® Chem

Fume Hood) was purchased from Erlab® (Rowley, USA). Gamma-Counting was done using 2480 WIZARD^2 Gamma Counter (PerkinElmer®, Waltham, USA).

Figure 16: LigandTracer® Instrumentation
LigandTracer® Yellow, Grey and White in the Department of Biomedical Imaging and Image-guided Therapy, Medical University of Vienna, Austria

4.3 Stock solutions and dilution series of known ADRB3 ligands and test compounds

Stock solutions and dilution series of the known ADRB3 ligands as well as the MCHR1 ligands were prepared prior to the performed experiments and are listed in Table 3. The ADRB3 agonists carazolol and pindolol and the ADRB1/ADRB2 antagonist propranolol were solved and diluted to the final concentrations with DMSO. Stock solutions and dilution series of the test compounds SNAP-7941 and FE@SNAP were prepared in ethanol. ADRB3 agonist CL 316243 was solved and then further diluted to achieve desired concentrations using bi-distilled water. The active sequence of MCH was diluted in bi-distilled water to achieve 1 mM concentration and divided into aliquots of 30 µL. The aliquots where stored at -20°C until further use.

Table 3: Test compounds with their solvents and target receptors

Chemical	Solvent	Target
Carazolol	DMSO	ADRB3
Pindolol	DMSO	ADRB3
Propranolol	DMSO	ADRB3
CL 316243	Bi-distilled water	ADRB3
SNAP-7941	Ethanol	MCHR1 ADRB3 ?
FE@SNAP	Ethanol	MCHR1 ADRB3 ?
MCH	Bi-distilled water	MCHR1

4.4 Competitive binding studies with membranes using filtration method

The competitive binding studies using a Brandel® Harvester were performed with CHO-K1 cell membranes expressing hADRB3 (Product No.: ES-035-M400UA, PerkinElmer®, Waltham, USA) (64) or in-house prepared cell membranes.

First, experiments using commercial membranes were conducted. After the assay was established with the known ADRB3 ligands, membranes were also prepared in-house from the CHO-K1-ADRB3 cell line and further experiments with the test compounds SNAP-7941 and FE@SNAP as well as carazolol were performed using these membranes.

4.4.1 Membranes

4.4.1.1 Preparation of commercial membranes

One batch of the commercial CHO-K1 cell membranes expressing hADRB3 (400µL) was thawed and quickly divided into 11 aliquots with 36 µL membrane solution each and stored at -80°C until further use. The protein concentration was determined by manufacturer using bicinchoninic acid (BCA) method (69) and was according to the technical data sheet 2 µg/µL (64).

Prior to every experiment, an aliquot containing 36 µL membrane suspension was thawed and mixed with 5.4 mL of an assay buffer (for composition see section 4.4.2). This approximate 1:150 dilution resulted in 2 µg of protein in one test tube (2 µg/500 µL).

4.4.1.2 Preparation of membranes from CHO-K1-ADRB3 cell line

The CHO-K1 cells stably expressing hADRB3 (CHO-K1-ADRB3) (Product No: ES-035-CV, PerkinElmer®, Waltham, USA) (65) were grown as described in section 4.5.1. Cell membranes were produced from this cell line according to Klotz *et al.* (70) with slight modifications.

The CHO-K1-ADRB3 cells were split into several T175 cm^2 cell culture flasks. The amount of used cells was chosen according to a preliminary experiment to obtain about 6.8 µg protein per tube and enough membrane suspension for 3 independent experiments. After reaching about 80% confluence, the cells were harvested. The medium was removed and cells were washed with ice-cold DPBS. Ice-cold buffer (10 mM Tris/HCl, 1 mM EDTA, pH 7.4) was added and cells were scraped off the flask and transferred to Eppendorf tubes.

Protease Inhibitor Cocktail (Catalog No: P2714, Sigma-Aldrich, St. Louis, USA) was prepared in advance. The lyophilized powder was solved in 2 mL bi-distilled water and stored at -20°C in form of 100 µL aliquots. The producer recommends to solve the cocktail in 100 mL; the prepared Protease Inhibitor Cocktail stock solution was therefore 50-fold concentrated. 20 µL of the concentrated Protease Inhibitor Cocktail was added per 1mL membrane-buffer-suspension.

The suspension was homogenized on ice using an insulin syringe and the homogenate was centrifuged for 10 min afterwards (4°C, 1000 g, Hettich® ROTANTA 460 RC centrifuge).

The supernatant was pipetted off into the SETON centrifuge tubes and centrifuged for 30 min at 100 000 g at 4°C using Ultracentrifuge SORVALL OTD Combi. Supernatant was discarded and pellet was suspended in ice-cold 50 mM Tris/HCl buffer (pH 7.4). The membrane suspension was divided into aliquots in CryoTube™ Vials, shock frozen in liquid nitrogen and transferred into -80°C until further use. The protein concentration was determined.

4.4.1.3 Determination of the protein concentration of the generated membranes

The protein concentration of the cell membranes prepared from the CHO-K1-ADRB3 cell line was determined using BCA Protein Assay Kit according to the manufacturer's instructions (68). The assay kit uses a measurement method based on BCA for the colorimetric detection and quantification of the protein amount first described by Smith and colleagues in 1985 (69). The method used is the same as the one used for the determination of the protein concentration of the applied commercial membranes from PerkinElmer® (64).

Protein concentration was determined with reference to standards of BSA. First, the series of dilutions of BSA standard were made according to the instruction sheet (68). The necessary amount of the BCA

Working Reagent was prepared by mixing 50 parts of BCA Reagent A with 1 part of BCA Reagent B. The unknown sample (prepared membrane solution) as well as standards were assayed in duplicates. 1:1 dilution of the unknown sample was assessed alongside. 25 µL of each standard or unknown sample was pipetted into a microplate well, 200 µL of the BCA Working Reagent was added to each well. The microplate was covered and incubated at 37°C for 30 min. Absorbance of the solution was measured at 562 nm on a plate reader.

Concentration of the unknown sample as well as of the 1:1 dilution was determined based on the standard curve and the value is expressed as mean ± standard error of the mean (SEM).

4.4.2 Buffers

Two types of buffers were prepared; an assay buffer, which was used for incubation and a wash buffer for washing after filtration of the samples through filter paper. While the assay buffer needed to be prepared only once, about 500 mL of wash buffer was used for every experiment and this was therefore made fresh prior to every second experiment.

The assay buffer consisted of 25 mM HEPES, 1 mM EDTA and 0.5% BSA, in accordance with the technical data sheet from PerkinElmer® (64). Sodium hydroxide (NaOH) was used to adjust pH to 7.4 after HEPES was solved. The wash buffer consisted of 10 mM HEPES and 500 mM NaCl, pH was also adjusted to 7.4 using NaOH. Until further use, buffers were stored at 4-7°C.

4.4.3 Radioligand

According to the Technical Data Sheet (64), PerkinElmer® recommends the usage of [^{125}I]CYP, but since the harvester tygon tubings are not suitable for iodine-125, [^{3}H]-CGP-12177 (Product No.: NET1061, PerkinElmer®, Waltham, USA) (66) was used instead (K_d=109.2 nM for ADRB3 (50)).

Prior to every experiment, [^{3}H]-CGP-12177 was diluted with assay buffer in order to achieve the desired final concentration of 5 nM as follows:

Taking into account the specific activity (1258 GBq/mmol) and activity concentration (9.25 MBq/250 µL) of the purchased product, 3.4 µL of radioligand were diluted with 2 mL of assay buffer. This radioligand stock solution (50 nM) was used 1:10 (50 µL radioligand in final volume of 500 µL) to yield 5 nM radioligand concentration. Due to the extremely long half-life of tritium (12.32 y), correction for radioactive decay was not necessary.

4.4.4 Assay procedure

The binding assay did not follow the recommendations of the manufacturer (64), since a different radioligand was used. In order to find the ideal assay conditions, several experimental settings were tested including different incubation time, incubation temperature, membrane concentration, shaking or no shaking before measurement of radioactivity, different solutions for presoaking of the filter as well as filter type.

The competition binding studies with filtration method consisted of four main steps: preparation of incubation mixture, incubation, filtration and measurement of radioactivity. The experiments were carried out in 500 µL total volume per test tube and at least three independent experiments were carried out in triplicates. For the representative experimental setting see Table 4. The incubation mixture was prepared as follows: 295 µL of the assay buffer, 5 µL of the test substance (competitor), 50 µL of the radioligand [^{3}H]-CGP-12177 stock solution (5 nM final concentration) and 150 µL of membrane suspension were added to the tubes.

Test substances were added in rising concentrations. The known ADRB3 ligands carazolol, pindolol and propranolol were applied in concentrations ranging from 0.1 nM to 1 µM. Highly concentrated standards of the MCHR1 ligands SNAP-7941 and FE@SNAP were prepared and used 1:100 in final assay volume: tested final concentrations were 10-50 µM (SNAP-7941) and 10-100 µM (FE@SNAP).

Total binding was determined using 5 µL respective solvent. The determination of non-specific binding was carried out in presence of 10 µM ADRB3 ligand (carazolol or propranolol). In total, 36 samples were possible to be processed at the same time using the 36-well harvester.

After the pipetting step, each tube was swiftly closed, shortly vortexed and the mixture was incubated at 27°C using a water bath for 90 min in order to allow the binding to achieve equilibrium. In the meantime, Whatman GF/B Filter Paper were presoaked in 0.05% PEI. Free and bound [^{3}H]-CGP-12177 was separated by filtration through the presoaked filter paper using Brandel® Harvester. The tubes were washed three times with wash buffer and filters were punched out into dedicated scintillation vials. 4 ml scintillation cocktail was added and the vials were shaken for 30 min. The radioactivity was determined using Hidex 300SL Beta Counter and expressed as counts per minute.

Table 4: Representative experimental setting for competitive binding experiments using filtration method (Exp. 3 with self-made membranes)

Position	Radioligand	Competitor	Final concentration of competitor	Membrane suspension	Buffer
1-3	50 µL	5 µL DMSO[1]		150 µL	295 µL
4-6	50 µL	5 µL ethanol[2]		150 µL	295 µL
7-9	50 µL	5 µL carazolol[3]	10 µM	150 µL	295 µL
10-12	50 µL	5 µL carazolol	1.5 nM	150 µL	295 µL
13-15	50 µL	5 µL carazolol	2.5 nM	150 µL	295 µL
16-18	50 µL	5 µL carazolol	5 nM	150 µL	295 µL
19-21	50 µL	5 µL SNAP-7941	10 µM	150 µL	295 µL
22-24	50 µL	5 µL SNAP-7941	15 µM	150 µL	295 µL
25-27	50 µL	5 µL SNAP-7941	50 µM	150 µL	295 µL
28-30	50 µL	5 µL FE@SNAP	10 µM	150 µL	295 µL
31-33	50 µL	5 µL FE@SNAP	50 µM	150 µL	295 µL
34-36	50 µL	5 µL FE@SNAP	100 µM	150 µL	295 µL

Experiment was performed in 500 µL total volume per test tube, always in triplicate and using 36 tubes per experiment. Single tube was filled with 50 µL [^{3}H]-CGP-12177 diluted to achieve 5 nM in final volume, 150 µL of membrane suspension, 295 µL of assay buffer as well as 5 µL of different competitors used in final concentration mentioned in the table. For more details see section 4.4.4.

[1,2] Total binding was determined using 5 µL of the respective solvent as vehicle control. For carazolol, DMSO was the solvent[1], SNAP-7941 and FE@SNAP were solved using ethanol[2].

[3] The non-specific binding was determined using 10 µM ADRB3 agonist carazolol.

4.4.5 Data analysis

The data are expressed as mean ± SEM from at least three independent experiments performed in triplicates. The analysis was conducted using GraphPad Prism (GraphPad Software, San Diego, USA). On the x-axis, the logarithmic concentrations of the competitors are depicted, on the y-axis the measured radioactivity expressed as counts per minute (cpm) of the bound radioligand.

The half-maximum inhibitory constant IC_{50} as well as the competitive binding curve were obtained after the concentrations of the test compounds were transformed to logarithmic scales ("Analyze" → "Transform of" → "x=log X") under "Analyze" → "Non linear regression (curve fit)" → "log(inhibitor) vs response – variable slope". The inhibition constant K_i was calculated from IC_{50} values using Cheng-Prusoff equation (55).

4.5 CHO-K1-ADRB3 and CHO-K1 cell line

4.5.1 Cell culture

4.5.1.1 Thawing of cells

CHO K1 cell line stably expressing hADRB3 (CHO-K1-ADRB3) (Product No: ES-035-CV, PerkinElmer®, Waltham, USA) (65) and parental CHO-K1 cells, a generous gift from Professor Karl-Norbert Klotz (University of Würzberg, Germany), were stored at -80°C.

Frozen cells were quickly thawed and added to 9 mL medium (F-12 Nut Mix (Ham) (1X), gibco®, Grand Island, USA). Cells were centrifuged (1200 rpm, 4 min, Hettich® ROTANTA TRC centrifuge) and after supernatant was discarded, resuspended in 1 mL of fresh medium. 75 cm^2 cell culture flask was filled with 13 mL medium and cell suspension was added. Cells were incubated as described in section 4.5.1.2. The next day, medium was changed to get rid of residual DMSO. After reaching at least 80% confluence, cells were split for the first time.

4.5.1.2 Splitting of cells

The CHO-K1 cells were grown in the F-12 Nut Mix (Ham) medium containing 10% FBS, 1% Pen Strep, 2 mM L-glutamine. The medium for CHO-K1-ADRB3 cell line was supplemented instead of 1% Pen Strep with 0.4 mg/mL Geneticin®. Cells were cultured in humidified atmosphere containing 5% CO_2 at 37°C (CO_2-Incubator C200, Labotect GmbH). Cell growth and confluency were examined using Olympus CK2 Inverted Microscope.

Every two to four days (after reaching about 80% confluence), the adherent cells were split. The old medium was removed, cells were washed with DPBS and incubated with trypsin for about 4 min at 37°C. After cells have detached, medium was added (at least the amount of trypsin) and cell suspension was centrifuged (1200 rpm, 4 min, Hettich® ROTANTA TRC centrifuge). Supernatant was discarded, cells resuspended in 1 mL fresh medium and split in the desired ratio to the new labelled flask/flasks (filled with appropriate amount of the new medium with all necessary additives).

4.5.2 Real-time assays conducted with CHO-K1-ADRB3 and CHO-K1 cell line

The real-time binding experiments (LigandTracer® experiments) were performed using the LigandTracer® Technology (Ridgeview Instruments AB, Uppsala, Sweden) according to the manufacturer with small deviations (61, 71). This semi-automated method measures the interaction

of radiolabelled ligands with cell surface receptors or targets inside the cell. Experiments were conducted on adherent CHO-K1 cells expressing the hADRB3 and CHO-K1 cells as a reference.

4.5.2.1 Cell dish preparation

Cells were seeded onto one side of a cell culture dish, while this was tilted. 250 000 cells (in 3 mL medium) were seeded two days prior the experiment. The cells were allowed to attach only on to this one side of the cell dish (target area) and replicate, while they were in incubator for about 24 hours in tilted position. Afterwards, medium was changed and cells were incubated for one more day, this time in horizontal position with 10 mL medium, since they were already attached.

LigandTracer® experiment was performed two days after seeding of the cells. Cell culture medium was changed in the corresponding cell culture dish to supplement-free medium (3 mL new medium) just before the experiment (Figure 17). This is important especially because of FBS that may interact with radioligand.

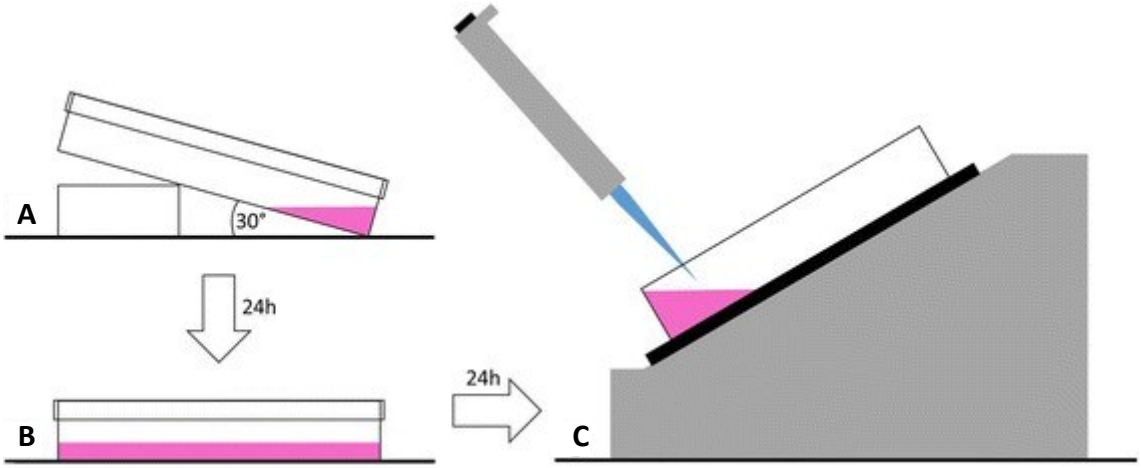

Figure 17: Schematic illustration of the cell dish preparation
250 000 CHO-K1-ADRB3 or CHO-K1 cells were seeded onto one side of a tilted cell culture dish and incubated in 3 mL of medium for about one day (**A**). On the next day, cell dish was changed into a horizontal position and the cells were cultured with 10 mL of fresh medium for additional day (**B**). On the third day, binding experiment was performed in 3 mL of fresh medium with no additives (**C**) (adapted from (72)).

4.5.2.2 Assay procedure

At the beginning of every LigandTracer® experiment, background measurement was performed for at least 5 min to make sure there are no interfering substances nearby as well as to ensure a stable

system. The cell dish was afterwards placed on an inclined support of the LigandTracer® instrument and radioligand was added.

For experiments using LigandTracer® Technology with CHO-K1-ADRB3 and CHO-K1 cell lines, highly affine [^{125}I]CYP was used. Couple of experiments were also conducted with CHO-K1-ADRB3 cell line and radiolabelled MCHR1 ligands, [^{11}C]SNAP-7941 and [^{18}F]FE@SNAP.

Different instrumentation was used depending on the label. LigandTracer® experiments with [^{125}I]CYP were performed using LigandTracer® Grey, a dedicated instrument for low energy gamma radiation. The experiments using [^{11}C]SNAP-7941, [^{18}F]FE@SNAP as well as [^{18}F]FDG were conducted using LigandTracer® Yellow, a scintillator-based solid state gamma-ray detector for PET or single photon emission computed tomography (SPECT) markers and LigandTracer® White with solid state electron/positron detector for beta emitters.

4.5.2.3 CHO-K1-ARBD3 and CHO-K1 cells with [^{125}I]CYP as radioligand

According to the Technical Data Sheet from PerkinElmer® for human adrenergic β_3 cell line used, the dissociation constant of [^{125}I]CYP for this cell line is K_d = 3,9 nM (65). Two types of experiments were performed using CHO-K1 and CHO-K1-ADRB3 cells and [^{125}I]CYP as radioligand: real-time kinetic association (and dissociation) experiments (designated as “kinetic measurements” in this thesis) and real-time kinetic competitive measurements (refered to “competitive experiments” in the following text). CHO-K1 cells were used as a negative reference, since there is no specific binding of [^{125}I]CYP to these cells.

4.5.2.3.1 Kinetic real-time binding experiments

Binding kinetics of [^{125}I]CYP to the seeded cells was examined using different concentrations of the mentioned radioligand (144 – 944 pM) either in a single step (145 – 581 pM) or two consecutive steps with increasing radioligand concentrations (194 – 315 pM for the first step, 387 – 629 pM for the next step). After the end of the association phase, as soon as an equilibrium was visually achieved (45 – 60 min), the medium was replaced with a fresh one and the dissociation of [^{125}I]CYP from the dedicated cells was observed until a new equilibrium was established.

4.5.2.3.2 Competitive real-time binding experiments

After the baseline measurement, [^{125}I]CYP was added. The competing substance was introduced following the radioligand either in one step or in two or three consecutive steps with increasing concentrations of the competitor. In the initial experiments, the competitor was introduced first after the equilibrium (signal plateau) was achieved (55 – 77 min after [^{125}I]CYP (145 or 194 pM)) in different concentrations. ADRB3 ligands carazolol, pindolol and propranolol were added in concentrations ranging from 0.1 nM to 3 µM, test compounds SNAP-7941 and FE@SNAP from 1 nM to 100 µM.

The competitor was added at different time points after radiotracer (10, 15, 30, 40, 50, 60 min after [^{125}I]CYP or simultaneously with [^{125}I]CYP (290, 581 or 629 pM)).

Vehicle control was performed using the same amount of the respective solvents, which were used for solving the competitors in a similar experimental setting. SNAP-7941 and FE@SNAP were solved using ethanol, DMSO was the solvent for carazolol, pindolol and propranolol. For more details regarding solving and diluting of test compounds see section 4.3.

4.5.2.4 CHO-K1-ADRB3 with [^{11}C]SNAP-7941 as radioligand

[^{11}C]SNAP-7941 was prepared by Cécile Philippe in a fully automated synthesizer (TRACERlab™ FX C Pro, GE Healthcare, Uppsala, Sweden) (11).

The molar activity of the produced radiotracer varies. Furthermore, as already mentioned, the half-life of radionuclides fluorine-18 and especially carbon-11 is very short. This means that the activity per quantity of the radiotracer may differ.

Two types of binding studies were conducted on CHO-K1-ADRB3 cells using [^{11}C]SNAP-7941. First, binding kinetics of [^{11}C]SNAP-7941 to CHO-K1 cells stably expressing hADRB3 was examined. [^{11}C]SNAP-7941 (8 nM, 65 kBq or 300 nM, 53 kBq depending on the molar activity) was added into the cell dish. After 42 min, medium was removed and fresh one was added to observe the dissociation of the radiolabelled tracer from CHO-K1-ADRB3 cells.

Secondly, the effect of two ADRB3 agonists, CL 316243 and carazolol, on [^{11}C]SNAP-7941 accumulation was examined, with both substances in a final concentration of 2 µM. The tested substances were added 30 min after [^{11}C]SNAP-7941 (231 nM, 42 kBq or 300 nM, 55 kBq) after the binding equilibrium was reached.

4.5.2.5 CHO-K1-ADRB3 with [^{18}F]FE@SNAP as radioligand

Radiosynthesis of [^{18}F]FE@SNAP was performed by Cécile Philippe using a microfluidic device (Advion NanoTek®, Ithaca, USA) with purification performed on a conventional synthesizer unit (Nuclear Interface®, GE Medical Systems, Uppsala, Sweden) (18).

Competition real-time cell-binding studies were performed by adding [^{18}F]FE@SNAP in two consecutive steps (first concentration added 104 pM, 19 – 48 kBq, second concentration 375 pM, 39 kBq or 625 pM, 73 kBq) or using one single concentration (625 pM, 73 kBq). 15 to 37 min after the addition of the second portion of radioligand, when a binding equilibrium was reached, the competing substance was introduced. 2 µM carazolol, 2 µM CL 316243 or the solvent for carazolol, DMSO, was added. CL 316243 was solved using bi-distilled water and no vehicle control was therefore necessary. For every substance, two independent experiments were performed.

4.5.2.6 Data analysis

The binding curves obtained using LigandTracer® Technology were not further subject to quantitative analysis, the data were only qualitatively analysed and the representative real-time binding curves will be discussed. The curves were processed using TraceDrawer™ (Ridgeview Instruments AB, Uppsala, Sweden). For better comparison, overlays of binding curves generated in similar experimental settings were created using TraceDrawer™ Software.

4.6 Brown adipocytes

Murine brown preadipocytes, kindly donated by the Department of Medicine III, Clinical Division of Endocrinology and Metabolism of Medical University of Vienna (Vienna, Austria) were cultured and differentiated according to Kiefer *et al.* (34). MCHR1 ligands were evaluated on the mature brown adipocytes.

4.6.1 Cell culture

Frozen fibroblast-like preadipocytes were thawed and split in the same way as described in section 4.5.1. For growth of preadipocytes Dulbecco's modified eagle medium (DMEM (1X), No: 41965-039, gibco®, Paisley, UK) (high glucose DMEM) was used. DMEM was supplemented with 10% FBS, 1% pyruvate and 1% Pen Strep and used as maintenance medium (Table 5).

4.6.1.1 Induction and post differentiation

Preadipocytes were seeded into suitable containers (6-well plates or cell dishes). Cells were grown to confluence in the maintenance medium detailed above. After reaching confluence, or the day after, the medium was changed for induction medium.

The induction medium consisted of the maintenance medium supplemented with 10 mg/mL insulin (human recombinant), 1 nM T_3, 0.5 mM IBMX, 125 nM indomethacin and 1 µM dexamethasone (Table 5).

Cells were cultured in the induction medium for 48 h, afterwards, it was replaced with the post differentiation medium. The post differentiation medium consisted of the maintenance medium supplemented with 10 mg/mL insulin and 1 nM T_3. Cells were incubated for 4 to 6 days until the characteristics of brown adipocytes were clearly visible. For the composition of the three media used for differentiation of adipocytes see Table 5.

Table 5: Cell culture media for differentiation of brown adipocytes

	Maintenance medium	**Induction medium**	**Post differentiation medium**
Use	For culturing of preadipocytes, until they reach confluence	After reaching confluence, 48 h induction	After induction medium, 4 to 6 d post differentiation
Medium	DMEM high glucose	DMEM high glucose	DMEM high glucose
Serum	10% FBS	10% FBS	10% FBS
Antibiotics	1% Pen Strep	1% Pen Strep	1% Pen Strep
Supplements	1% pyruvate	1% pyruvate	1% pyruvate
		10 mg/mL insulin	10 mg/mL insulin
		1 nM T_3	1 nM T_3
		0.5 mM IBMX	
		125 nM indomethacin	
		1 µM dexamethasone	

The use and composition of three media used for differentiation of fibroblast-like murine preadipocytes into brown adipocytes. For more details regarding the use or different components, see text section 4.6.1.

Both, the induction as well as post differentiation media, were used for two weeks. The mixed aliquots were filtered through a sterile filter under the Laminar-Flow Hood and stored at -20°C until further use.

The cells were documented during the differentiation process. Images of non-stained cells in cell dishes were made using the camera from smartphone Samsung S3 Neo and Olympus CK2 Inverted Microscope.

4.6.2 Oil Red O staining of differentiated murine brown adipocytes

The differentiated brown adipocytes were stained using Oil Red O stain according to the working protocol from Lonza (73) with minor deviations. Preadipocytes were seeded into a 6-well plate and differentiated into mature brown adipocytes as described above. At the 7th day of post differentiation, cells were stained.

A 10% solution of formalin was prepared in advance by diluting 37% formaldehyde solution with bi-distilled water. 60% isopropanol was made as a dilution from 2-propanol with bi-distilled water. All procedures involving formalin were performed under the Captair® Chem Fume Hood.

The 6-well plate with differentiated brown adipocytes was removed from the incubator and the medium was aspired. Wells were thereafter washed using DPBS. Cells were fixed using 1 mL of 10% formalin per well for 45 min at room temperature.

Oil Red O stock solution was prepared by diluting 375 mg of the Oil Red O powder in 100 mL of 99% 2-propanol. 15 mL of the Oil Red O stock solution was mixed with 10 mL of bi-distilled water and allowed to sit for 10 min at room temperature. This working solution was filtered before usage.

Formalin was carefully removed from the wells and cells were washed with tap water. 1 mL of 60% isopropanol was added to each well for 5 min. This was replaced with 1 mL Oil Red O working solution. Incubation took place for 5 or 15 min.

The wells were washed with tap water again until the water was clear (4 times). Stained cells were kept in 1 mL tap water while being examined under the microscope or cells were subjected to haematoxylin counterstaining. To this, undiluted or 1:7 diluted haematoxylin in H_2O was added for 3 min.

The cells were thoroughly washed with tap water and clean tap water was left in the wells. Images were recorded on an inverted microscope Axio Observer in the Department of Pathophysiology and

Allergy Research of Medical University of Vienna (Vienna, Austria), using a 20- or 40-fold magnification.

4.6.3 Real-time assays with preadipocytes and differentiated brown adipocytes

LigandTracer® experiments were conducted on differentiated murine brown adipocytes (after 6 days in post differentiation medium) and with undifferentiated preadipocytes. [^{11}C]SNAP-7941 and [^{18}F]FDG were employed as radioligands. The method is described in detail in section 4.5.2. The cell dish was tilted during the whole process of differentiation of the preadipocytes.

4.6.3.1 LigandTracer® experiments with [^{18}F]FDG as radioligand

Before starting the experiment, the post differentiation medium (differentiated cells) or growth medium (preadipocytes) was changed to DMEM without glucose (No: 11966-025, gibco®, Paisley, UK) and any further additives. The cells were starved for 1 h 12 min ± 3 min before starting the LigandTracer® experiment. After placing the cell dish into the instrument, the PET tracer was added (161 ± 2.9 kBq [^{18}F]FDG). The uptake of [^{18}F]FDG was also studied in the absence or presence of the ADRB3 agonist CL 316243, β-blocker propranolol or MCHR1 ligand SNAP-7941.

4.6.3.2 LigandTracer® experiments with [^{11}C]SNAP-7941 as radioligand

One kinetic and several competitive real-time binding experiments were conducted on differentiated brown adipocytes with [^{11}C]SNAP-7941 as radioligand. Here, post differentiation medium was changed against high glucose DMEM (No: 41965-039, gibco®, Paisley, UK) without any further additives. In contrast to the experiments with [^{18}F]FDG, cells did not need to be starved.

After the background measurement, the cell dish was placed onto the inclined support of the instrument and [^{11}C]SNAP-7941 was added (72 ± 8.6 kBq (114 ± 66.2 nM)). For the kinetic experiment, 1 nM [^{11}C]SNAP-7941 (50 kBq) was added and after the binding equilibrium was reached (46 min), the medium containing radioligand was changed to fresh one.

For the competitive binding experiments, the competing substances were added after binding equilibrium was reached (42 ± 2 min). The effect of β-blocker propranolol (2 µM), ADRB3 agonists CL 316243 and carazolol (2 µM) and MCHR1 ligands MCH (1.3 or 10 µM) and SNAP-7941 (20 or 40 µM) on binding or uptake of [^{11}C]SNAP-7941 by brown adipocytes was tested.

4.6.3.3 Data analysis

The data were analysed as detailed above in section 4.5.2.6.

4.6.4 Well plate radioligand assays with differentiated brown adipocytes

Radioligand binding assays with differentiated murine adipocytes were performed in 6-well plates with [^{18}F]FDG and [^{11}C]SNAP-7941 as radioligands.

4.6.4.1 Well plate assays with [^{18}F]FDG as radioligand

Uptake of fluorine-18 labelled 2-deoxy-glucose was measured with adherent differentiated brown adipocytes and influence of different substances was assessed in triplicate. The effects of CL 316243, ADRB3 agonist known to stimulate the glucose uptake in brown adipocytes (37, 38), β-blocker propranolol and both MCHR1 ligands, SNAP-7941 and FE@SNAP, were evaluated.

Cells were starved with supplement-free DMEM without glucose (No: 11966-025, gibco®, Paisley, UK) for 1 h 12 min ± 1 min. The test substances (or dedicated solvents – baseline) were added during this starving period. The pre-blocking was carried out for 39 ± 1 min with 20 µM SNAP-7941 and FE@SNAP and with 2 µM CL 316243 and propranolol. [^{18}F]FDG was diluted in tap water and added to the cells (50.9 ± 0.65 kBq) and incubated for 38 ± 1 min. All incubation steps were carried out in humidified atmosphere containing 5% CO_2 at 37°C.

After incubation, three fractions were collected from each well into Eppendorf tubes and the radioactivity was measured. First, the supernatant was removed (1. fraction – supernatant). The cells were then washed with 1 mL ice-cold DPBS (2. fraction – wash) and incubated with 0.5 mL trypsin for 5 min at 37°C. The reaction was stopped by addition of 0.5 mL of the supplement-free DMEM without glucose and the cell suspension was removed (3. fraction – cells).

The Eppendorf tubes containing the different radioactive fractions were measured using 2480 WIZARD^2 Gamma Counter.

4.6.4.2 Well-plate assays with [^{11}C]SNAP-7941 as radioligand

The well plate experiments using the MCHR1 PET tracer [^{11}C]SNAP-7941 were performed as those using the radiolabelled glucose analogue described in detail in section 4.6.4.1 with minor adaptions:

In contrast to the experiments using [^{18}F]FDG, no starving was necessary. The medium was changed prior to the beginning of an experiment to unsupplemented DMEM with high glucose content (No: 41965-039, gibco®, Paisley, UK). The test substance (2 or 20 µM SNAP-7941, 2 µM CL 316243, 2 µM propranolol) was added and incubated with brown adipocytes for 43 ± 4 min. [^{11}C]SNAP-7941 was diluted using DPBS and 2.7 ± 0.70 nM (49.8 ± 0.91 kBq) were added to each well and incubation was carried out for 32 ± 1 min.

4.6.4.3 Data analysis

The counts per minute obtained from Gamma Counter measurements were manually ([^{18}F]FDG) or automatically ([^{11}C]SNAP-7941) corrected for decay. The mean cpm was calculated from the triplicate of the cell fractions of the baseline (dedicated solvent instead of tested substance) (100% binding/well). Percentage of radioligand binding to cells was calculated referring to baseline. GraphPad Prism (GraphPad Software, San Diego, USA) was used to generate graphs with the y-axis expressed in % binding/uptake per well and to determine mean, standard deviation, standard error of the mean as well as p-value. $p < 0.05$ have been considered significant. Values are expressed in % binding/well ± SEM from at least two individual experiments performed in triplicates.

5. Results and Discussion

5.1 Competitive binding studies with membranes using filtration method

Competitive binding studies were conducted on CHO-K1 cell membranes stably expressing human β_3-adrenergic receptor. For the experiments, one concentration of radioligand [^{3}H]-CGP-12177 and various concentrations of test compounds were used. The assay was established using cell membrane preparations purchased from PerkinElmer® (Waltham, USA) and the well-described ADRB3 ligands carazolol, pindolol and propranolol. The obtained inhibition constants were subsequently compared with published K_i-values.

Since low total binding was observed with commercial membranes, cell membranes were prepared in-house from cultured CHO-K1-ADRB3 cells and used for further experiments. Determination of the affinity of MCHR1 ligands SNAP-7941 and FE@SNAP was conducted in parallel with the ADRB3 agonist carazolol as standard.

Low affinity of the two MCHR1 ligands to ADRB3 was found, whereas SNAP-7941 is distinctly more affine (K_i = 14.5 ± 0.3 µM, n=3) than FE@SNAP (K_i = 65.1 ± 2.9 µM, n=3). Table 6 comprises the obtained K_i-values as well as the comparison with values reported in literature.

The value for carazolol was not significantly different when self-made membranes were used (2.0 ± 0.3 nM, n=3) compared to commercially available ones (2.3 ± 0.4 nM, n=3) as well as when compared with the K_i-value published by Méjean *et al.* (2 ± 0.2 nM) (49). The experiments with commercially available membranes resulted in a K_i-value for pindolol of 44.5 ± 11.8 nM (n=4), which corresponds to the value from Hoffman *et al.* (K_i = 44.1 nM (CI: 30.9-63.0 nM)) (45), but is distinct from the affinity value obtained by Emorine *et al.* (K_i = 11 ± 2 nM) (39). However, this is still in the same affinity range. The obtained K_i of propranolol (67.4 ± 14.4 nM, n=3) was lower than that reported by Hoffman *et al.* (186 nM (CI: 134-259nM)) (45) or by Blin *et al.* (145 ± 8 nM) (46).

Different K_i-values may be the result of different experimental settings. The working groups of Méjean *et al.*, Emorine *et al.* and Blin *et al.* conducted whole cell binding studies with CHO-K1 cells transfected with ADRB3 (39, 46, 49). Whereas, Hoffman *et al.* performed the experiments with cell membranes in presence of 100 µM guanosine triphosphate (GTP) (45). All mentioned publications were performed with [^{125}I]CYP as radioligand (39, 45, 46, 49) in contrast to the experiments performed within this thesis where [^{3}H]-CGP-12177 was used as radioligand (with membranes and in absence of GTP).

Table 6: Inhibition constants (K_i-values) obtained by competitive binding assay using filtration method and comparison with literature

Test compound	K_i using commercial membranes	K_i using self-prepared membranes	K_i from literature	Reference
Carazolol	2.3 ± 0.4 nM (n=3)	2.0 ± 0.3 nM (n=3)	2 ± 0.2 nM	(49)
Pindolol	44.5 ± 11.8 nM (n=4)		44.1 nM (CI: 30.9-63.0) 11 ± 2 nM	(45) (39)
Propranolol	67.4 ± 14.4 nM (n=3)		186 nM (CI: 134-259) 145 ± 8 nM	(45) (46)
SNAP-7941	> 19 µM (n=3)	**14.5 ± 0.3 µM** (n=3)		
FE@SNAP	> 25 µM (n=2)	**65.1 ± 2.9 µM** (n=3)		

Competitive binding studies using filtration method were conducted with CHO-K1 cell membranes expressing ADRB3 with [^{3}H]-CGP-12177. Radioligand in one and competitors in various concentrations were used. For more details regarding the competitive binding assay see section 4.4. Experiments were performed using commercially available membranes or self-prepared membranes from CHO-K1-ADRB3 cell line.
n is the number of independent experiments performed in triplicates.
CI is 95% confidence interval.
All K_i-values represent the mean ± SEM except for values by Hoffman *et al.* (45) where CI is in brackets.

These discrepancies are of interest because in intact cells, compared to cell membranes, endogenous GTP is always present. The complex of GPCR and G protein will dissociate in presence of GTP thereby leaving the receptor in a low affinity state. In membrane preparations GTP is absent and G protein is unable to dissociate from GPCR. GPCR therefore exists also in high affinity (G protein-bound) state. Whole cell-binding studies and studies with membranes in presence of GTP would therefore be expected to yield affinities similar to low affinity state only (50, 74). This may partly explain the differences observed between the obtained K_i for propranolol and the values from literature (45, 46). Another minor limitation is the fact, that the K_d-value of [^{3}H]-CGP-12177 used for the calculation of K_i-values was also determined in whole cell-binding studies (50). Furthermore, K_i-values, obtained from experiments using commercially available membranes, varied significantly due to low reproducibility, evident from rather high standard error of mean (Table 6).

Representative competitive binding curves of carazolol, pindolol and propranolol from experiments using commercially available CHO-K1 cell membranes expressing ADRB3 are shown in Figure 18.

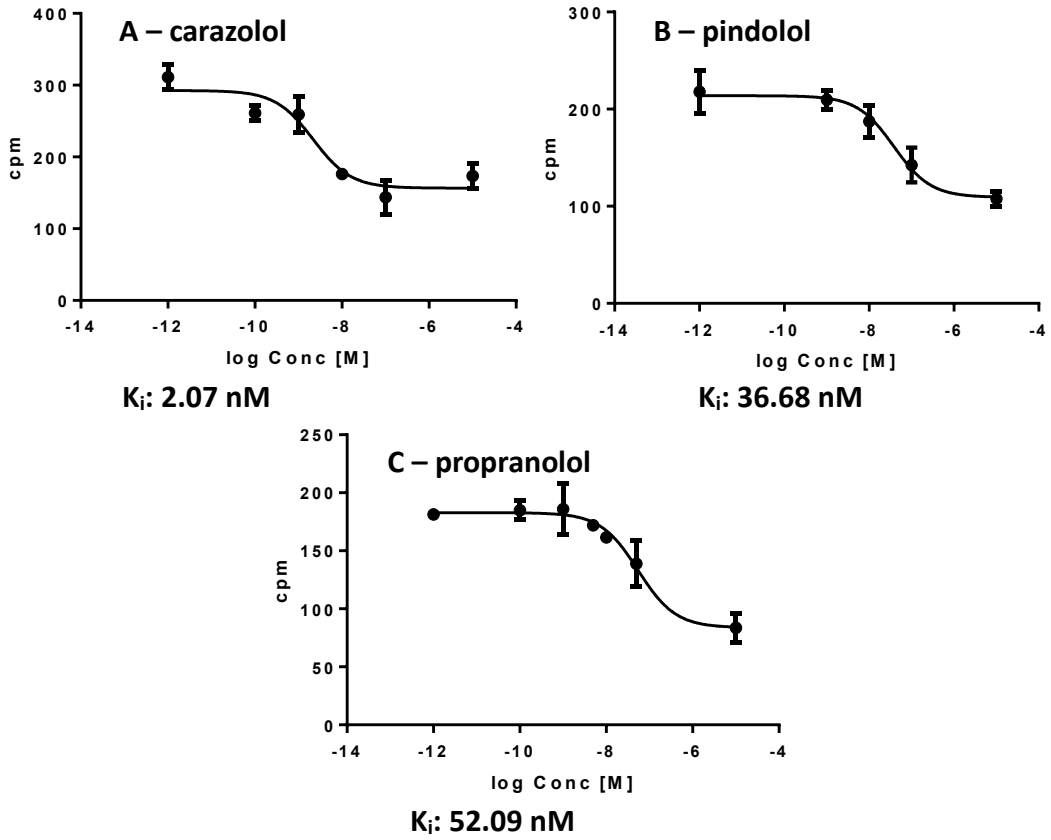

Figure 18: Representative competitive binding curves of carazolol, pindolol and propranolol when using commercially available membranes

Competitive binding studies using filtration method were conducted with CHO-K1 cell membranes expressing hADRB3 and with [^{3}H]-CGP-12177. Radioligand was used in one concentration, competitors were applied in several concentrations. For more detailed description of the assay see section 4.4. The depicted binding curves are representative curves from different experiments using commercially available membranes. Competitive binding curves with carazolol (**A**), pindolol (**B**) and propranolol (**C**) and the corresponding inhibition constants obtained in the respective experiment are shown.

Figure 19 depicts binding curves and K_i-values of carazolol, SNAP-7941 and FE@SNAP obtained from competitive experiments using the self-prepared membranes. The detailed experimental setting from this experiment is described in Table 4 (section 4.4.4).

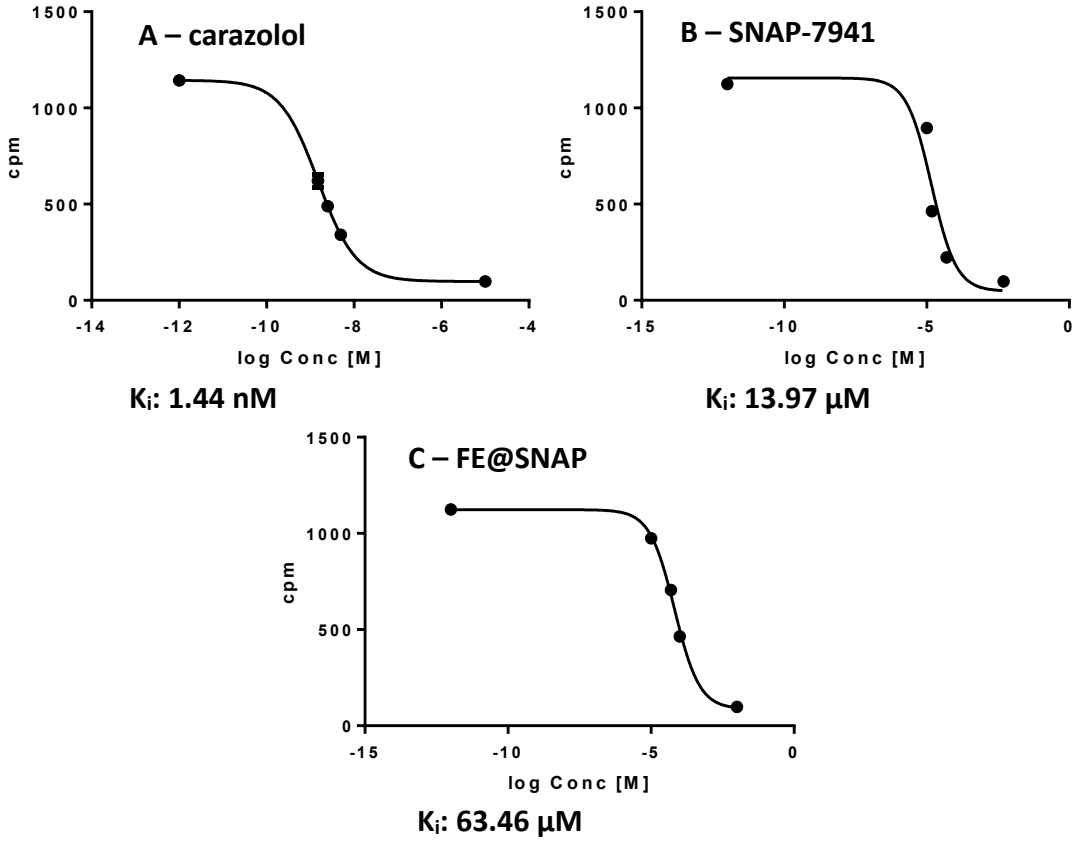

Figure 19: Representative competitive binding curves of carazolol, SNAP-7941 and FE@SNAP when using self-made membranes

Competitive binding studies were conducted as described in legend of Figure 18 and more detailed in section 4.4. The depicted binding curves are from Exp. 3 with self-made membranes. Experimental setting from the very same experiment is in detail in Table 4. Competitive binding curves with carazolol (**A**), SNAP-7941 (**B**) and FE@SNAP (**C**) and their corresponding K_i-values are shown.

5.2 Evaluation of self-prepared membranes

Cell membranes were produced from CHO-K1 cell line expressing hADRB3, since protein expression of the commercial membranes was insufficient. The commercially available membranes were used in a concentration of 2 µg protein per tube. In one experiment, the concentration of commercially available membranes was doubled without effecting total binding. Thus, assay reproducibility as well as the price of the commercially available membranes were not favourable. In a preliminary experiment, self-prepared membranes were tested in the same protein amount (2 µg/tube), leading to higher total binding than with the commercially available membranes, while non-specific binding remained unaffected (data not shown). This suggests a higher expression rate of ADRB3 in the self-made membranes. Self-preparation of cell membranes yielded 1125 µL membrane suspension with protein concentration 655 ± 6.2 µg/mL. Aliquotation of membrane suspension was performed to achieve 6.8 µg protein per test tube.

Figure 20 shows comparison of two representative binding curves obtained from competitive binding studies using the filtration method with commercial membranes and with self-made membranes for the ADRB3 agonist carazolol and the MCHR1 ligand SNAP-7941. Both examples show obvious difference regarding the counts (cpm). The total radioligand binding was significantly higher using the self-made membranes, which was primarily due to higher protein concentration (6.4 µg vs 2 µg per test tube), while the non-specific binding remained unaffected. Furthermore, the obtained binding affinities were much better reproducible and the standard error smaller.

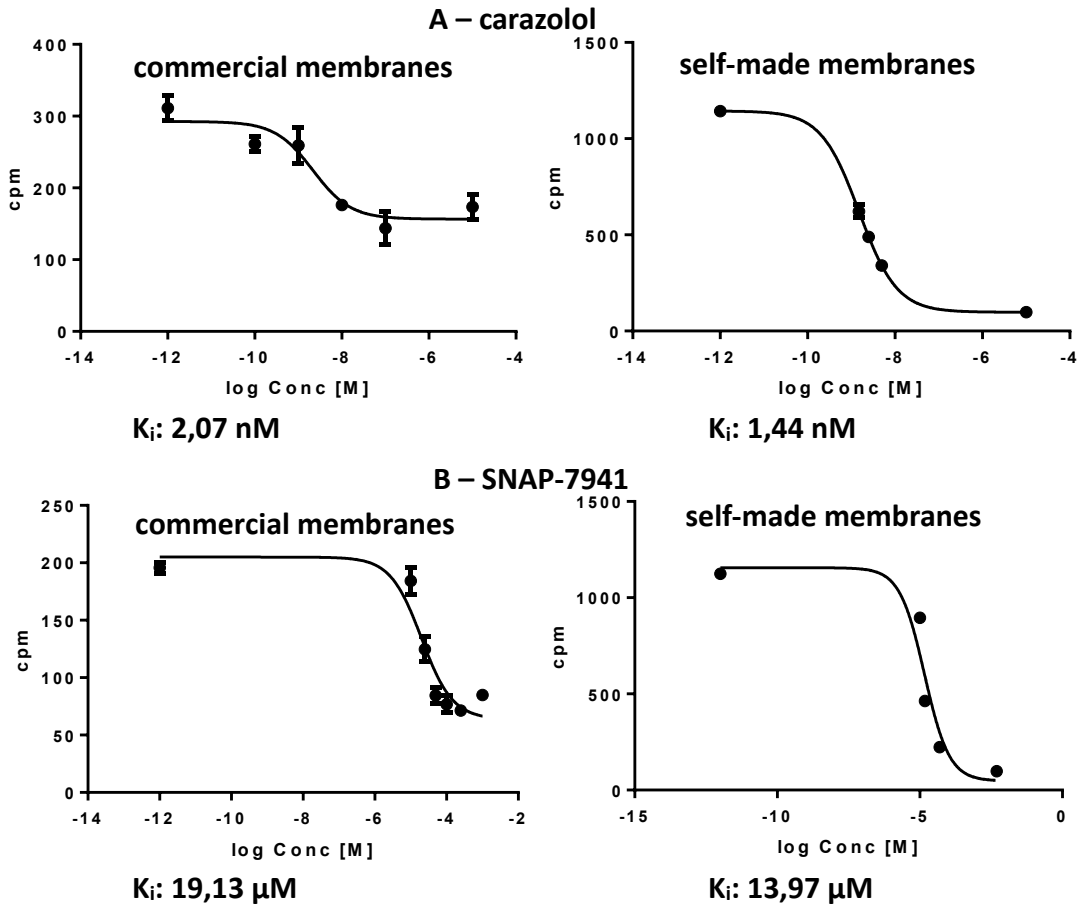

Figure 20: Comparison of representative competitive binding curves using commercially available or self-prepared membranes with carazolol or SNAP-7941 as competitor
Competition experiments were performed as described in legend to Figure 18 and more detailed in section 4.4. Competitive binding curves are depicted using carazolol (**A**) or SNAP-7941 (**B**) as competitor. Binding curves obtained using commercially available membranes are compared with those obtained using self-made ones. Corresponding K_i-values are mentioned.

5.3 Real-time assays using CHO-K1-ADRB3 and CHO-K1 cell line

Real-time binding studies were conducted on CHO-K1 cells stably expressing hADRB3 and CHO-K1 cell line (control) using LigandTracer® Technology. Two types of experiments were performed. First,

kinetic evaluation, where the radioligand was added (once or twice) and after reaching binding equilibrium, the medium was replaced with unsupplemented fresh one. It was therefore possible to examine in real-time the association as well as the dissociation of the radioligand from seeded cells. The second type was a competition assay, where the radioligand was added and after certain amount of time (either after achieving equilibrium or sooner), the test substance was introduced. It was possible to observe, if there is a competition between the radioligand and the non-labelled test substance for the receptor.

The studies on CHO-K1-ADRB3 and CHO-K1 cell line were performed with [^{125}I]CYP and the radiolabelled analogues of the MCHR1 ligands – [^{11}C]SNAP-7941 and [^{18}F]FE@SNAP.

In the following Figures, "Background" means measurement of the reference region of cell dish without cells and "Target-Background" the reference-subtracted signal. In the overlay view, different reference-subtracted binding curves are compared.

5.3.1 CHO-K1-ADRB3 and CHO-K1 cells with [^{125}I]CYP as radioligand

Kinetic evaluation of association and dissociation of [^{125}I]CYP on CHO-K1-ADRB3 cells is shown in Figure 21. Figure 21A shows the association of the radioligand (0.6 nM) on CHO-K1-ADRB3 cells and following dissociation after the medium was replaced with fresh one with the measurement of the background as comparison. The radioligand dissociation led to about 15% decrease in the signal. Due to this slow dissociation, it was decided to add the competing substance not only after the equilibrium has been reached, but also at various time points before, to allow a better competition.

Figure 21B shows the same binding curve as the one in Figure 21A, but depicted in comparison with the binding of [^{125}I]CYP to the reference cell line CHO-K1. Binding of the same amounts of [^{125}I]CYP to the seeded CHO-K1 cells is significantly lower than to the cells stably expressing ADRB3, as the reference cell line does not express the respective target.

Moreover, the association using two concentrations of the radioligand can be observed in Figure 21C. In order to more accurately analyse interaction dynamics and affinity, the manufacturer recommends using at least two ligand concentrations during one measurement (75). Interaction with CHO-K1-ADRB3 cells is also here compared to the interaction with reference cell line CHO-K1. Binding to cells not expressing the respective target is about 20% of the binding to cells expressing ADRB3 protein. This represents the non-specific binding and maybe diffusion (Figure 21).

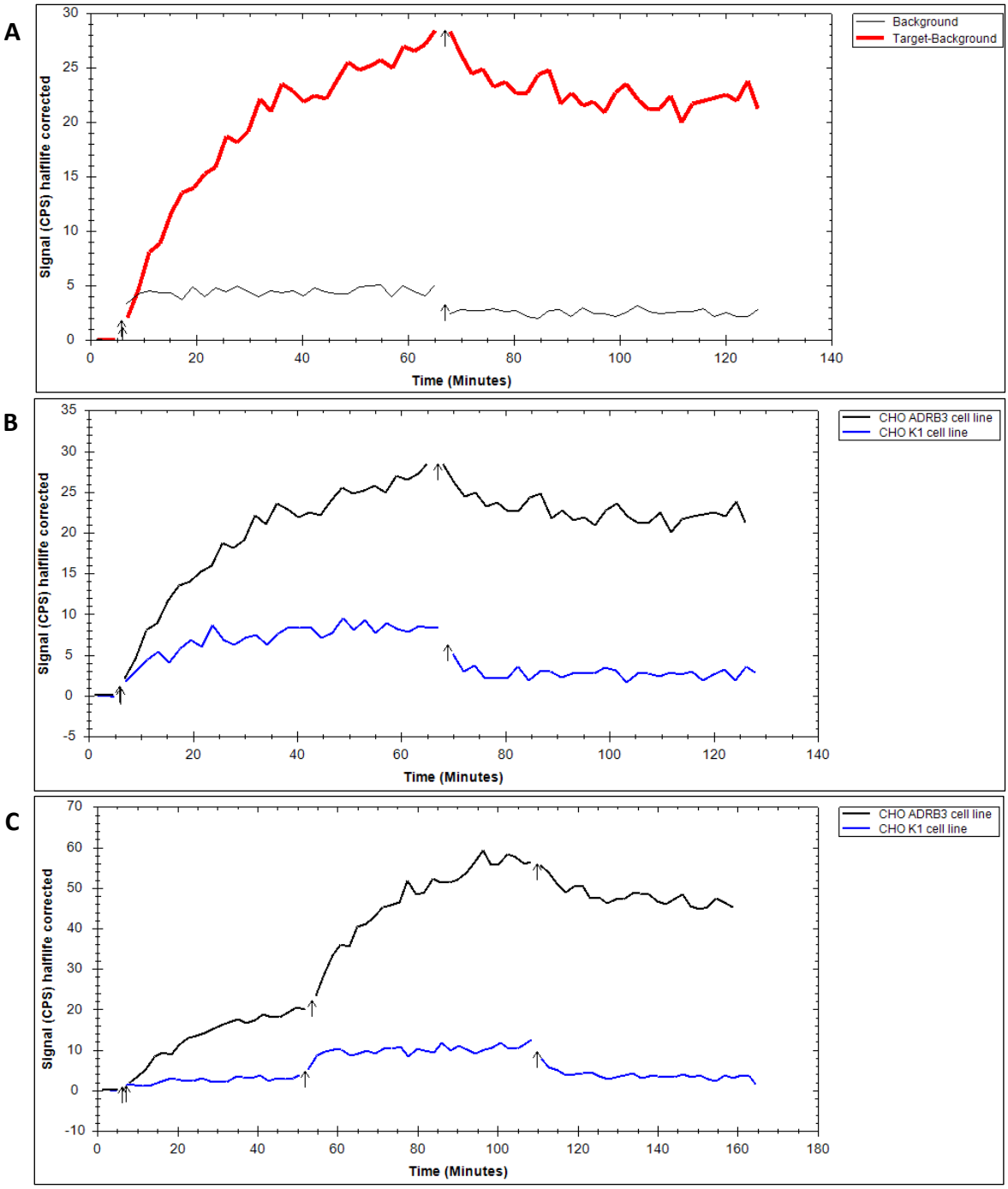

Figure 21: Representative binding curves of kinetic evaluation of [^{125}I]CYP on CHO-K1-ADRB3 and CHO-K1 cells Association of [^{125}I]CYP on CHO-K1-ADRB3 cells and the following dissociation after replacing medium with the fresh one. Arrows represent the interruption of LigandTracer® measurement, during which radioligand was added or medium was changed, respectively. **A**) Association of [^{125}I]CYP (0.6 nM, 62 kBq) on CHO-K1-ADRB3 cells and the following dissociation. Black line represents Background, the red line Target-Background. **B**) Comparison of association of [^{125}I]CYP (0.6 nM, 61.0 ± 0.7 kBq) on CHO-K1-ADRB3 cells (black line) and CHO-K1 cells (blue line) and the following dissociation after replacing medium with fresh one. **C**) Association of [^{125}I]CYP added in two consecutive steps (0.3 nM, 32.8 ± 0.4 kBq and after 45 min 0.6 nM, 66.1 ± 0.7 kBq) on CHO-K1-ADRB3 cells (black line) and CHO-K1 cells (blue line) and the following dissociation after replacing medium with the fresh one (57 min after addition of second batch of radioligand).

The effect of the known ADRB3 ligands (carazolol, pindolol, propranolol) as well as of MCHR1 ligands can be seen in Figure 22. The signal measured as counts per second was normalized in Figure 22 in order to allow better comparison. Signal height at the end of association phase was defined as 100%. This was 30 min after addition of the radioligand and as it can be seen in Figure 21A, the equilibrium is not reached at this time point. The time point was chosen because of the apparently poor dissociation of [^{125}I]CYP from CHO-K1-ADRB3 cells (Figure 21B, 21C), in order to allow a better competition. Therefore, if the test substance has no affinity to the hADRB3, the signal will be further increasing. If the substance is affine, further signal increase will be prevented and the signal may even start to decrease, since [^{125}I]CYP will be displaced.

In Figure 22A, the effect of the already known ADRB3 ligands in concentrations 15- to 50-fold their experimentally obtained K_i-values (Table 6) can be observed.

35 µM SNAP-7941 as well as 75 µM FE@SNAP caused a decrease of [^{125}I]CYP binding (Figure 22A). The kinetic of the displacement is similar to that of the known ADRB3 ligands. In Figure 22B, different concentrations of FE@SNAP show different effects on the normalized signal. We can observe that 1 µM FE@SNAP is insufficient to displace [^{125}I]CYP from the receptor on CHO-K1-ADRB3 cells and the signal further increases, although the competing substance was introduced. The increase in the signal after addition of 10 µM FE@SNAP is almost no more apparent; concentration of 25 µM hinders further rising of the signal completely; 35 µM FE@SNAP causes a slight decrease in the signal measured (Figure 22B). A very similar effect can be observed with SNAP-7941, although already 20 µM SNAP-7941 causes a slight decrease in the signal (Figure 22C).

The overlays depicted in Figure 22 provide additional strength to the K_i-values obtained with the previous method (Table 6). Test substances SNAP-7941 and FE@SNAP displace [^{125}I]CYP in concentrations that are in agreement with the obtained K_i-values.

A

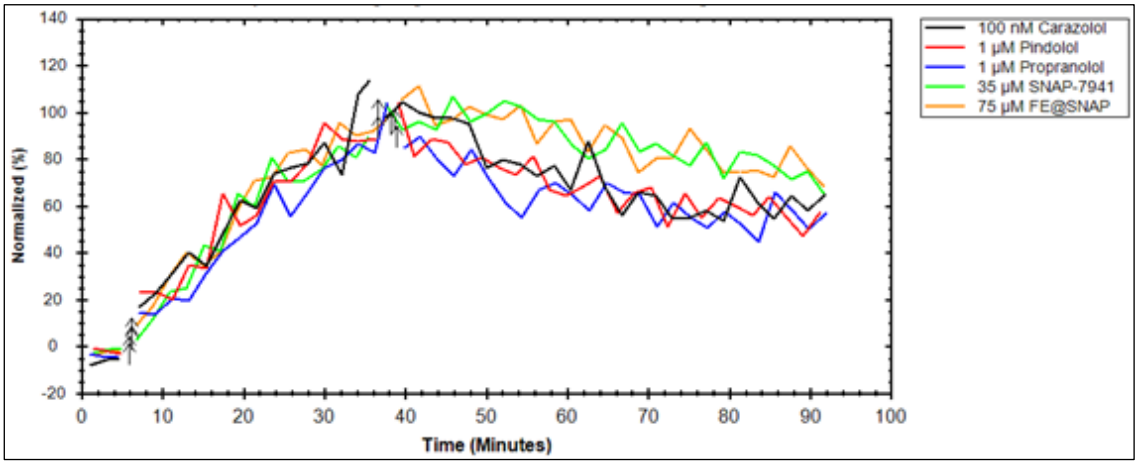

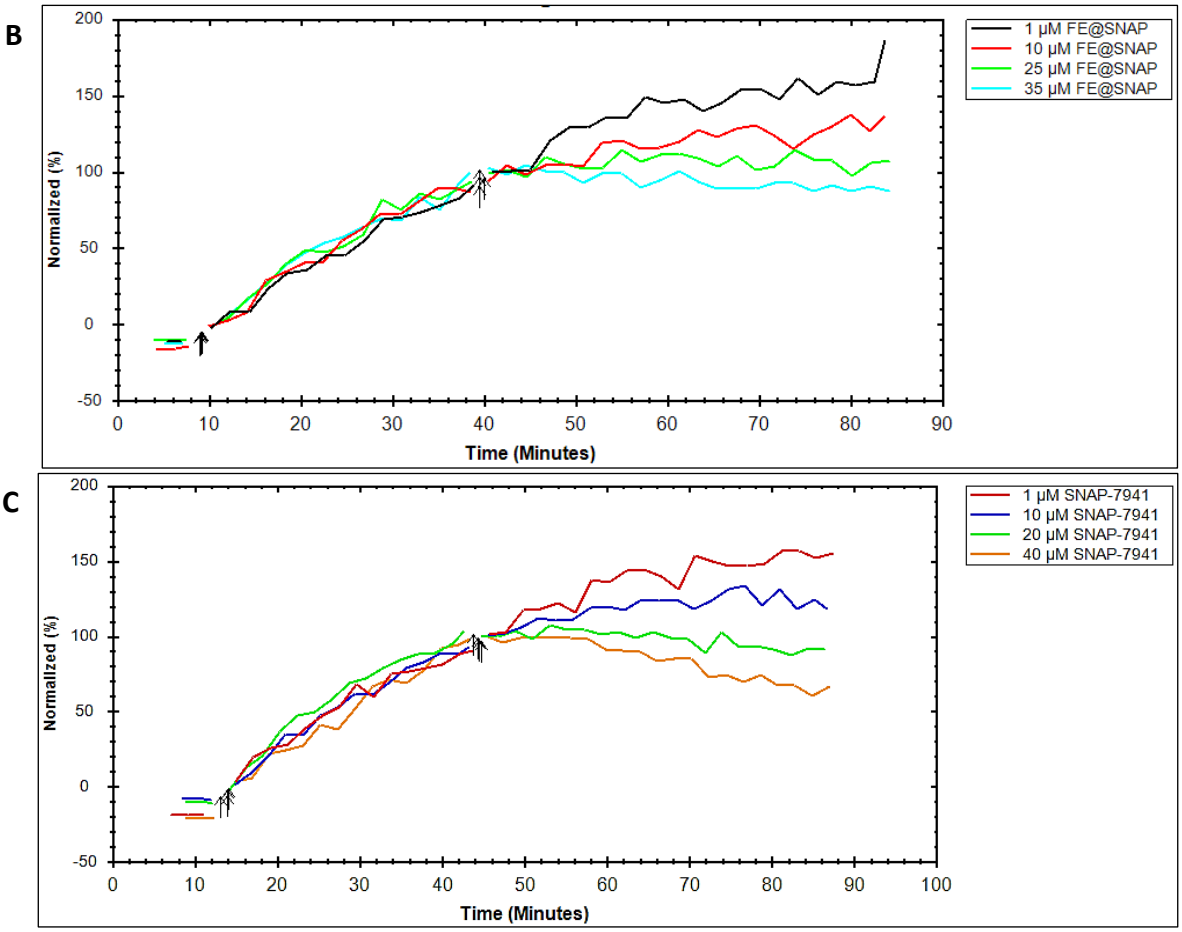

Figure 22: Overlays of competitive binding curves with competitors given 30 min after [^{125}I]CYP
For better comparison of the competitive curves, the signal in cps was normalized. As 100% was chosen signal height at the end of association phase, after 30 min, although equilibrium was not achieved yet. **A**) Different competitors (different line colours) were added 30 min after [^{125}I]CYP (0.3 nM, 20.2 ± 0.5 kBq). **B**) FE@SNAP was added in different concentrations (different line colours) 30 min after [^{125}I]CYP (0.4 nM, 52.5 ± 0.4 kBq). **C**) Different concentrations of SNAP-7941 (different line colours) were added 30 min after [^{125}I]CYP (0.4 nM, 58.5 ± 2.5 kBq).

Figure 23A and 23B show that the effect of carazolol, pindolol and propranolol (Figure 23A) as well as of SNAP-7941 and FE@SNAP (Figure 23B) on CHO-K1-ADRB3 cells is indeed caused by the respective substances and not by their solvents (ethanol, DMSO). For those experiments, the test substances were added in more steps in increasing concentrations. It can be observed, that the solvents have no effect on radioligand binding, as the signal stays on the same niveau after ethanol or DMSO is added. However, after the addition of the test substances in sufficient concentrations, the signal decreases.

Figure 23C shows the non-specific binding of [^{125}I]CYP to the reference cell line CHO-K1. The signal is very weak, scattered and not influenced by addition of carazolol.

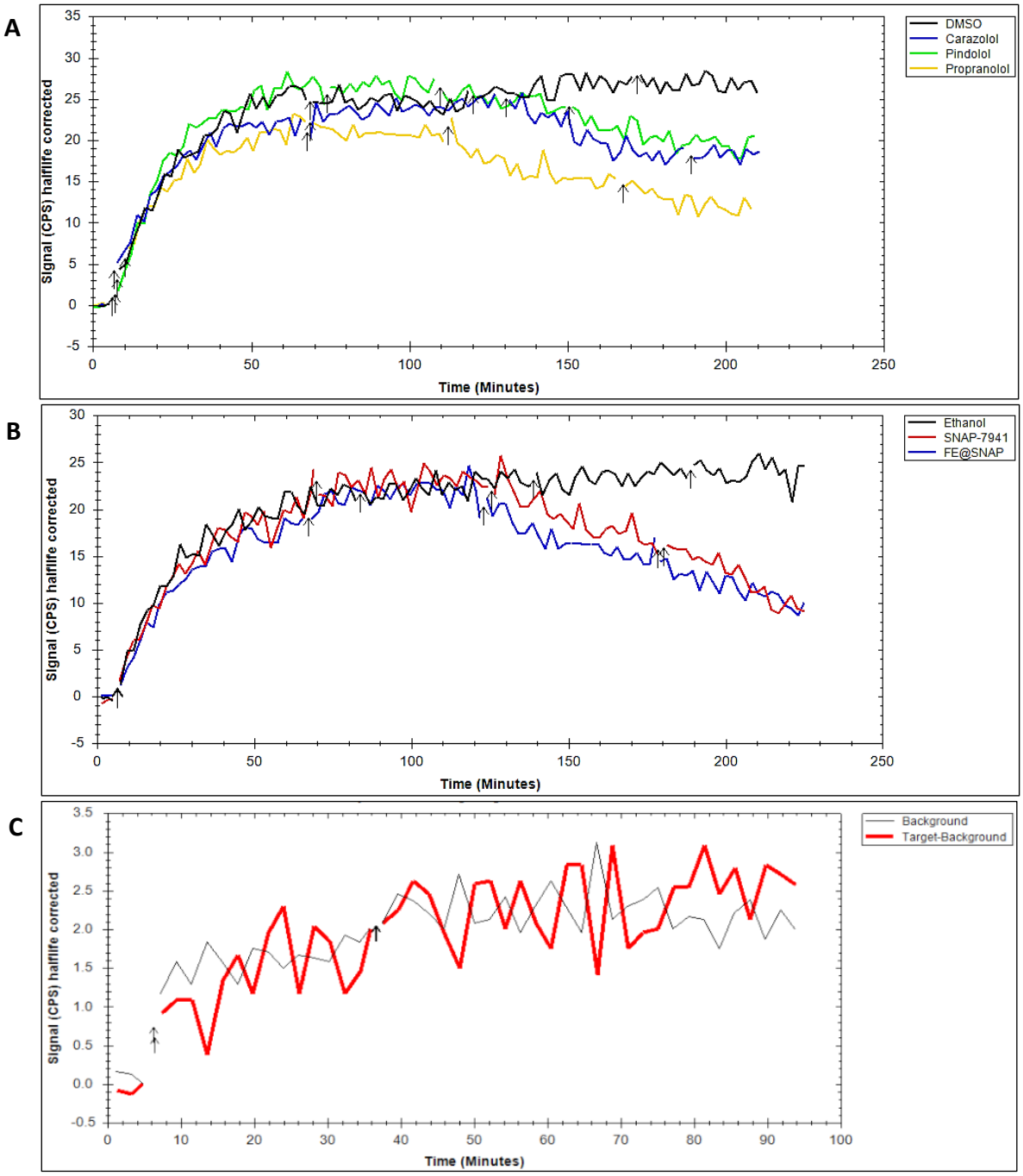

Figure 23: Overlays of competitive binding curves using different competitors and comparison with their respective solvents (vehicles)

A) Vehicle control (DMSO) for carazolol, pindolol and propranolol (different line colours). About 1 h after addition of [^{125}I]CYP the competitors or DMSO were added at three different time points (in consecutive steps using always higher concentrations) to the CHO-K1-ADRB3 cells. **B**) Vehicle control (ethanol) for SNAP-7941 and FE@SNAP (different line colours). About 1 h after addition of [^{125}I]CYP the competitors or ethanol were added at three different time points (in consecutive steps using always higher concentrations) to the CHO-K1-ADRB3 cells. **C**) Carazolol (100 nM) given 30 min after [^{125}I]CYP (290 pM, 20.8 kBq) to CHO-K1 cells (reference cell line).

Changes in binding kinetics of [^{125}I]CYP to CHO-K1-ADRB3 in presence of carazolol, pindolol, propranolol, SNAP-7941 and FE@SNAP can be observed in Figure 24. The measurement of association of [^{125}I]CYP on the cells was performed either in absence or in presence of the mentioned test substances. In presence of the competitors, the initial increase in the signal was slower (except for 52.5 µM SNAP-7941) and the equilibrium was reached sooner, in contrast to literature reporting that the presence of an unlabelled competitor will lengthen the equilibrium time of the radioligand (51).

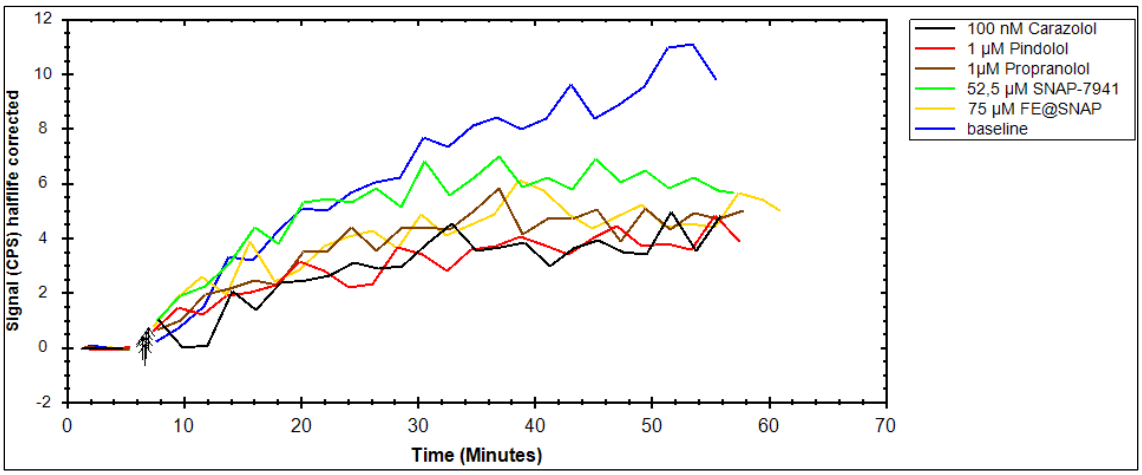

Figure 24: Overlay of binding curves in presence or absence of different test substances
Different competing substances (lines of different colours) were given simultaneously with [^{125}I]CYP (290 pM, 19.8 ± 0.7 kBq) to CHO-K1-ADRB3 cells.

5.3.2 CHO-K1-ADRB3 cells with [^{11}C]SNAP-7941 as radioligand

Few experiments were performed using the radiolabelled analogue of SNAP-7941 ([^{11}C]SNAP-7941). The binding kinetic of [^{11}C]SNAP-7941 to CHO-K1-ADRB3 cells was examined and was identified to be concentration-dependent (Figure 25A). No binding kinetic was observed when [^{11}C]SNAP-7941 was applied at low concentration (8 nM, 60 kBq, n=2). 300 nM [^{11}C]SNAP-7941 (53 kBq, n=2) led to an increase in the cell-associated signal measured in cps. It was, however, not possible to displace the MCHR1 ligand [^{11}C]SNAP-7941 from the cells using the ADRB3 agonist carazolol (Figure 25B) or CL 316243 (data not shown). These data suggest, that the binding of [^{11}C]SNAP-7941 on the CHO-K1-ADRB3 cell line is concentration-dependent, but not ADRB3 specific.

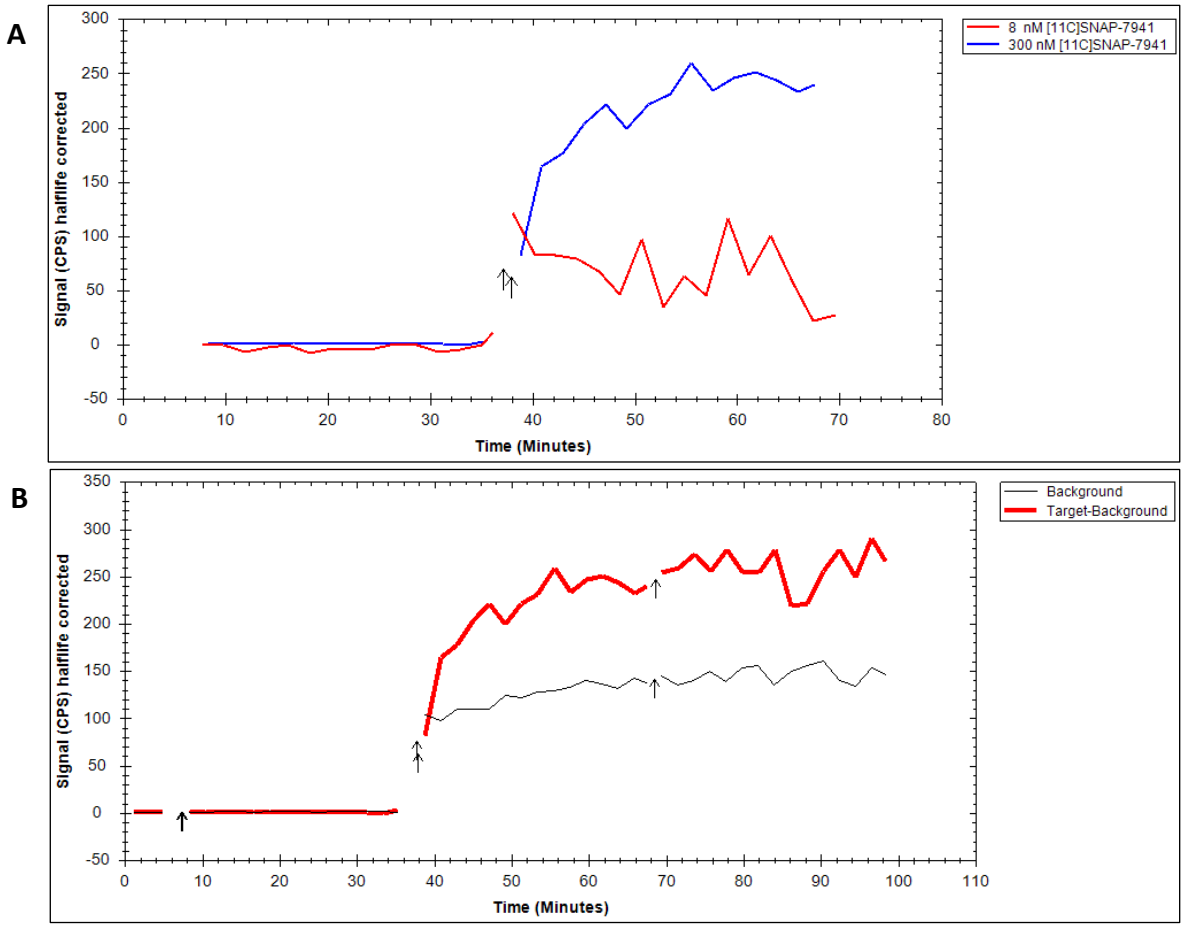

Figure 25: Representative binding curves using [^{11}C]SNAP-7941 and CHO-K1-ADRB3 cells
The arrows show the time points of introduction of different substances into the measurement. **A**) Binding kinetic of [^{11}C]SNAP-7941 was tested using two different concentrations of radioligand. [^{11}C]SNAP-7941 was added either in small concentration (red curve) (8 nM, 60 kBq) or in higher concentration (blue curve) (300 nM, 53 kBq). Both curves are Target-Background and in overlay view. **B**) Competitive binding curve using [^{11}C]SNAP-7941 as radioligand and carazolol as a competitor. Radioligand was added in two consecutive steps (first 1.3 kBq, 2.3 nM and second 53 kBq, 300 nM). Carazolol (100 nM) was introduced 30 min after the second addition of [^{11}C]SNAP-7941. The black line shows Background, the red one Target-Background.

5.3.3 CHO-K1-ADRB3 cells with [^{18}F]FE@SNAP as radioligand

A couple of experiments were performed using [^{18}F]FE@SNAP, the radiolabelled analogue of FE@SNAP. Unexpectedly, a binding enhancement was observed after the test substance, ADRB3 agonist carazolol, was added to the cell dish in a 2 µM concentration (n=2). The steep and very distinct increase in the measured cps can be seen in Figure 26A after the last arrow. To rule out the effect of the solvent DMSO, a similar experimental setting was performed with the vehicle (Figure 26B). No such effect of this respective solvent was observed. Interestingly, also the known ADRB3 agonist CL 316243 (2 µM) had no binding enhancing effect (Figure 26C). Each experiment was performed in duplicate (n=2).

At this point it is necessary to mention that the amount of tracer varies between the different experiments because of the half-life of the radioligand. To obtain a clearly visible signal during the LigandTracer® experiment, a sufficient amount of radioligand must be used. To compensate for the radioactive decay, the concentration of the used radioligand must further increase with elapsed time. The application of rising substance amounts over time is even more pronounced when carbon-11 labelled PET tracers are used. The observed effect of carazolol might be therefore a result of a favorable choice of a concentration of the radioligand, the competing test substance, or both. The potential effect of CL 316243 might be present, but due to the mentioned limitations, overlooked. A further limitation is the limited number of experiments that were performed with [^{11}C]SNAP-7941 and [^{18}F]FE@SNAP, since these research tracers are synthesized only irregularly. Therefore, some of the interesting observations could not be examined further.

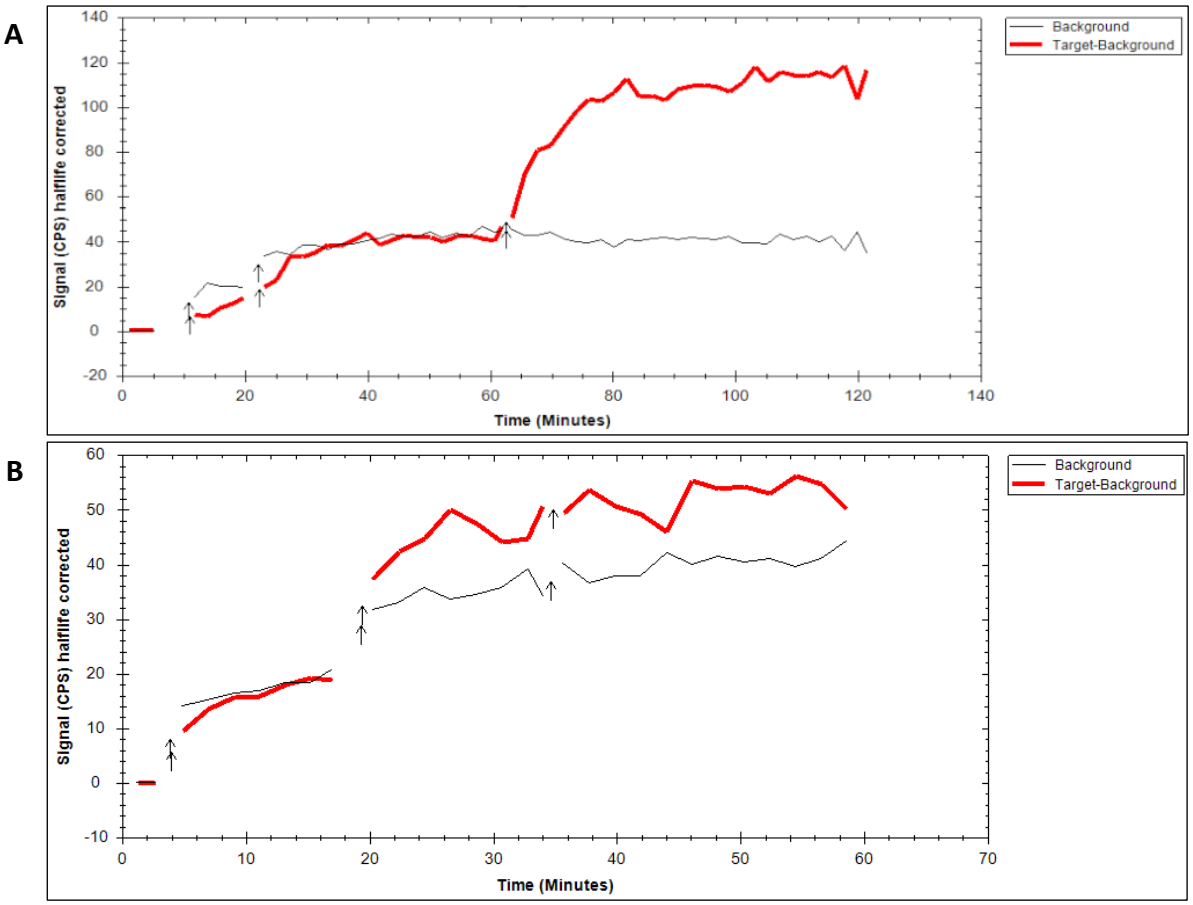

C

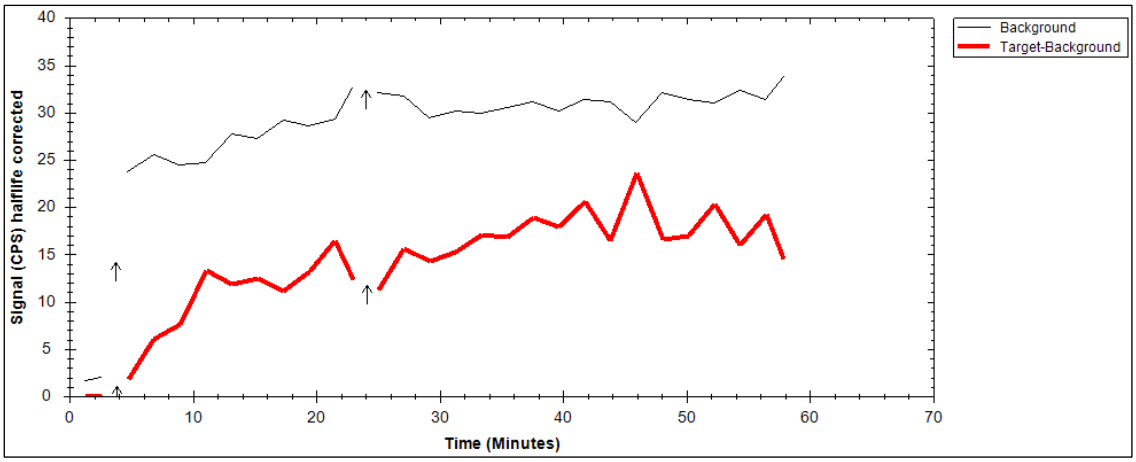

Figure 26: Representative binding curves using [^{18}F]FE@SNAP and CHO-K1-ADRB3 cells Target-Background (red line) is compared with Background (black line). Arrows show time points of introduction of different substances into the measurement. **A**) [^{18}F]FE@SNAP was added to the cells in two consecutive steps (both times 0.1 nM, first 48 kBq, second 42 kBq). 30 min after the second addition of [^{18}F]FE@SNAP carazolol (2µM) was introduced (last arrow). **B**) Vehicle control (DMSO) for experiments with carazolol. [^{18}F]FE@SNAP was added to the cells in two consecutive steps (first 0.63 nM, 73 kBq, second additional 0.38 nM and 39 kBq). 16 min after the second batch of [^{18}F]FE@SNAP, DMSO was added in volume corresponding with the experiments using carazolol. **C**) [^{18}F]FE@SNAP was added to the cells (0.63 nM, 73 kBq) and after 20 min the 2 µM CL 316243 was introduced.

5.4 Experiments with brown adipocytes

5.4.1 Induction and post differentiation

Shortly after thawing, murine brown preadipocytes were spherical, but soon attained a fibroblast-like shape (Figure 27). After reaching confluence, cells were either split or the induction begun with a specific cocktail described in detail in section 4.6.1.1. The morphological changes during the differentiation were followed under the microscope even if the cells were not stained. The cells began to be more spherical and filled with lipids organized in many small vacuoles usually around the nucleus in the centre of cell, as described for the mature brown adipocytes (26, 27). Figure 28A shows brown preadipocytes during differentiation when the induction medium has to be exchanged for the post differentiation medium. In Figures 28B and 28C, differentiated brown adipocytes with many small lipid filled vacuoles can be observed but also some undifferentiated cells retaining the more oblong shape.

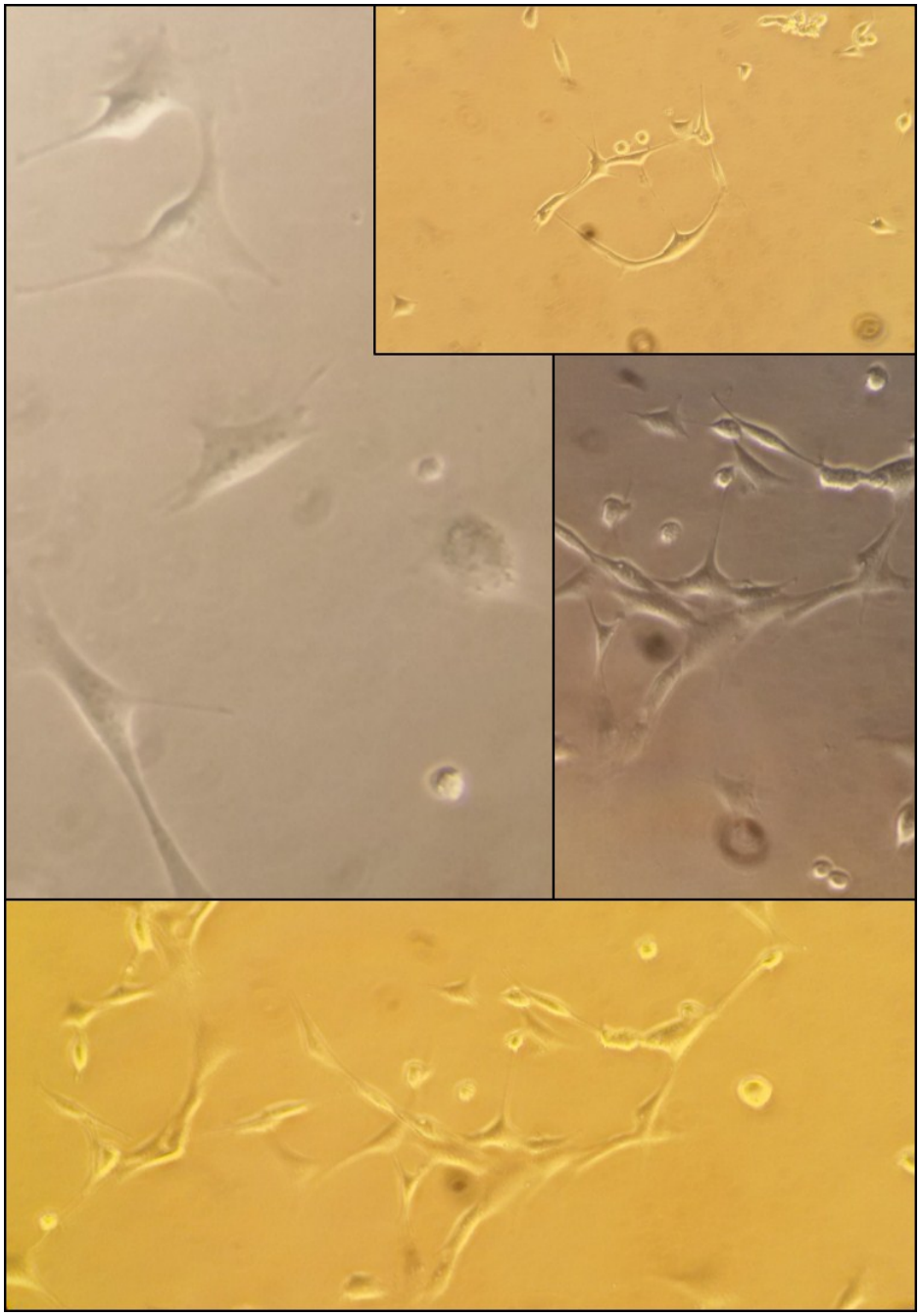

Figure 27: Murine brown preadipocytes
Original magnification: x80, picture in right upper corner: x20

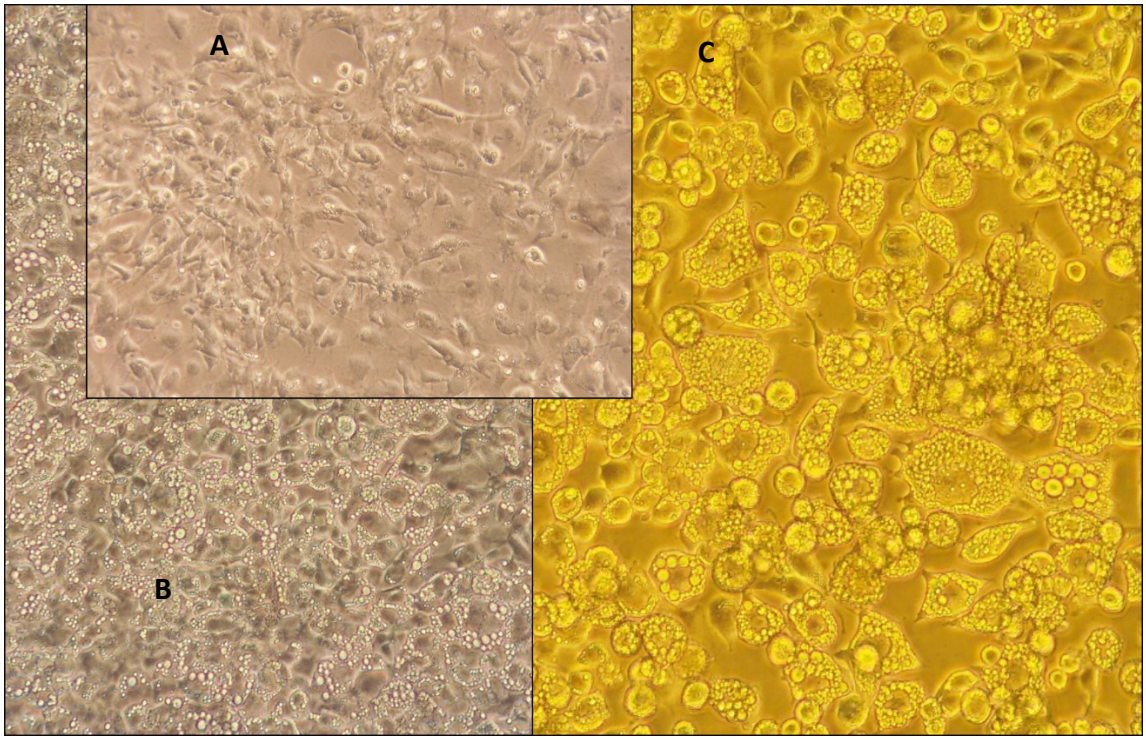

Figure 28: Murine brown fat cells during and after the differentiation
A) Murine brown preadipocytes during differentiation, shortly before post differentiation. **B**,**C**) Differentiated murine brown fat cells. Original magnification: x20

Fully differentiated brown adipocytes were obtained after 6 days. When post differentiation was carried out for a longer time period (eg 8 d), three-dimensional cell clumps occurred (Figure 29A). When differentiation of preadipocytes was not induced with the respective cell culture medium, spontaneous differentiation of small percent of preadipocytes could be observed (Figure 29B) as previously described (76). Furthermore, the cells flocked and were not regularly distributed anymore, but clusters were formed as depicted in Figures 29C and 29D.

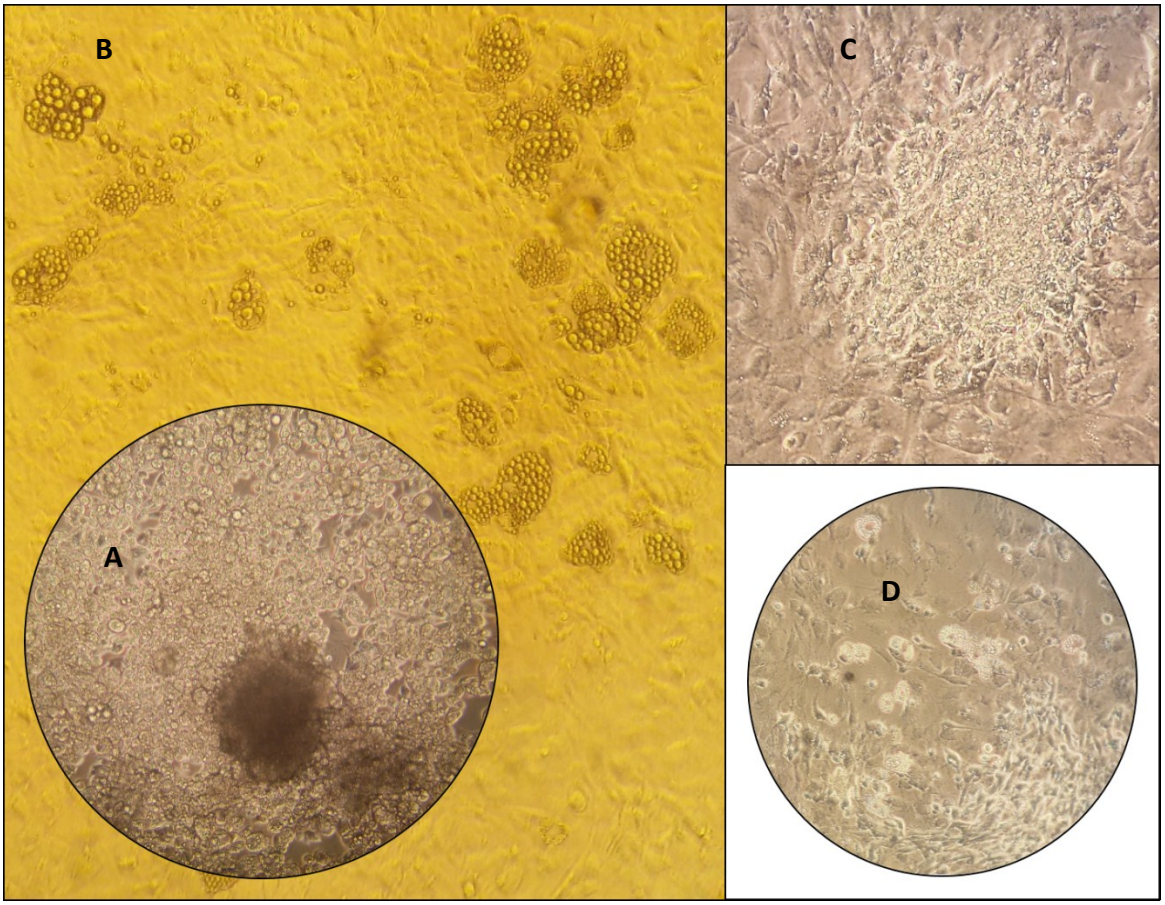

Figure 29: Observations during the differentiation of murine brown preadipocytes
A) Longer post differentiation (8 d) led to "3D"-cell clumps. **B**) Spontaneous differentiation of some of the preadipocytes as well as formation of clusters (**C**,**D**) occurred when preadipocytes were not induced with respective cell medium on time. Original magnification: x20

5.4.2 Oil Red O staining of differentiated murine brown adipocytes

Mature differentiated murine brown adipocytes were stained using Oil Red O as described detailed in section 4.6.2. Under light microscopy, lipid droplets stained with Oil Red O appear bright orange or red (Figure 30) and the remainder of the cellular constituents is non-stained. The nuclei can be counterstained with haematoxylin (77). The less densely coloured areas were photographed on purpose, in order to be able to better observe the morphology of the cells.

For Figures 30A and 30B, cells have been stained with Oil Red O for 15 min without counterstaining and show the lipid droplets organized either on the border of the cells or around the nucleus. For Figures 30C and 30D, nuclei have been counterstained using haematoxylin (1:7 dilution) for 3 min. The counterstaining does not seem to have worked, since the whole cell seems to be somewhat blueish and not only the nucleus. It is possible, that the cells were not properly washed, or that the exposure to haematoxylin was too long. In these Figures, but also when Oil Red O was used only for 5 min and

counterstaining carried out with undiluted haematoxylin (Figure 30E, 30F), non-differentiated preadipocytes with their fibroblast-like shape and the blueishly stained nuclei can be distinguished.

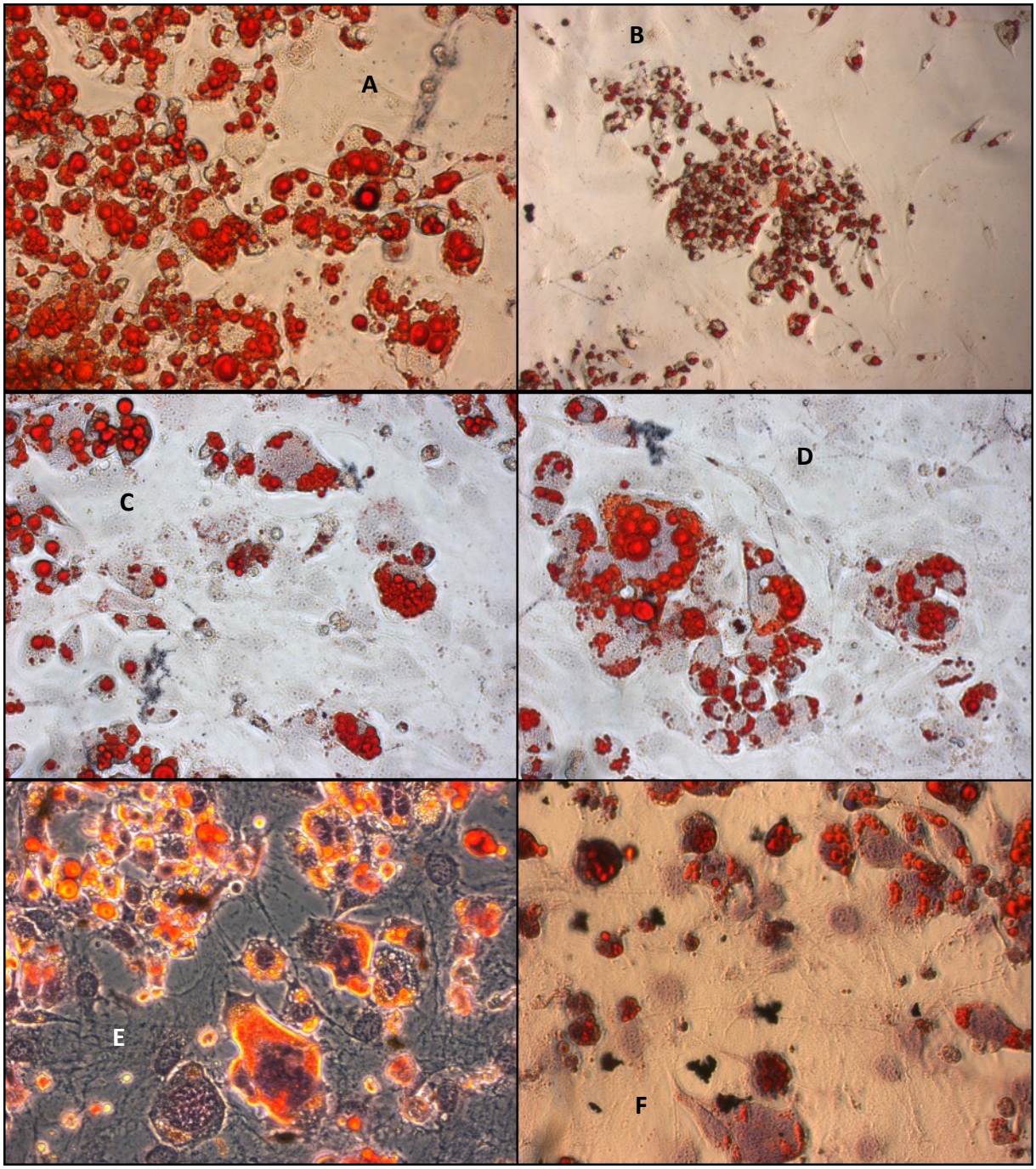

Figure 30: Oil Red O staining of mature murine brown adipocytes
Mature murine brown adipocytes have been stained only with Oil Red O (**A**,**B**) for 15 min, or also counterstained using haematoxylin. **C**,**D**) Oil Red O – 15 min, 1:7 diluted haematoxylin, **E**,**F**) Oil Red O – 5 min, haematoxylin undiluted. Original magnification: x20 (**B**), or x40 (**A**,**C**,**D**,**E**,**F**).

5.4.3 Real-time assays with preadipocytes and differentiated brown adipocytes

5.4.3.1 LigandTracer® experiments with [^{18}F]FDG as radioligand

Uptake of [^{18}F]FDG by differentiated murine brown adipocytes has been studied in real-time binding experiments using LigandTracer® Technology. The uptake kinetic was linear and very distinct (Figure 31A) in contrast to murine brown preadipocytes (Figure 31B), where the uptake was very weak. Figure 31C shows the overlay of the two experiments, pointing at the higher glucose consumption of mature brown adipocytes compared to their precursor cells *in vitro*, although very similar conditions were employed (155 kBq [^{18}F]FDG and 1 h 8 min starving or 146 kBq [^{18}F]FDG and 1 h 32 min starving).

Qualitatively, no effect of the ADRB3 ligands CL 316243 and propranolol on the [^{18}F]FDG uptake were observed for mature brown adipocytes nor preadipocytes. The MCHR1 ligand SNAP-7941 showed no effect either in these experiments (data not shown). This stands in contrast to the *in vivo* findings, where SNAP-7941 has increased the uptake of [^{18}F]FDG (63) similarly to ADRB3 agonists (37, 38). Thus, we decided to perform competitive binding experiments using 6-well plates to be able to further elicit potential effects.

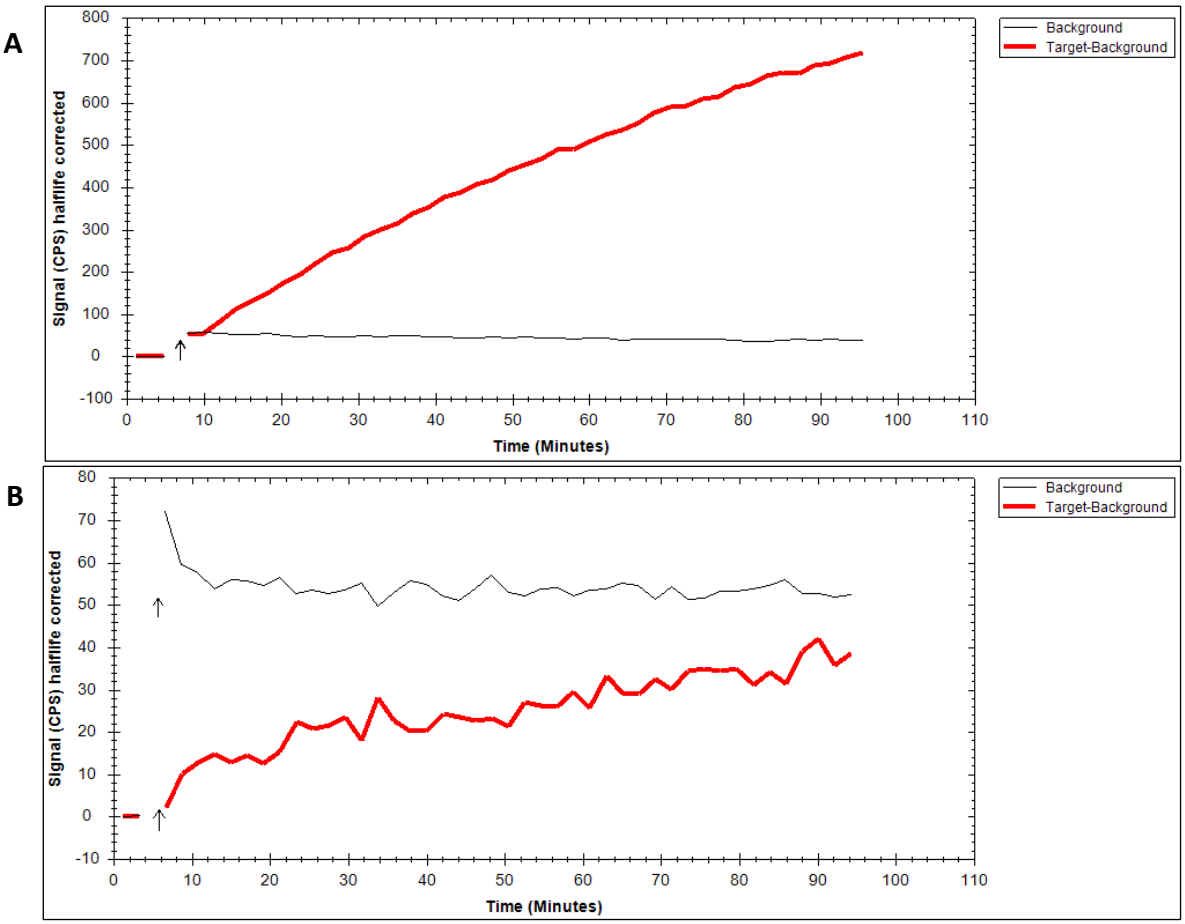

C

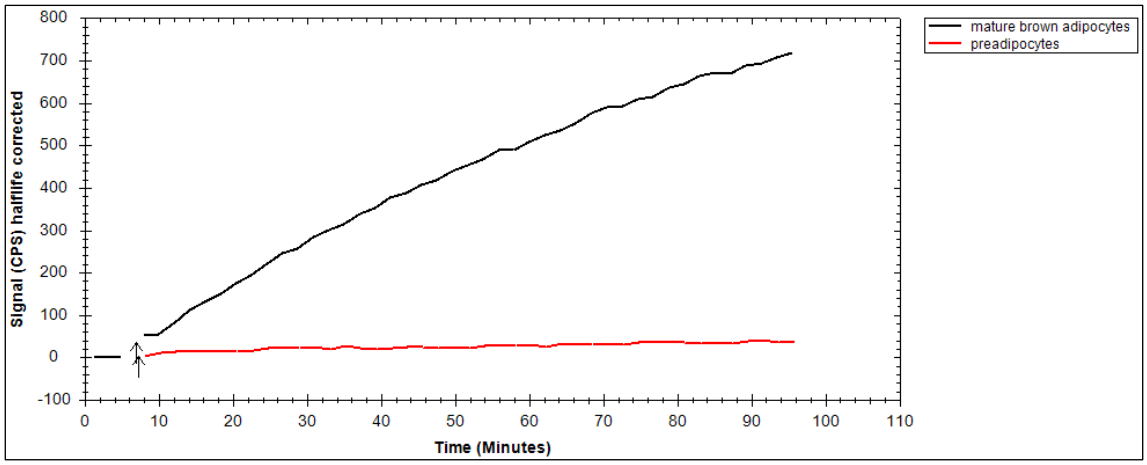

Figure 31: Kinetic uptake curves using murine brown adipocytes or preadipocytes and [^{18}F]FDG as radioligand Arrow shows time point of introduction of radioligand into the measurement. **A**) [^{18}F]FDG was added to the differentiated murine brown adipocytes (155 kBq) after the cells were starved for 1 h 8 min. Target-Background (red line) is compared with Background (black line) (**A**,**B**). **B**) [^{18}F]FDG was introduced to the murine brown preadipocytes (146 kBq) after the cells were starved for 1 h 32 min. **C**) Comparison of [^{18}F]FDG uptake of differentiated murine brown adipose cells (black line) (155 kBq, 1 h 8 min starving) and murine brown preadipocytes (red line) (146 kBq, 1 h 32 min starving).

5.4.3.2 LigandTracer® experiments with [^{11}C]SNAP-7941 as radioligand

Kinetic murine brown adipocyte measurement using [^{11}C]SNAP-7941 is shown in Figure 32A. After changing the medium to allow for radioligand dissociation, cell-associated radioactivity decreased by about 50%. However, it was not possible to displace the radioligand with 2 µM propranolol, carazolol, CL 316243 (2 or 10 µM) or with 1.3 or 10 µM MCH (data not shown). Figure 32B shows minor displacement by the unlabelled analogue SNAP-7941 (20 µM) leading us to suggest, that the observed binding is not specific for ADRB3 nor MCHR1. Thus, measured cell-associated radioactivity may be rather due to partial passive diffusion into the cell.

A

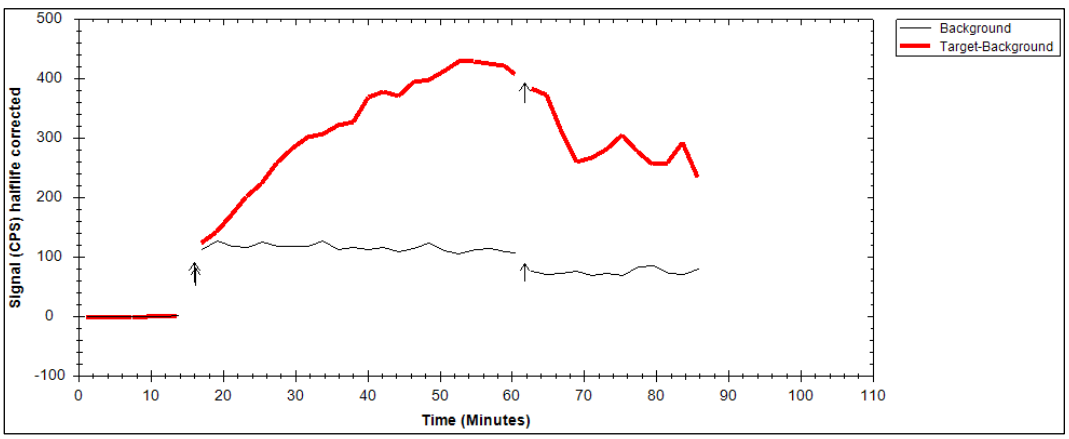

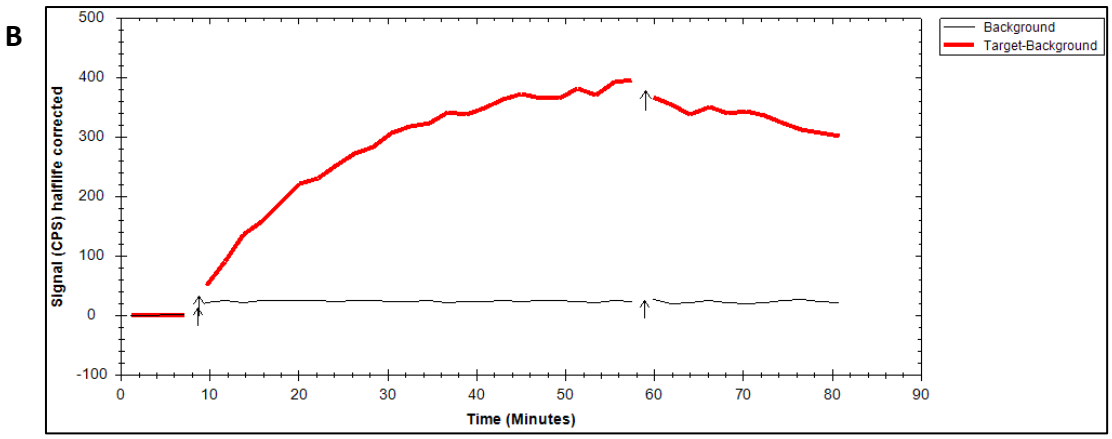

Figure 32: Binding curves with [^{11}C]SNAP-7941 and differentiated murine brown adipocytes Target-Background (red line) is compared with Background (black line). **A**) Association and dissociation of [^{11}C]SNAP-7941 to and from the mature brown adipose cells. 50 kBq (1 nM) [^{11}C]SNAP-7941 was added and after visual equilibrium was reached (46 min), medium was exchanged. The first arrow shows the time point of introduction of radioligand to the measurement, the second one the medium change. **B**) 38 kBq [^{11}C]SNAP-7941 (70 nM) was added and after visually reaching equilibrium (51 min), SNAP-7941 (20 µM) was added. Arrows show time points of introduction of radioligand and of the unlabelled compound into the measurement.

5.4.4 Well plate radioligand assays with differentiated brown adipocytes

In order to better understand the observations made in *in vivo* experiments with rats (62, 63), radioligand binding assays were performed in well plates using mature brown adipose cells. The two radioligands used in *in vivo* studies and anterior LigandTracer® experiments, [^{18}F]FDG and [^{11}C]SNAP-7941, were applied.

5.4.4.1 Well plate assays with [^{18}F]FDG as radioligand

After starving in glucose-free unsupplemented medium, cells were pre-incubated with test substances prior to the addition of the radioligand. The radioactivity of the cell fraction when pre-incubated with test substance was compared to the cell-associated radioactivity when pre-incubated with the solvent of the respective substance.

An explicit uptake of fluorine-18 labelled glucose analogue by the differentiated cells (data not shown) in accordance with performed LigandTracer® experiments (Figure 31A) could be observed. However, the basal uptake of [^{18}F]FDG differed significantly between some individual days, probably due to the state of differentiation of cells or passage number, despite the effort to keep the conditions similar. There was a significant influence of three test substances on the uptake of [^{18}F]FDG into brown adipocytes (Table 7, Figure 33).

Both, SNAP-7941 and FE@SNAP (20 µM concentration), decreased the uptake of [^{18}F]FDG by brown adipose cells significantly. Only 70 ± 4.2% of [^{18}F]FDG was taken up when pre-incubated with 20 µM SNAP-7941 (n=3, p<0.0001) and 74 ± 8.8% when pre-incubated with 20 µM FE@SNAP (n=2, p<0.005) compared to the pre-incubation with ethanol (100% uptake) (Table 7, Figure 33). Interestingly, this is the direct opposite effect of what has been observed *in vivo*. In anaesthetized rats, administration of a pharmacological dose of SNAP-7941 (15 mg/kg BW) led to increased uptake of labelled glucose analogue in BAT (63), which was suggestive of an adrenergic stimulation of glucose uptake in brown adipose cells by SNAP-7941 similarly as described for catecholamine norepinephrine or β_3-adrenergic agonists like CL 316243 (37, 38) via the ADRB3. Due to countless differences, there are difficulties when trying to extrapolate the observations from *in vitro* to *in vivo* and vice-versa. Not only are the *in vitro* studied mature brown adipocytes not the only cells in brown adipose tissue in living organism (25), this tissue is also a secretory organ (33) communicating with its surroundings and possibly affected by other factors impossible to account for in an *in vitro* experiment. Furthermore, the test substances are applied to the cells under standardized conditions, whereas if the substance is injected to the animal, it needs to reach the tissue of interest first and the comparison of the cell-associated dose is therefore much harder. The *ad libitum* feeding of test animal but also the anaesthetic agent pose other possibly influencing factors.

Table 7: Uptake of [^{18}F]FDG in well plate radioligand assays

pre-incubation with	corresponding solvent	20 µM SNAP-7941	20 µM FE@SNAP	2 µM CL 316243	2 µM propranolol
% uptake/well	100%	70 ± 4.2% (n=3)	74 ± 8.8% (n=2)	135 ± 8.2% (n=2)	105 ± 4.8% (n=2)

Mature brown adipocytes have been starved and then pre-incubated with the test substances or their solvents (baseline) and the effect of those substances on [^{18}F]FDG uptake was assessed as % uptake of radioligand per well relative to baseline. Results are from at least two independent experiments performed in triplicates. For more details regarding the method see section 4.6.4.1.
n is the number of independent experiments performed in triplicates.

Even more interesting, the glucose transport increasing effect of the β_3-adrenergic agonist CL 316243, which was previously reported (37, 38), was reproduced *in vitro*. 2 µM CL 316243 significantly increased glucose uptake up to 135 ± 8.2% (n=2, p<0.005) while 2 µM propranolol had no significant effect on [^{18}F]FDG uptake by differentiated brown adipose cells (105 ± 4.8%, n=2, p>0.05) (Table 7, Figure 33). The beta-blocker propranolol exhibited differing effects in previous studies behaving as a

very weak and partial agonist on ADRB3 (40, 46) or even having very weak inverse agonistic effects (almost antagonist) (45).

In this *in vitro* setting, the MCHR1 ligands do not influence [^{18}F]FDG uptake in the same way as ADRB3 agonist CL 316243, contrary to what was expected according to their glucose uptake enhancing effects *in vivo* measured by [^{18}F]FDG µPET (63).

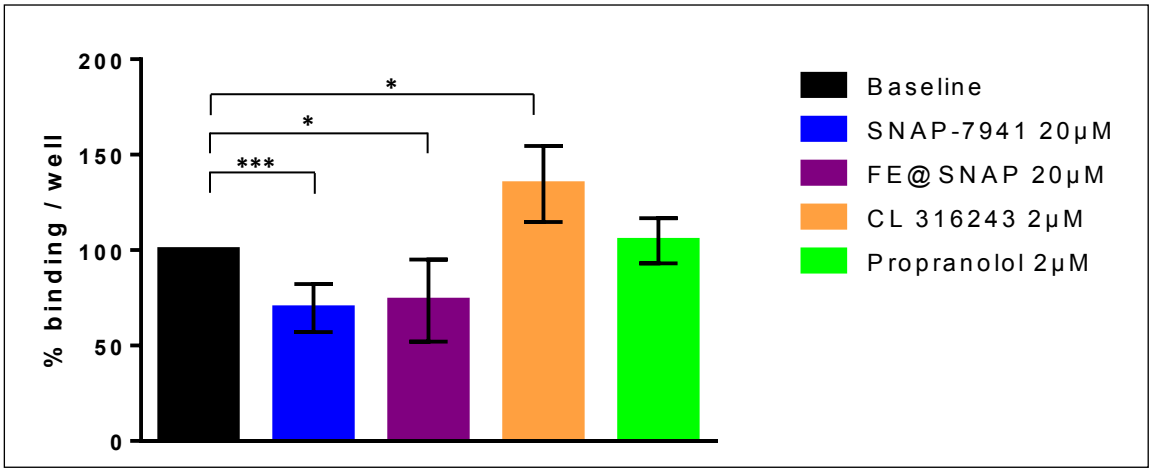

Figure 33: Uptake of [^{18}F]FDG per well assessed with well plate radioligand assays
Experiments were performed as described in legend to Table 7 and more detailed in section 4.6.4.1. Results were considered significant if $p<0.05$. * $p<0.005$, *** $p<0.0001$

5.4.4.2 Well plate assays with [^{11}C]SNAP-7941 as radioligand

Well plate experiments with [^{11}C]SNAP-7941 were performed similarly as those conducted with [^{18}F]FDG, but without starving. Significant blocking effects of the uptake or binding could be observed with all test substances (Table 8, Figure 34).

MCHR1 ligand SNAP-7941 blocked the accumulation of its radiolabelled analogue by about 25%. There was no significant difference between two different concentrations of SNAP-7941, 2 µM (76 ± 2.7% uptake, n=2) or 20 µM (75 ± 1.7% uptake, n=2) (Table 8, Figure 34). The blocking effect of SNAP-7941 is not surprising, since the radioactive analogue is applied in much smaller nM-range (2.7 ± 0.70 nM). Furthermore, the non-labelled analogue is longer in contact with the cells, since pre-blocking experiments were performed. Therefore, binding of the non-labelled analogue has a higher probability. The results are in accordance with LigandTracer® experiments performed with [^{11}C]SNAP-7941 (Figure 32B), where radiolabelled SNAP-7941 was slightly displaced after addition of its non-labelled analogue. Real-time cell-binding competitive experiments using LigandTracer® Technology were performed as displacement experiments, where after reaching equilibrium the competing substance was added. This could explain the slightly different effect of SNAP-7941 in well plate

experiments (25% blocking) and the LigandTracer® experiment (minor displacement). Main part of [^{11}C]SNAP-7941 accumulation in BAT cells observed in well plate assays was not abolished by the addition of the unlabelled compound, suggesting irreversible or nonspecific binding processes or passive diffusion.

In pre-blocking experiments, radioligand is added after pre-incubation with the competing substance. Within well plate assays, brown adipocytes were incubated with [^{11}C]SNAP-7941 for 32 min and binding equilibrium is not reached at this time point (Figure 32). Furthermore, according to literature, it takes longer for equilibrium to be established when a competitor is present (51), although the LigandTracer® experiments with [^{125}I]CYP as radioligand indicate the opposite (Figure 24). In well plate assays where no K_i nor K_d is determined, experiments can be performed also before the equilibrium is established.

Two tested ADRB3 ligands, ADRB3 agonist CL 316243 and β_1-/β_2-adrenergic antagonist propranolol caused about 10% reduction in cell-associated fraction of [^{11}C]SNAP-7941. Cells pre-incubated with 2 µM CL 316243 accumulated 89 ± 2.6% (n=2) and when pre-incubated with 2 µM propranolol 91 ± 1.8% [^{11}C]SNAP-7941 (n=3) compared to the respective vehicle control (baseline measurement) (Table 8, Figure 34). This is in contrast to LigandTracer® experiments, where no displacement of [^{11}C]SNAP-7941 accumulation by ADRB3 ligands could be observed. However, as described above, different experimental settings were performed: blocking and displacement experiments.

The low affinity of SNAP-7941 and FE@SNAP towards ADRB3 elicited in competitive binding studies using filtration method is in accordance with these experiments, where 10% of [^{11}C]SNAP-7941 signal was blocked by ADRB3 ligands. This indicates, that the accumulation of [^{11}C]SNAP-7941 is partly caused by binding to ADRB3. But since only 10% of the binding can be blocked, this is with high probability not the main cause of the accumulation of the potential MCHR1 PET tracers in BAT of rats (62). Since the non-radioactive analogue SNAP-7941 decreases the uptake of [^{11}C]SNAP-7941 by only 25%, it seems that the effect could be best explained by very high non-specific binding to the cells or passive diffusion. [^{11}C]SNAP-7941 could theoretically also bind to MCHR1 in BAT, although the receptor has not been described in BAT yet. The preliminary investigations of the group around Cécile Philippe running in parallel with this master thesis indicate that there might be MCHR1 expression in membranes of brown adipocytes.

The accumulation of [^{11}C]SNAP-7941 in BAT of rats (63), could therefore be explained by more events: partial binding to the ADRB3, strong passive diffusion or non-specific binding and potential binding to its main target, the MCHR1.

Table 8: Accumulation of [^{11}C]SNAP-7941 in well plate radioligand assays

Pre-incubation with	Corresponding solvent	2 µM SNAP-7941	20 µM SNAP-7941	2 µM CL 316243	2 µM propranolol
% Accumulation per well	100%	76 ± 2.7% (n=2)	75 ± 1.7% (n=2)	89 ± 2.6% (n=2)	91 ± 1.8% (n=3)

Differentiated brown adipocytes have been pre-incubated with test substances or their solvents (baseline) and the effect of those substances on [^{11}C]SNAP-7941 accumulation assessed as % binding/uptake of radioligand per well relative to baseline. Results are from at least two experiments performed in triplicates. For more details see section 4.6.4.2.
n is the number of independent experiments performed in triplicates.

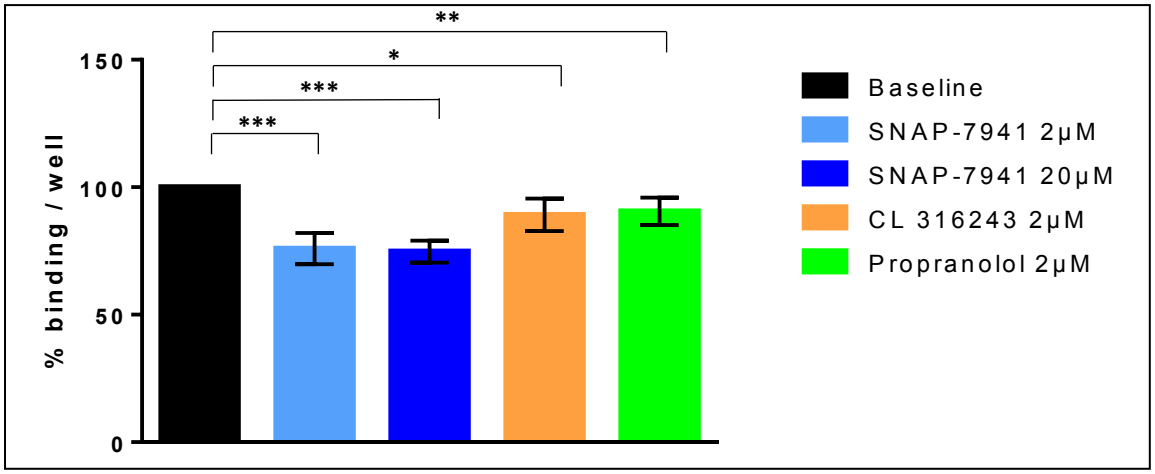

Figure 34: Accumulation of [^{11}C]SNAP-7941 per well assessed with well plate radioligand assays
Experiments were performed as described in legend to Table 8 and more detailed in section 4.6.4.2. Results were considered significant if $p<0.05$. * $p<0.005$, ** $p<0.001$, *** $p<0.0001$

The difference between anaesthetized and non-anaesthetized rats could be theoretically explained by pharmacological effects caused by the used anaesthetic. The research group uses isoflurane (1.5 – 2.5%), a volatile anaesthetic that has been shown to inhibit the thermogenesis in isolated hamster brown adipocytes after stimulation with norepinephrine. Maximal observed inhibition of norepinephrine response by isoflurane in the study was 69% (above 2% isoflurane), IC_{50} was 0.6 ± 0.06% (78). If the thermogenesis would be blocked by isoflurane after administration of a pharmacological dose of SNAP-7941 in rats, this would support the theory that MCHR1 ligand SNAP-7941 acts indeed as ADRB3 agonist *in vivo*, though acting differently regarding effects on glucose uptake *in vitro*.

6. Conclusion

Competitive binding studies using filtration method have been a useful tool to investigate the affinity of the non-labelled MCHR1 ligands SNAP-7941 and FE@SNAP to the ADRB3 after optimizing the experimental assay and employing self-made cell membranes. The affinity of these substances was low. The affinity of SNAP-7941 expressed as equilibrium inhibition constant K_i was 14.5 µM, FE@SNAP evinced even lower affinity with a K_i of 65.1 µM for ADRB3. Hence, both K_i values ranged in a µM-range, which is only achieved *in vivo*, when using the ligands in pharmacological doses.

The results could be confirmed with real-time cell-binding studies using LigandTracer® Technology. Both MCHR1 ligands displaced [^{125}I]CYP, a radioligand highly affine for ADRB3, when added in a two-digit µM-range.

The binding kinetic of the PET tracer [^{11}C]SNAP-7941 to the ADRB3 was also examined with LigandTracer® experiments and seems to be concentration-dependent. No specific binding to the CHO-K1-ADRB3 cells could be observed using small concentrations of the radioligand. Furthermore, there was no displacement with the ADRB3 agonist carazolol. Interestingly, an enhancing effect of carazolol on the binding of [^{18}F]FE@SNAP to the CHO-K1-ADRB3 cells could be observed using the same experimental setting.

Murine brown preadipocytes were differentiated into mature brown adipocytes and when stained with Oil Red O stain evinced typical brown adipose cell morphology with numerous small fat vacuoles and often centrally located nucleus.

Real-time binding assays and well plate radioligand assays have shown distinct uptake of [^{18}F]FDG into mature brown adipocytes. This uptake was significantly higher compared to the uptake in undifferentiated preadipocytes. In contrast to previously conducted *in vivo* experiments (63), the MCHR1 ligands SNAP-7941 and FE@SNAP (20 µM) decreased the [^{18}F]FDG uptake into mature brown adipocytes *in vitro* (25-30% blocking), showing a difference between studies in cells and animals. In well plate assays, the ADRB3 agonist CL 316243 increased the [^{18}F]FDG uptake (35% increase) as expected.

Real-time binding assays using the potential MCHR1 PET tracer [^{11}C]SNAP-7941 have shown accumulation of the radiotracer in differentiated brown adipocytes, that could however not be displaced with ADRB3 ligands or with MCH. On the other hand, pre-blocking well plate radioligand binding assays have shown about 10% blocking by ADRB3 ligands CL 316243 and propranolol. SNAP-7941 has concentration-independently displaced its radioactive labelled analogue by about 25% which is in accordance with the LigandTracer® experiments.

In conclusion, the obtained affinity values of SNAP-7941 and FE@SNAP in µM-range do not explain the *in vivo* observed effects of the PET tracers [^{18}F]FE@SNAP and [^{11}C]SNAP-7941, since these are applied in pM-concentration. The observed accumulation of the PET tracers in BAT of rats could be a combined effect of partial binding to ADRB3, non-specific binding and passive diffusion into the cells. Furthermore, an expression of MCHR1 in BAT cannot be excluded yet. The difference between anaesthetized and conscious freely moving rats could be ascribed to the anaesthetic used. Interactions between anaesthetics and target regions are reported in literature (78). Nevertheless, the pharmacological concentrations of the respective nonradioactive compounds, as they were used in µPET experiments for blocking/displacement studies, may exert effects in BAT via ADRB3. However, there seem to be differences between *in vivo* and *in vitro* conditions, since it was not possible to reproduce the *in vivo* observed enhancing effect of SNAP-7941 on the [^{18}F]FDG uptake in cultured brown adipocytes. On the contrary, a blocking effect of SNAP-7941 was obvious.

Employing different assay types, radioligands, cell lines, cells or membrane suspensions, many observations were made and some of those could not be explained. Couple of observations have been opposite to those made in animal studies. Seek of all explanations would greatly exceed the scope of this master thesis and inevitably provide new questions. Many further experiments are necessary to shed light onto some of the observations. Although not serving the ultimate answer, the thesis offers on one hand robust values to eliminate some theories and on the other hand intriguing observations to make alternative theories, raise new questions and direct further research, as is usual in science.

Abstract

Melanin-concentrating hormone is a hypothalamic neuropeptide playing a key role in energy homeostasis and body weight (1, 2). Two PET tracers targeting MCHR1, the receptor for this peptide, have recently been developed, [^{11}C]SNAP-7941 and [^{18}F]FE@SNAP (11, 13). Specific uptake of [^{18}F]FE@SNAP into BAT of conscious freely moving rats was observed after blocking with a pharmacological dose of SNAP-7941 (15 mg/kg BW), although the expression of MCHR1 in BAT has not been described yet. However, contradictory observations were made in µPET studies: a trend towards uptake enhancement of [^{18}F]FE@SNAP into BAT of anaesthetized rats after displacement with SNAP-7941 (15 mg/kg BW) was observed. Moreover, administration of SNAP-7941 (15 mg/kg BW) led to an increased uptake of [^{18}F]FDG into BAT of anaesthetized rats (62, 63), suggestive of activating BAT in a similar way as it was described for ADRB3 agonists (37). ADRB3 is expressed primarily in adipose tissue (25), where it is essential for lipolysis (47) and in BAT for thermogenesis (25).

The hypothesis was, that these two MCHR1 ligands bind to ADRB3 in BAT and the first aim of this thesis was therefore to elicit the affinity of SNAP-7941 and FE@SNAP for ADRB3. Competitive binding studies using the filtration method with membranes expressing hADRB3 and [^{3}H]-CGP-12177 as radioligand were employed. In order to confirm the results obtained with this method, real-time whole cell-binding studies using LigandTracer® Technology with CHO-K1 cells stably expressing hADRB3 and [^{125}I]-(-)-Iodocyanopindolol as well as [^{11}C]SNAP-7941 and [^{18}F]FE@SNAP were performed.

The second aim of this work was to characterize the interaction of [^{11}C]SNAP-7941 with brown adipocytes and to elicit the effect of the two MCHR1 ligands as well as known ADRB3 ligands on the uptake of [^{18}F]FDG into BAT. Murine brown preadipocytes were differentiated into mature brown adipocytes, stained with Oil Red O and real-time binding LigandTracer® experiments and well plate radioligand binding assays were performed.

K_i-values for the known ADRB3 ligands were reproduced in competitive binding studies using the filtration method. For economic reasons membranes were prepared from CHO-K1-ADRB3 cells in-house. Moreover, higher total binding was achieved than when using commercially available membrane preparations. Studies with these self-prepared membranes attained the K_i = 2.0 ± 0.3 nM for carazolol, which is in accordance with K_i = 2 ± 0.2 nM from literature (49). The affinities of the two MCHR1 ligands for ADRB3 were in two-digit µM-range. SNAP-7941 was more affine (K_i = 14.5 ± 0.3 µM) than FE@SNAP (K_i = 65.1 ± 2.9 µM). In real-time whole cell-binding studies, similar concentrations (20 µM SNAP-7941, 35 µM FE@SNAP) led to displacement of [^{125}I]CYP. [^{11}C]SNAP-7941 accumulated in concentration-dependent manner to CHO-K1-ADRB3 cells and could not be displaced from the cells with ADRB3 agonists (carazolol, CL 316243). Interestingly, 2 µM carazolol led to an increase in

accumulation of [^{18}F]FE@SNAP to the cell line, while CL 316243 had no effect. [^{18}F]FDG was linearly taken up to the mature brown adipocytes in contrast to undifferentiated preadipocytes. In well plate assays, as expected, ADRB3 agonist CL 316243 increased the uptake of [^{18}F]FDG into brown adipocytes (35% increase). MCHR1 ligands SNAP-7941 and FE@SNAP however behaved differently than *in vivo* (63) and in 20 µM concentration decreased [^{18}F]FDG uptake significantly (30% and 26% decrease, respectively). [^{11}C]SNAP-7941 was accumulated in murine brown adipocytes *in vitro* and this was partly reversible. 20 µM SNAP-7941 displaced its radiolabeled analogue only slightly in LigandTracer® experiment, in pre-blocking well plate experiment the accumulation was reduced by about 25% and there was no significant difference between 2 and 20 µM SNAP-7941. 2 µM of the ADRB3 ligands CL 316243 and propranolol reduced the accumulation by approximately 10% in the well plate assay, which is in agreement with the low affinity of SNAP-7941 and FE@SNAP for ADRB3. In LigandTracer® experiments, no effect of substances could be detected.

The affinities of SNAP-7941 and FE@SNAP in µM-range do not explain the specific accumulation of [^{18}F]FE@SNAP into BAT *in vivo*, PET tracers are applied in pM-concentrations in µPET experiments. The accumulation of potential MCHR1 PET tracers in BAT can partly be caused by binding to ADRB3 in brown adipocytes, but there is probably an extensive non-specific binding or at least partial passive diffusion into brown fat cells. Preliminary investigations show that there might be a small amount of MCHR1 expressed in BAT and the tracer could partly bind here as well. According to the literature (78), the difference between anaesthetized and conscious freely moving rats could be ascribed to the anaesthetic used. Taking into account the affinity of SNAP-7941 and FE@SNAP to ADRB3, the effect of a pharmacological (µM) dose of SNAP-7941 on [^{18}F]FDG uptake could be via ADRB3. However, SNAP-7941 had a directly opposite effect on [^{18}F]FDG uptake in mature brown adipocytes *in vitro* compared to *in vivo* in anaesthetized rats and acted differently than ADRB3 agonist CL 316243. Further experiments are necessary to explain some of the observations and discrepancies.

Zusammenfassung

Das hypothalamische Neuropeptid Melanin-konzentrierendes Hormon spielt eine wichtige Rolle für die Aufrechterhaltung der Energiehomeostase und des Körpergewichts (1, 2). Zwei PET-Tracer sind vor kurzem entwickelt worden, welche am MCHR1 – der Rezeptor für MCH – binden. [^{11}C]SNAP-7941 und [^{18}F]FE@SNAP (11, 13) haben in präklinischen Untersuchungen ein großes Potential für die Bildgebung des MCHR1 gezeigt (16, 17, 19). [^{18}F]FE@SNAP zeigte eine spezifische Aufnahme in braunem Fettgewebe von wachen, nicht-anästhesierten Ratten, welche durch die Applikation von SNAP-7941 signifikant reduziert wurde (62). Jedoch ist die MCHR1 Expression in braunem Fettgewebe in der Literatur noch nicht beschrieben. Gegenteiliges wurde in µPET Studien bei anästhesierten Ratten beobachtet: Die Applikation einer pharmakologischen Dosis von SNAP-7941 (15 mg/kg Körpergewicht) führte zu einer gesteigerten [^{18}F]FE@SNAP-Anreicherung im braunen Fettgewebe. Weiters konnte SNAP-7941 in pharmakologischer Dosis die Aufnahme von [^{18}F]FDG in braunem Fettgewebe von anästhetisierten Ratten steigern (63). Dies war ähnlich einer Aktivierung von braunem Fettgewebe durch ADRB3 Agonisten (37). Der ADRB3 wird hauptsächlich im Fettgewebe exprimiert (25), wo er für die Lipolyse (47) und in braunem Fettgewebe auch für die Thermogenese unerlässlich ist (25).

Die Hypothese der Arbeit war, dass die zwei MCHR1 Liganden an ADRB3 in braunem Fettgewebe binden und somit war das erste Ziel dieser Masterarbeit, die Affinität von SNAP-7941 und FE@SNAP zu ADRB3 zu bestimmen. Kompetitive Bindungsstudien mittels Filtrationsmethode mit Membranen, die ADRB3 exprimieren, und mit [^{3}H]-CGP-12177 als Radioligand sind durchgeführt worden. Um diese Ergebnisse bekräftigen zu können, wurden zusätzlich Echt-Zeit-Zellbindungsstudien mit CHO-K1 Zellen, die ADRB3 exprimieren, und mit [^{125}I]-(-)-Iodocyanopindolol als Radioligand durchgeführt. Außerdem wurden Bindungsstudien mit den PET-Tracern [^{11}C]SNAP-7941 and [^{18}F]FE@SNAP vorgenommen. Das zweite Ziel von dieser Arbeit war, die Interaktion von [^{11}C]SNAP-7941 und braunen Fettgewebszellen zu charakterisieren sowie den Effekt von den bekannten ADRB3 Liganden und MCHR1 Liganden SNAP-7941 und FE@SNAP auf die Aufnahme von [^{18}F]FDG im braunen Fettgewebe zu untersuchen. Murine braune Präadipozyten sind in braune Adipozyten differenziert worden und mit Oil Red O gefärbt worden. Es wurden Echt-Zeit-Zellbindungsstudien, die LigandTracer® Experimente, sowie konventionelle Radioligand-Bindungsstudien (“well plate assays“) durchgeführt.

Zwar konnten die K_i-Werte für die bekannten ADRB3 Liganden mittels Filtrationsmethode reproduziert werden, die kommerziell erhältlichen und relativ kostenintensiven Membranen lieferten aber eine unzureichende Gesamtbindung bei geringer Proteinkonzentration. Deshalb wurden die Membranen für die weiteren Experimente selbst aus CHO-K1-ADRB3 Zellen hergestellt. K_i = 2.0 ± 0.3 nM für

Carazolol war nicht signifikant unterschiedlich von dem publizierten Wert (K_i = 2 ± 0.2 nM) (49). SNAP-7941 (K_i = 14.5 ± 0.3 µM) und FE@SNAP (K_i = 65.1 ± 2.9 µM) zeigten eine mittlere Affinität für den ADRB3. Kompetitive LigandTracer® Experimente zeigten, dass FE@SNAP (35µM) und SNAP-7941 (20µM) in jenem Konzentrationsbereich eine Verdrängung vom [^{125}I]CYP verursachen, was auf eine Interaktion mit dem ADRB3 hindeutet. Die Anreicherung von [^{11}C]SNAP-7941 in CHO-K1-ADRB3 Zellen erfolgte konzentrationsabhängig, konnte aber mittels ADRB3 Agonisten Carazolol oder CL 316243 nicht verdrängt werden. Interessanterweise wurde durch Carazolol (2 µM) eine verstärkte [^{18}F]FE@SNAP-Akkumulation in dieser Zelllinie verursacht, wobei CL 316243 keinen Effekt hatte. Im Gegensatz zu Präadipozyten wurde [^{18}F]FDG von differenzierten Adipozyten stark und linear aufgenommen. Wie erwartet, konnte durch konventionelle Radioligand-Bindungsstudien eine um 35% gesteigerte [^{18}F]FDG-Aufnahme in braune Fettzellen beobachtet werden, welche durch den ADRB3 Agonist CL 316243 ausgelöst wurde. Die MCHR1 Liganden SNAP-7941 und FE@SNAP wiesen hingegen ein anderes Verhalten als *in vivo* (63) auf. Die Aufnahme von [^{18}F]FDG wurde in den *in vitro* Experimenten signifikant reduziert (um 30% im Falle von SNAP-7941 und um 26% bei FE@SNAP). *In vitro* wurde [^{11}C]SNAP-7941 von den differenzierten braunen Fettzellen akkumuliert, wobei diese teilweise verdrängbar war. In LigandTracer® Experimenten konnte durch 20 µM SNAP-7941 nur eine gerinfügige Verdrängung von [^{11}C]SNAP-7941 Bindung erzielt werden. Die konventionellen Radioligand-Bindungsstudien zeigten eine 25%ige Reduktion der [^{11}C]SNAP-7941-Akkumulation, wenn mit SNAP-7941 (2 oder 20 µM) vorbehandelt wurde. Die ADRB3 Liganden CL 316243 und Propranolol (2 µM) haben die Bindung bzw. die Aufnahme von [^{11}C]SNAP-7941 um ungefähr 10% reduziert, was bedeutet, dass nur ein kleiner Teil der [^{11}C]SNAP-7941 Bindung ADRB3 vermittelt ist. In kompetitiven LigandTracer® Experimenten konnte kein Effekt von den Substanzen beobachtet werden.

Die mittlere Affinität von SNAP-7941 und FE@SNAP zu ADRB3, die in µM-Bereich liegt, kann die Anreicherung von [^{11}C]SNAP-7941 und [^{18}F]FE@SNAP in braunem Fettgewebe *in vivo* nicht erklären, da in µPET Experimenten lediglich pM-Konzentrationen der PET-Tracer appliziert werden. Vermutlich liegen hier neben der ADRB3 Bindung auch andere Prozesse wie eine nicht-spezifische Anreicherung im Fettgewebe sowie eine passive Diffusion vor. Im Moment laufen Untersuchungen zum Nachweis des MCHR1 Proteins in braunem Fettgewebe, welche weitere Aufklärung schaffen sollen. Laut der Literatur konnte der Unterschied zwischen anästhetisierten und nicht-anästhetisierten Tieren mit der Art des Anästhetikums zusammenhängen (78). Anhand der Affinität von SNAP-7941 und FE@SNAP zu ADRB3 deutet der Effekt der pharmakologischen (µM) Dosis auf die Aufnahme von [^{18}F]FDG jedoch auf einen ADRB3-vermittelten Effekt hin. SNAP-7941 hat allerdings einen gegenteiligen Effekt bezüglich [^{18}F]FDG Aufnahme in differenzierte braune Fettzellen *in vitro* im Vergleich zu *in vivo* und

hat sich auch anders als der ADRB3 Agonist CL 316243 verhalten. Weitere Untersuchungen sind notwendig um einige Beobachtungen und Diskrepanzen zu erklären.

References

1. Qu D, Ludwig DS, Gammeltoft S, Piper M, Pelleymounter MA, Cullen MJ, Mathes WF, Przypek J, Kanarek R, Maratos-Flier E. A role for melanin-concentrating hormone in the central regulation of feeding behaviour. Nature 1996;380(6571):243-247

2. Kokkotou EG, Tritos NA, Mastaitis JW, Slieker L, Maratos-Flier E. Melanin-Concentrating Hormone Receptor Is a Target of Leptin Action in the Mouse Brain. Endocrinology 2001;142(2):680-686

3. Borowsky B, Durkin MM, Ogozalek K, Marzabadi MR, DeLeon J, Heurich R, Lichtblau H, Shaposhnik Z, Daniewska I, Blackburn TP, et al. Antidepressant anxiolytic and anorectic effects of a melanin-concentrating hormone-1 receptor antagonist. Nat Med 2002;8(8):825-830

4. Ludwig DS, Tritos NA, Mastaitis JW, Kulkarni R, Kokkotou E, Elmquist J, Lowell B, Flier JS, Maratos-Flier E. Melanin-concentrating hormone overexpression in transgenic mice leads to obesity and insulin resistance. J Clin Invest 2001;107(3):379-386

5. Mashiko S, Ishihara A, Gomori A, Moriya R, Ito M, Iwaasa H, Matsuda M, Feng Y, Shen Z, Marsh DJ, et al. Antiobesity Effect of a Melanin-Concentrating Hormone 1 Receptor Antagonist in Diet-Induced Obese Mice. Endocrinology 2005;146(7):3080-3086

6. Saito Y, Nothacker H-P, Wang Z, Lin SHS, Leslie F, Civelli O. Molecular characterization of the melanin-concentrating-hormone receptor. Nature 1999;400(6741):265-269

7. Sailer AW, Sano H, Zeng Z, McDonald TP, Pan J, Pong S-S, Feighner SD, Tan CP, Fukami T, Iwaasa H, et al. Identification and characterization of a second melanin-concentrating hormone receptor, MCH-2R. Proc Natl Acad Sci U S A 2001;98(13):7564–7569

8. Philippe C, Mitterhauser M. The Potential Role of the MCHR1 in Diagnostic Imaging: Facts and Trends. In: Blumenberg M, ed. Melanin. Rijeka, Croatia: InTechOpen, 2017:27-43

9. Kokkotou E, Moss AC, Torres D, Karagiannides I, Cheifetz A, Liu S, O'Brien M, Maratos-Flier E, Pothoulakis C. Melanin-concentrating hormone as a mediator of intestinal inflammation. Proc Natl Acad Sci U S A 2008;105(30):10613-10618

10. Pissios P, Ozcan U, Kokkotou E, Okada T, Liew ChW, Liu S, Peters JN, Dahlgren G, Karamchandani J, Kudva YC, et al. Melanin Concentrating Hormone Is a Novel Regulator of Islet Function and Growth. Diabetes 2007;56(2):311-319

11. Philippe C, Schirmer E, Mitterhauser M, Shanab K, Lanzenberger R, Karanikas G, Spreitzer H, Viernstein H, Wadsak W. Radiosynthesis of [^{11}C]SNAP-7941 – the first PET-tracer for the melanin concentrating hormone receptor 1 (MCHR1). Appl Radiat Isot 2012;70(10):2287-2294

12. Philippe C, Nics L, Zeilinger M, Kuntner C, Wanek T, Mairinger S, Shanab K, Spreitzer H, Viernstein H, Wadsak W, et al. Preclinical *in vitro* & *in vivo* evaluation of [^{11}C]SNAP-7941 – the first PET tracer for the melanin concentrating hormone receptor 1. Nucl Med Biol 2013;40(7):919-925

13. Philippe C, Ungersboeck J, Schirmer E, Zdravkovic M, Nics L, Zeilinger M, Shanab K, Lanzenberger R, Karanikas G, Spreitzer H, et al. [^{18}F]FE@SNAP – A new PET tracer for the melanin concentrating hormone receptor 1 (MCHR1): Microfluidic and vessel-based approaches. Bioorg Med Chem 2012;20(19):5936-5940

14. Ametamey SM, Honer M, Schubiger PA. Molecular Imaging with PET. Chem Rev 2008;108(5):1501-1516

15. Wadsak W, Mitterhauser M. Basics and principles of radiopharmaceuticals for PET/CT. Eur J Radiol 2010;73(3):461-469

16. Zeilinger M, Dumanic M, Pichler F, Budinsky L, Wadsak W, Pallitsch K, Spreitzer H, Lanzenberger R, Hacker M, Mitterhauser M, et al. *In vivo* evaluation of radiotracers targeting the melanin-concentrating hormone receptor 1: [^{11}C]SNAP-7941 and [^{18}F]FE@SNAP reveal specific uptake in the ventricular system. Sci Rep 2017;7(1):8054

17. Philippe C, Haeusler D, Fuchshuber F, Spreitzer H, Viernstein H, Hacker M, Wadsak W, Mitterhauser M. Comparative autoradiographic *in vitro* investigation of melanin concentrating hormone receptor 1 ligands in the central nervous system. Eur J Pharmacol 2014;735:177-183

18. Philippe C, Nics L, Zeilinger M, Schirmer E, Spreitzer H, Karanikas G, Lanzenberger R, Viernstein H, Wadsak W, Mitterhauser M. Preparation and First Preclinical Evaluation of [^{18}F]FE@SNAP: A Potential PET Tracer for the Melanin-Concentrating Hormone Receptor-1 (MCHR1). Sci Pharm 2013;81:625-639

19. Philippe C, Haeusler D, Scherer T, Fürnsinn C, Zeilinger M, Wadsak W, Shanab K, Spreitzer H, Hacker M, Mitterhauser M. [^{18}F]FE@SNAP – a specific PET tracer for melanin-concentrating hormone receptor 1 imaging? EJNMMI Res 2016;6:31

20. Rosen ED, Spiegelman BM. What We Talk About When We Talk About Fat. Cell 2014;156:20-44

21. Kiefer FW. Browning and thermogenic programing of adipose tissue. Best Pract Res Clin Endocrinol Metab 2016;30(4):479-485

22. Peirce V, Carobbio S, Vidal-Puig A. The different shades of fat. Nature 2014;510(7503):76-83

23. Fenzl A, Kiefer FW. Brown adipose tissue and thermogenesis. Horm Mol Biol Clin Invest 2014;19(1):25-37

24. Klaus S. Brown Adipose Tissue: Thermogenic Function and Its Physiological Regulation. In: Klaus S, ed. Adipose Tissues. Austin, Texas: Landes Bioscience, 2001:56-81

25. Cannon B, Nedergaard J. Brown Adipose Tissue: Function and Physiological Significance. Physiol Rev 2004;84(1):277-359

26. Cinti S. Morphology of the Adipose Organ. In: Klaus S, ed. Adipose Tissues. Austin, Texas: Landes Bioscience, 2001:11-26

27. Slot JW, Geuze HJ, Gigengack S, Lienhard GE, James DE. Immuno-localization of the Insulin Regulatable Glucose Transporter in Brown Adipose Tissue of the Rat. J Cell Biol 1991;113(1):123-135

28. Seale P, Bjork B, Yang W, Kajimura S, Kuang S, Scime A, Devarakonda S, Chin S, Conroe HM, Erdjument-Bromage H, et al. PRDM16 Controls a Brown Fat/Skeletal Muscle Switch. Nature 2008;454(7207):961-967

29. Enerbäck S. Brown adipose tissue in humans. Int J Obes 2010;34:S43-S46

30. Cypess AM, Lehman S, Williams G, Tal I, Rodman D, Goldfine AB, Kuo FC, Palmer EL, Tseng Y-H, Doria A, et al. Identification and Importance of Brown Adipose Tissue in Adult Humans. N Engl J Med 2009;360(15):1509-1517

31. Virtanen KA, Lidell ME, Orava J, Heglind M, Westergren R, Niemi T, Taittonen M, Laine J, Savisto N-J, Enerbäck S, et al. Functional Brown Adipose Tissue in Healthy Adults. N Engl J Med 2009;360(15):1518-1525

32. Saito M, Okamatsu-Ogura Y, Matsushita M, Watanabe K, Yoneshiro T, Nio-Kobayashi J, Iwanaga T, Miyagawa M, Kameya T, Nakada K, et al. High Incidence of Metabolically Active Brown Adipose Tissue in Healthy Adult Humans: Effects of Cold Exposure and Adiposity. Diabetes 2009;58(7):1526-1531

33. Kiefer FW. The significance of beige and brown fat in humans. Endocr Connect 2017;6(5):R70-R79

34. Kiefer FW, Vernochet C, O'Brien P, Spoerl S, Brown JD, Nallamshetty S, Zeyda M, Stulnig TM, Cohen DE, Kahn CR, et al. Retinaldehyde dehydrogenase 1 regulates a thermogenic program in white adipose tissue. Nat Med 2012;18(6):918-925

35. Dallner OS, Chernogubova E, Brolinson KA, Bengtsson T. β_3-Adrenergic Receptors Stimulate Glucose Uptake in Brown Adipocytes by Two Mechanisms Independently of Glucose Transporter 4 Translocation. Endocrinology 2006;147(12):5730-5739

36. Shimizu Y, Satoh S, Yano H, Minokoshi Y, Cushman SW, Shimazu T. Effects of noradrenaline on the cell-surface glucose transporters in cultured brown adipocytes: novel mechanism for selective activation of GLUT1 glucose transporters. Biochem J 1998;330:397-403

37. Nikami H, Shimizu Y, Sumida M, Minokoshi Y, Yoshida T, Saito M, Shimazu T. Expression of β3-Adrenoceptor and Stimulation of Glucose Transport by β3-Agonists in Brown Adipocyte Primary Culture. J Biochem 1996;119:120-125

38. Chernogubova E, Cannon B, Bengtsson T. Norepinephrine Increases Glucose Transport in Brown Adipocytes via β_3-Adrenoceptors through a cAMP, PKA, and PI3-Kinase-Dependant Pathway Stimulating Conventional and Novel PKCs. Endocrinology 2004;145(1):269-280

39. Emorine LJ, Marullo S, Briend-Sutren MM, Patey G, Tate K, Delavier-Klutchko C, Strosberg AD. Molecular Characterization of the Human β_3-Adrenergic Receptor. Science 1989;245:1118-1121

40. Baker JG. Evidence for a Secondary State of the Human β3-Adrenoceptor. Mol Pharmacol 2005;68(6):1645-1655

41. Coman OA, Păunescu H, Ghiţă I, Coman L, Bădărău A, Fulga I. Beta 3 adrenergic receptors: molecular, histological, functional and pharmacological approaches. Rom J Morphol Embryol 2009;50(2):169-179

42. Bylund DB, Eikenberg DC, Hieble JP, Langer SZ, Lefkowitz RJ, Minneman KP, Molinoff PB, Ruffolo RR Jr, Trendelenburg U. International Union of Pharmacology Nomenclature of Adrenoceptors. Pharmacol Rev 1994;46(2):121-136

43. D'Allaire F, Claude A, Mauriège P, Simard P-M, Bukowiecki LJ. Characterization of β_1- and β_3-adrenoceptors in intact brown adipocytes of the rat. Br J Pharmacol 1995;114(2):275-282

44. Skeberdis VA. Structure and function of β_3-adrenergic receptors. Medicina (Kaunas) 2004;40(5):407-413

45. Hoffman C, Leitz MR, Oberdorf-Maass S, Lohse MJ, Klotz K-N. Comparative pharmacology of human β-adrenergic receptor subtypes – characterization of stably transfected receptors in CHO cells. Naunyn-Schmied Arch Pharmacol 2004;369:151-159

46. Blin N, Camoin L, Maigret B, Strosberg AD. Structural and Conformational Features Determining Selective Signal Transduction in the β3-Adrenergic Receptor. Mol Pharmacol 1993;44:1094-1104

47. Chaudhry A, Granneman JG. Differential regulation of functional responses by β-adrenergic receptor subtypes in brown adipocytes. Am J Physiol 1999;277:R147-R153

48. Klingenberg M, Huang S-G. Structure and function of the uncoupling protein from brown adipose tissue. Biochim Biophys Acta 1999;1415(2):271-296

49. Méjean A, Guillaume J-L, Strosberg AD. Carazolol: a potent, selective β_3-adrenoceptor agonist. Eur J Pharmacol 1995;291:359-366

50. Baker JG. The selectivity of β-adrenoceptor antagonists at the human β1, β2 and β3 adrenoceptors. Br J Pharmacol 2005;144:317-322

51. Hulme EC, Trevethick MA. Ligand binding assays at equilibrium: validation and interpretation. Br J Pharmacol 2010;161(6):1219-1237

52. Hein P, Michel MC, Leineweber K, Wieland T, Wettschureck N, Offermanns S. Receptor and Binding Studies. In: Dhein S, Mohr FW, Delmar M, eds. Practical Methods in Cardiovascular Research. Berlin, Germany: Springer, Berlin, Heidelberg, 2005:723-783

53. Motulsky HJ, Mahan LC. The Kinetics of Competitive Radioligand Binding Predicted by the Law of Mass Action. Mol Pharmacol 1984;25(1):1-9

54. Motulsky HJ, Neubig RR. Analyzing Binding Data. Curr Protoc Neurosci 2010;Suppl52:Unit7.5

55. Cheng Y-C, Prusoff WH. Relationship between the inhibition constant (K_I) and the concentration of inhibitor which causes 50 per cent inhibition (I_{50}) of an enzymatic reaction. Biochem Pharmacol 1973;22(23):3099-3108

56. Qume M. Overview of Ligand-Receptor Binding Techniques. In: Keen M, ed. Receptor Binding Techniques. Totowa, USA: Humana Press, 1999: 3-23

57. Björke H, Andersson K. Measuring the affinity of a radioligand with its receptor using a rotating cell dish with in situ reference area. Appl Radiat Isot 2006;64(1):32-37

58. Björke H, Andersson K. Automated, high-resolution cellular retention and uptake studies in vitro. Appl Radiat Isot 2006;64(8):901-905

59. Ridgeview Instruments AB. LigandTracer Technology. Internet: http://www.ridgeviewinstruments.com/instruments/technology/ (accessed 10 April 2018)

60. Ridgeview Instruments AB. Quantify biomolecular interactions in real-time using LigandTracer. Internet: http://www.ridgeviewinstruments.com/instruments/ (accessed 10 April 2018)

61. Ridgeview Instruments AB. Protocol: A typical LigandTracer® measurement. Internet: http://www.ridgeviewinstruments.com/docs/LigandTracer%20Protocol%20A%20typical%20LigandTracer%20measurement%201.3.pdf (accessed 10 April 2018)

62. Philippe C, Zeilinger M, Scherer T, Fürnsinn C, Dumanic M, Pilz J, Wadsak W, Hacker M, Mitterhauser M. MCHR1: a potential indicator for BAT activity. Nuklearmedizin 2016;55(2):A78 (abstr)

63. Balber T, Benčurová K, Mitterhauser M, Wadsak W, Viernstein H, Hacker M, Philippe C. Uptake of the MCHR1 PET-tracers [^{18}F]FE@SNAP and [^{11}C]SNAP-7941 in BAT: an adrenergic beta-3 receptor mediated effect? Eur J Nucl Med Mol Imaging 2017:44(Suppl 2):S526 (abstr)

64. PerkinElmer®. Technical Data Sheet: human Adrenergic β_3 Receptor. Internet: http://www.perkinelmer.co.uk/Content/TDLotSheet/ES-035-M400UA_1732440.pdf (accessed 30 March 2018)

65. PerkinElmer®. Technical Data Sheet: human Adrenergic β_3 Cell Line. Internet: http://www.perkinelmer.com/Content/TDLotSheet/ES-035-C_M1W-C3.pdf (accessed 30 March 2018)

66. PerkinElmer®. Technical Data Sheet: (-)-CGP-12177, [5,7-^{3}H]-. Internet: https://www.perkinelmer.com.cn/Content/TDLotSheet/NET1061_2219198.pdf (accessed 30 March 2018)

67. Schirmer E, Shanab K, Datterl B, Neudorfer C, Mitterhauser M, Wadsak W, Philippe C, Spreitzer H. Syntheses of Precursors and Reference Compounds of the Melanin-Concentrating Hormone Receptor 1 (MCHR1) Tracers [^{11}C]SNAP-7941 and [^{18}F]FE@SNAP for Positron Emission Tomography. Molecules 2013;18:12119-12143

68. Thermo Fisher Scientific. Instructions: Pierce™ BCA Protein Assay Kit. Internet: https://tools.thermofisher.com/content/sfs/manuals/MAN0011430_Pierce_BCA_Protein_Asy_UG.pdf (accessed 30 March 2018)

69. Smith PK, Krohn RI, Hermanson GT, Mallia AK, Gartner FH, Provenzano MD, Fujimoto EK, Goeke NM Olson BJ, Klenk DC. Measurement of Protein Using Bicinchoninic Acid. Anal Biochem 1985;150(1):76-85

70. Klotz K-N, Hessling J, Hegler J, Owman C, Kull B, Fredholm BB, Lohse MJ. Comparative pharmacology of human adenosine receptor subtypes – characterization of stably transfected receptors in CHO cells. Naunyn-Schmiedeberg's Arch Pharmacol 1998;357(1):1-9

71. Ridgeview Instruments AB. Protocol: Seeding cells for LigandTracer®. Internet: http://www.ridgeviewinstruments.com/docs/LigandTracer%20Protocol%20Seeding%20cells%20for%20LigandTracer%201.3.pdf (accessed 31 March 2018)

72. Zeilinger M, Pichler F, Nics L, Wadsak W, Spreitzer H, Hacker M, Mitterhauser M. New approaches for the reliable in vitro assessment of binding affinity based on high-resolution real-time data acquisition of radioligand-receptor binding kinetics. EJNMMI Res 2017;7(1):22

73. Lonza Walkersville, Inc. Protocol: Oil red o stain for *in vitro* adipogenesis. Internet: http://bio.lonza.com/uploads/tx_mwaxmarketingmaterial/Lonza_ManualsProductInstructions_Oil_Red_O_Stain_for_In_Vitro_Adipogenesis.pdf (accessed 10 April 2018)

74. Kobilka B. Adrenergic receptors as models for G protein-coupled receptors. Annu Rev Neurosci 1992;15:87-114

75. Ridgeview Instruments AB. Technology note: Understanding how your ligand interacts with living cells. Internet: http://www.ridgeviewinstruments.com/docs/LigandTracer%20Technology%20Note%201.6.pdf (accessed 4 April 2018)

76. Cannon B, Nedergaard J. Adrenergic regulation of brown adipocyte differentiation. Biochem Soc Trans 1996;24(2):407-412

77. Kinkel AD, Fernyhough ME, Helterline DL, Vierck JL, Oberg KS, Vance TJ, Hausman GJ, Hill RA, Dodson MV. Oil red-O stains non-adipogenic cells: a precautionary note. Cytotechnology 2004;46(1):49-56

78. Ohlson KBE, Mohell N, Cannon B, Lindahl SGE, Nedergaard J. Thermogenesis in Brown Adipocytes Is Inhibited by Volatile Anesthetic Agents. A Factor Contributing to Hypothermia in Infants? Anesthesiology 1994;81(1):176-183